NTNU

Norwegian University of
Science and Technology

Reduction of Pelletized Tyssedal Ilmenite and the Effect of Changing Gas Composition and Flow, Pellet Size and Pre Oxidation Condition

Steinar Jørstad

Materials Science and Engineering
Submission date: July 2011
Supervisor: Leiv Kolbeinsen, IMTE
Co-supervisor: Jan Martin Eriksen, ERAMET
Håvard Elstad, ERAMET

Norwegian University of Science and Technology
Department of Materials Science and Engineering

I hereby declare that this work has been carried out independently and in compliance with the examination regulations of the Norwegian University of Science and Technology, NTNU.

Steinar Jørstad

Trondheim, July 2011

ACKNOWLEDGEMENTS

This master thesis is carried out at the department of material science and engineering, at the Norwegian University of Science and Technology (NTNU) during the spring of 2010. The work is done in collaboration with ERAMET Titanium & Iron AS (ETI) in Tyssedal Norway.

I would first of all like to thank my supervisor Leiv Kolbeinsen for guidance, inspiration and advice during the work with this master thesis. I would also like to thank my co-supervisor Jan Martin Eriksen and Dr. Stian Seim for useful comments and help with organizing the analysis at ETI Tyssedal. For practical organization when I worked at the plant in Tyssedal during the summer of 2010, and for useful feedback, co-supervisor Haavard Elstad receives my gratefulness.

I would like to express my sincere gratitude to Arne Hildal for the discussion regarding the XRD results, as well as Knut Kaupang for the help with supplying the raw materials. The laboratory at ETI Tyssedal, under the supervision of Tora Lervik, also deserves my thanks.

When I began running experiments, Shawn Wilson from SINTEF, explained how to operate the DISvaDRI furnace. He also gave advice regarding the experiments which I am grateful for. I would like to thank Bendik Sægrov for help when anything unexpected occurred with the software. To understand the phase composition of the samples XRD analysis were done. Dr. Julian Tolchard told me how to operate the equipment and interpret the results, for which I am most grateful. I would also like to thank Morten Peder Raanes for assisting me during the EPMA analyzes. At last I would like to thank my classmates Jens E. Davidsen and Trine V. Salvesen for helping me out when I was stuck with LaTeX and for useful feedback towards the end.

ABSTRACT

This master thesis is based on reduction experiments of pelletized Tyssedal ilmenite. The focus is set on the effect of changing parameters such as gas composition, gas flow, pellet size and pre-oxidation condition. The results are interpret regarding values of conversion, degree of metalization, XRF-analysis and microstructure images. Based on these results the aim was to find out how these parameters influenced reduction. Another goal was to reveal what hampered reduction inside both grains and pellets and caused the two stage reduction behaviour. EPMA was used to examine pellets and grains and to look for explanation for the slow reduction. XRD-analysis was decisive for explaining the importance of optimum pre-oxidation for the subsequent reduction.

Pre-oxidized and green pellets with a size fraction of 8-10 mm were heated in a thermogravimetric analyzer. Ar was used during heating and cooling. Reduction occurred at 930-940 °C, with either CO, H_2 or both for up to 45 minutes. Gas flows used were 4.8, 7 and 9 Nl/min. In total 18 experiments were carried out. Weight before and after reduction was measured, calculations of degree of metalization, XRF- and XRD-analysis was done. Microstructure images, point analysis, line scan and mapping were obtained by EPMA.

Highest final values of conversion, c. 0.9, were obtained for pre-oxidized pellets from 2011 reduced with H_2. Maximum degree of metalization, 94-99 % were obtained after reduction of pre-oxidized pellets from 2010. Final value of conversion and degree of metalization were 0.23 and c. 24 % higher for pre-oxidized pellets from 2010 than from 2011. Only green pellets from 2011 was harder to reduce with CO. Reducibility was not increased with the pre-oxidation conditions at ETI Tyssedal in January 2011. In spite of that the pre-oxidized pellets from 2010 and 2011 are made in the same manner and from the same raw material they react differently during reduction. This should be kept in mind when comparing results from different sources.

Reduction of pre-oxidized pellets occurred in two distinct linear stages separated by a clear bend. A normal behaviour with steadily decreasing oxygen removal rate was observed with green pellets. An increased flow of CO from 7 Nl/min to 9 Nl/min resulted in decreased reduction.

Examination by EPMA confirmed the presence of the barrier effect and higher amount of oxygen 0.6-1.0 mm from the surface. This indicates hampered reduction in grains and pellets. This combined with slow migration of CO/CO_2 in the pellets can partly explain the unusual reduction behaviour. Pre-oxidized pellets from 2010 contains higher amount of the easily reducible M_3O_5, and less M_2O_3 compared to pre-oxidized pellets from 2011. The less reducible M_3O_4 was also found in the pre-oxidized pellets from 2011, making them harder to reduce.

Contents

1 INTRODUCTION

Ilmenite, $FeTiO_3$, is a mineral mainly consisting of iron and titanium oxides with the general formula M_2O_3. Amount of iron oxides and titanium oxides range from 20 - 35 wt % and 35 - 65 wt %, respectively. Manganese and magnesium can dissolve into the M_2O_3 structure while other impurities, like silicon and aluminium, are found as separate oxides (Jørstad, 2010).

There are two different types of ilmenite, rock and sand ilmenite. Rock ilmenite is mined and hardly exposed to air. It therefore contains more iron and harmful impurities such as manganese and magnesium. Sand ilmenite is naturally crushed and often agglomerated on beaches after exposure to air and water. This process is called weathering. Weathering and its influence on chemical properties was thoroughly studied by Gupta et al. (1989). The main effect of weathering is that divalent iron is oxidized to trivalent iron. As trivalent iron is more soluble in water, some iron will be removed from the ilmenite. The fraction of manganese can also be reduced by weathering. Local differences in grain structure and inter lamella spacing also affects the reduction (Jørstad, 2010).

At complete weathering all the ilmenite is converted into rutile (TiO_2), which is the main constituency in ”beach sand”. Rutile can be processed directly into $TiCl_4$ by the chloride upgrading process. This can be used as feedstock in the TiO_2 pigment process or reduced into Ti-metal by the use of Mg in the Kroll process. Synthetic rutile can be processed from ilmenite by several upgrading processes, for instance Beecher. Further treatment is the same as for natural rutile. Ilmenite can also form the basis for pigment production in the sulphate slag process. (Kolbeinsen, 2010)

The chemical properties mainly determine the choice of slag upgrading process. Generally, there are two different routes; sulphate slag and chloride slag upgrading. Low levels of impurities are most decisive for chloride processing as Mg and Ca form condensates in reaction with chloride gas, which harms the equipment in the chloride upgrading process (Borowiec et al., 1997; Sun et al., 1992).

Different processes are used to utilize the ilmenite depending on the ratio of iron to titanium, and amount and type of impurities. The hydro metallurgical route, which does not utilize the iron, is one possibility. Alternative processes are pyrometallurgical. These are direct reduction in an electric arc furnace, called ilmenite smelting, or a two stage process with pre-reduction in solid state, followed by smelting in a submerged arc furnace. The latter is called the Tyssedal process (Gupta et al., 1989; Elstad et al., 1992).

Prior to reduction, ilmenite pellets are pre-oxidized in order to gain strength and enhance the kinetics of reduction. Tangstad (1988*a*,*b*) and Jørstad (2010) investigated the effect of pre-oxidation on the ilmenite reduction of Tyssedal pellets, and Tangstad reported significant changes in kinetics during reduction. The variation in rate and extent of reduction for pellets with different state of pre-oxidation makes it crucial for the industry to control and optimize the pre-oxidation process. To achieve pre-oxidation in the Tyssedal process green pellets are heated and fired with air. The pellets are subsequently transferred to a rotary kiln where most of the iron oxide is reduced to solid metallic iron. Finally, the remaining iron oxide is smelted and partly reduced in a smelter. Some FeO is left in the slag to benefit the slag properties. With decreasing amount of FeO the viscosity of the slag increases, making the separation of slag and metal more difficult. Since the reducing potential is low, only minor amount of other oxides are reduced. This gives two valuable products; a titania enriched slag sold for upgrading to TiO_2 pigment and high purity pig iron used for special cast iron products (Elstad et al., 1992).

The original goal for this thesis was to investigate the kinetics of ilmenite reduction with alternating reducing potentials by the use of gas mixtures of CO/CO_2 and H_2/H_2O. The conversion results for some of the initial experiments deviated from general accepted knowledge and the aim of this master thesis was therefore changed. The new goal for this thesis has been to understand the differences related to ilmenite reduction and try to explain the odd results when parameters such as pre-treatment, pellet size, gas composition (CO or H_2) and gas flows are altered. Values of conversion, degree of metalization and data from the XRF-analysis are compared. In addition investigations by EPMA and XRD are performed to reveal the differences between grains inside the reduced pellets and changes in phase composition.

2 THEORY

This section is included to give the reader general knowledge about ilmenite reduction. The iron, titanium and oxygen system will be explained together with pre-oxidation and reduction of ilmenite. A brief section with kinetics is included to point out the rate determining steps. How ilmenite reduction is affected by temperature, gas composition and pre-oxidation is also explained.

2.1 Necessary definitions

The terms degree of metallization and degree of conversion are often used, but are not interchangeable.

2.1.1 Degree of metallization

The degree of metallization tells how much of the iron oxides that is reduced to metallic iron, value in wt.%, is given by Equation 2.1 (Elstad et al., 1992):

$$\text{Degree of metallization} = \frac{\text{metallic iron}}{\text{metallic iron + iron in iron oxides}} \times 100 \tag{2.1}$$

2.1.2 Degree of conversion

From the analysis of the pre-oxidized ilmenite pellets both the total amount of iron and the distribution between divalent (FeO) and trivalent iron (Fe_2O_3) can be found. Degree of oxidation (OX) is a measure of the actual amount of oxygen bound to iron, compared to the maximum amount of oxygen that can be bound to iron. The connection is shown in Equation (2.2), which is derived in Section A.1 in the Appendix (Elstad et al., 1992):

$$\text{OX} = \frac{\text{m}_\text{O} - \Delta_\text{Weight}}{\text{m}_\text{O,tot}} = \frac{(\text{n}_{\text{Fe}^{3+}} \times 1{,}5 + \text{n}_{\text{Fe}^{2+}} \times 1 + \text{n}_\text{Fe} \times 0) \times \text{M}_O - \Delta_\text{Weight}}{(\text{n}_{\text{Fe}^{3+}} + \text{n}_{\text{Fe}^{2+}} + \text{n}_\text{Fe}) \times 1{,}5 \times \text{M}_O} \tag{2.2}$$

In Equation (2.2) m_O and $m_{O,tot}$ measures amount of oxygen bound to iron [g] at a given analysis and at fully oxidized sample, respectively. M_O is the molar weight of oxygen [g/mole]. Δ_{Weight} is the weight loss during one experiment [g], and finally n_i is number of moles of specie i [mole]. Weight loss is assumed to be 100 % oxygen. Connection between degree of oxidation and conversion (X) is given in Equation (2.3):

$$\text{X} = 1 - \text{OX} \tag{2.3}$$

2.2 Phase relations in ilmenite

The following sections will give an introduction to three ilmenite phase diagrams where the most common phases are included.

2.2.1 Fe-Ti-O

The phase diagram for pure ilmenite above 1100 °C is according to Borowiec and Rosenqvist (1985) well understood. The spinell phase has a M_3O_4 structure, varying in composition from magnetite (Fe_3O_4) to ulvöspinell (Fe_2TiO_4). The α-oxide, characterized as M_2O_3, has a composition ranging from hematite (Fe_2O_3) to ilmenite ($FeTiO_3$). The M_3O_5 structure is a solid solution of ferric pseudobrookite (Fe_2TiO_5) and ferro pseudobrookite ($FeTi_2O_5$). Iron is trivalent in ferric pseudobrookite and divalent in ferro pseudobrookite. Pseudorutile with trivalent iron can be found in the M_5O_9 structure as $Fe_2Ti_3O_9$. In addition to these phases, $Fe_2Ti_2O_7$, representing the M_4O_7 structure and some iron and titanium oxide can be found as solid solution in the rutile phase (TiO_2) and wüstite phase "(FeO)", respectively.

For reduction purposes it is also interesting to understand the phase diagram at lower temperatures. The ternary phase diagram made by Borowiec and Rosenqvist (1981) for the system Fe-Fe_2O_3-TiO_2 can be seen in Figure 2.1. There are four different three phase areas:

1. Fe + wüstite + spinell
2. Fe + spinell + α-oxide
3. Fe + α-oxide + rutile
4. α-oxide + rutile + pseudobrookite

The N_{Ti} lines in Figure 2.1 gives the oxidation path for different ilmenite ores. N_{Ti} is calculated from Equation (2.4):

$$N_{Ti} = \frac{N_{TiO_2}}{N_{TiO_2} + N_{Fe_2O_3} + N_{FeO}} \tag{2.4}$$

Where N_x is mole fraction of specie x. From analysis of pre-oxidized Tyssedal ilmenite N_{Ti} is 0.60 and 0.55 for pellets acquired during autumn and winter respectively. Because of the high N_{Ti} values, wüstite and spinell phase should not occur under reduction at 950 °C. According to the phase diagram in Figure 2.2 metallic iron can dissolve 4 wt.% titanium at 1000 °C. This is therefore the

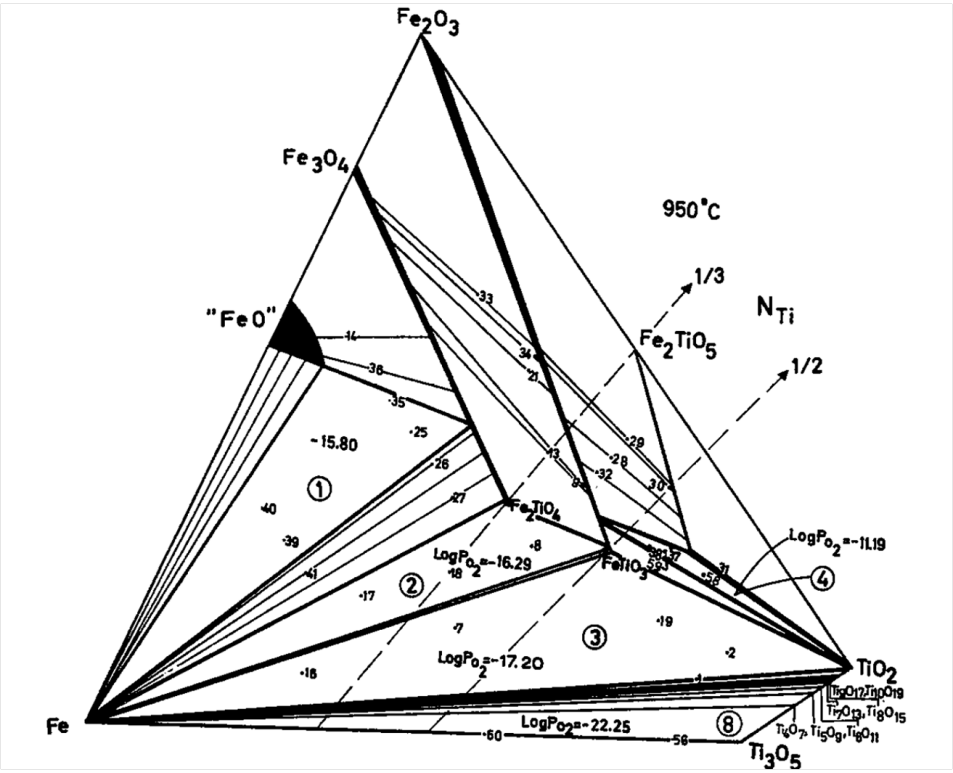

Figure 2.1: Equilibrium phase diagram for the system Fe-Fe_2O_3-TiO_2 at 950 °C. The Figure is taken from (Borowiec and Rosenqvist, 1981).

maximum content of titanium in the reduced iron phase after reduction. From the same phase diagram, some titanium will be precipitated as Fe_2Ti during cooling of a titanium saturated iron phase (Calphad, 2010).

2.2.2 Fe-Ti-Mg-O

The Fe-Ti-O system is quite simple. Addition of small amounts of Mg and Mn gives a much more complex system. Mn will stabilize the M_2O_3 phase and Mg forms solid solution with the M_2O_3 phase. According to Jones (1974) and Gupta et al. (1987) pure M_3O_5 is unstable below 1140 °C, but both Mn and Mg will stabilize this phase far below this temperature. A simplified three dimensional model of the system made by Borowiec and Rosenqvist (1982) is found in Figure 2.3.

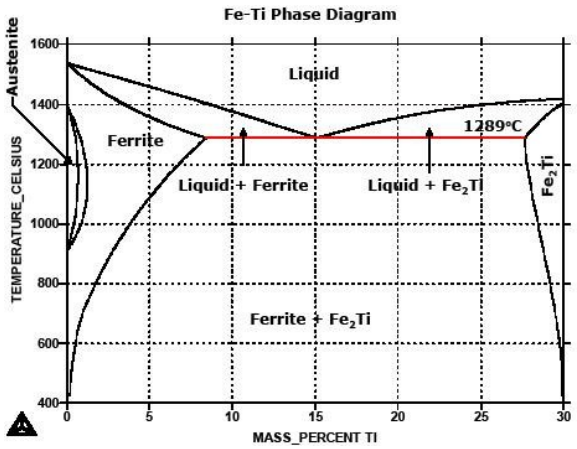

Figure 2.2: Fe-Ti Phase diagram from the SGTE phase diagram collection. The phase diagram is taken from (Calphad, 2010).

The four oxides FeO, Fe_2O_3, TiO_2 and MgO are chosen as components to represent each corner in the phase diagram. As a result of this some components will be represented outside the tetrahedral with negative concentrations. Based on this system each reduction path will follow a straight line drawn from the point O. The direction is dependent on the Mg:Ti:Fe-ratio. In Figure 2.3 a line in the plane of Mg:Ti-ratio of 0.2, which is close to the ratio found in the Tyssedal ilmenite (0.16), is drawn. Point C represents the ilmenite after pelletizing and D after complete pre-oxidation. If pellets are slightly reduced composition moves towards point B. A further Increase in the reducing potential will move the composition towards A, which is the hypothetical end point.

2.3 Ilmenite Reduction

This subsection describes pre-oxidation and the most common ilmenite reduction Equations with the use of CO and H_2 as reducing agents.

2.3.1 Pre-oxidation

In the pre-oxidation both microstructure and phase composition will change. Jones (1975) and Zhang and Ostrovski (2002) reported that this enhanced reducibility. Zhao (2010) found that pelletized Titania ilmenite pre-oxidized at 800 °C for two hours contained $Fe_2Ti_3O_9$, TiO_2 and Fe_2O_3. At 1200 °C the main phases are TiO_2 and Fe_2TiO_5. This confirms previous results by Borowiec and

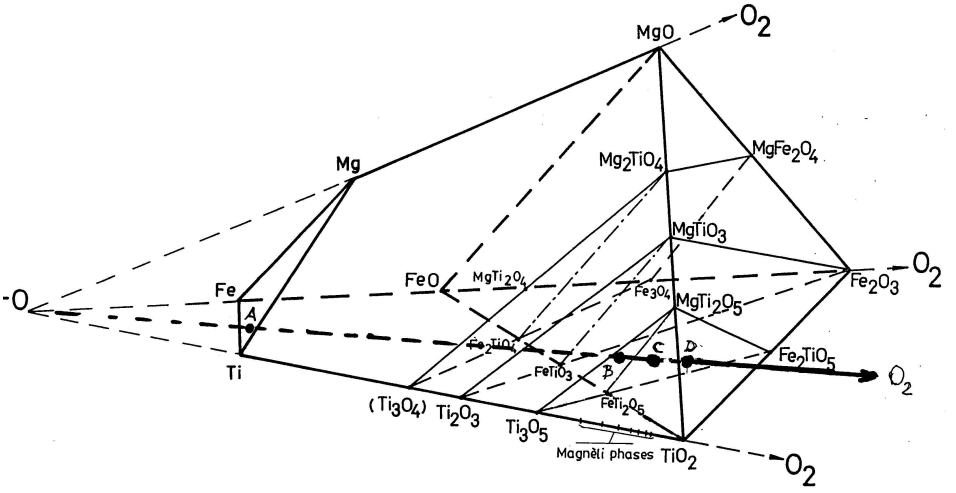

Figure 2.3: Pseudo ternary phase diagram for the system Fe-Ti-Mg-O. With the components: FeO, Fe_2O_3, TiO_2 and MgO. Figure after (Borowiec and Rosenqvist, 1982).

Rosenqvist (1981), that pre-oxidation up to 850 °C gives TiO_2 and Fe_2O_3. Above 900 °C ferric pseudobrookite also occurred. The main pre-oxidation products between 950 and 1000 °C are Fe_2TiO_5 and TiO_2.

Similar results were obtained by Tangstad (1988*a*). TiO_2 was found at pre-oxidation below 750 °C. Between 750 and 850 °C Fe_2O_3 and TiO_2 were the final phases obtained. The occurrence of pseudobrookite was first observed above 930 °C. In contradiction to this, Jasna (1978) found pseudobrookite already at 750 °C. Compared to the phase diagram for the pure Fe-Ti-O system, pseudobrookite was stable at temperature higher than 585 °C. With addition of Mg the three phase area M_3O_5 + M_2O_3 + TiO_2 was stabilized below 585 °C (Borowiec and Rosenqvist, 1985).

(Tangstad, 1988*b*) proposed two mechanisms for this:

1. Impurities could decrease the solubility of $FeTi_2O_5$ in Fe_2TiO_5. As a result of this the area of stability for M_2O_3 + TiO_2 increased, as the three phase area M_3O_5 + M_2O_3 + TiO_2 shifted towards higher degree of oxidation

2. Transformation to pseudobrookite is generally slow below 900 °C

The reason pseudobrookite did not form below 900 °C is most likely a combination of the two mechanisms. The phases obtained after pre-oxidation is therefore affected by both amount of impurities present and pre-oxidation time.

2.3.2 Reduction of pre-oxidized pellets

From the work on pre-oxidized Titania ilmenite at 800 °C with H_2, Zhao (2010) found that the following reactions occurred:

$$Fe_2O_3(s) + 3H_2(g) = 2Fe(s) + 3H_2O(g) \quad (2.5)$$
$$Fe_2Ti_3O_9(s) + H_2(g) = 2FeTiO_3(s) + TiO_2(s) + H_2O(g) \quad (2.6)$$
$$FeTiO_3(s) + H_2(g) = Fe(s) + TiO_2(s) + H_2O(g) \quad (2.7)$$
$$nTiO_2(s) + H_2(g) = Ti_nO_{2n-1}(s) + H_2O(g) \quad (2.8)$$

After pre-oxidation at 1200 °C pseudobrookite was also reduced with H_2 according to Equation (2.9) (Zhao, 2010):

$$Fe_2TiO_5(s) + H_2(g) + TiO_2(s) = 2FeTiO_3(s) + H_2O(g) \quad (2.9)$$

With CO as reducing agent the following reduction reactions could be obtained (Zhao, 2010):

$$Fe_2TiO_5(s) + CO(g) + TiO_2(s) = 2FeTiO_3(s) + CO_2(g) \quad (2.10)$$
$$FeTiO_3(s) + CO(g) = Fe(s) + TiO_2(s) + CO_2(g) \quad (2.11)$$
$$Fe_2O_3(s) + 3CO(g) = 2Fe(s) + 3CO_2(g) \quad (2.12)$$
$$nTiO_2(s) + CO(g) = Ti_nO_{2n-1}(s) + CO_2(g) \quad (2.13)$$

In addition to these reactions ulvöspinel can form during reduction of ferric pseudobrookite, see Equation 2.14. Ulvöspinell is then reduced to iron and ilmenite according to Equation 2.15. Formation of ulvöspinel is faster than the subsequent reduction to iron and ilmenite (Jones, 1973; Zhang and Ostrovski, 2001).

$$Fe_2TiO_5(s) + H_2(g) = Fe_2TiO_4(s) + H_2O(g) \quad (2.14)$$
$$Fe_2TiO_4(s) + H_2(g) = Fe(s) + FeTiO_3(s) + H_2O(g) \quad (2.15)$$

Depending on temperature and CO/CO_2 ratio the reverse Boudouard reaction, Equation (2.16), can occur. The impact of this reaction can be seen in Figure 2.4a.

$$2CO(g) = C(s) + CO_2(g) \quad (2.16)$$

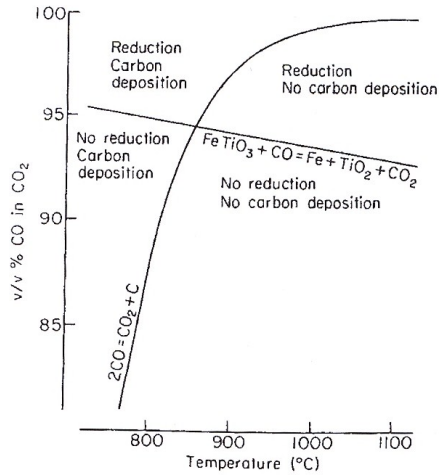

(a) CO/CO_2 in equilibrium with carbon and ilmenite. This Figure is copied from Jones (1975).

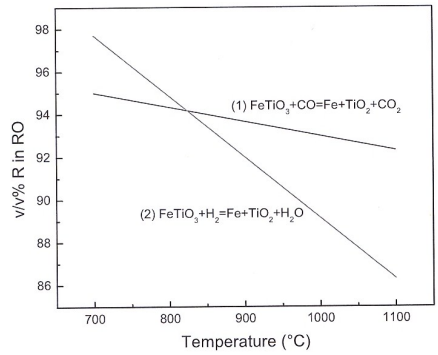

(b) (1) R=CO, RO=CO_2;(2) R=H_2, RO=H_2. Figure taken from Zhao (2010).

Figure 2.4: Gas compositions in equilibrium with ilmenite as a function of temperature.

Carbon is deposited according to Boudouard reaction in Equation (2.16), specially at low temperatures and high partial pressure of CO. From Figure 2.4a it can be seen that carbon deposition at 900 °C could be avoided with the addition of 3 at.% CO_2. Merk and Pickles (1988) and Towhidi and Szekely (1983) found that carbon deposition was proportional to amount of porous iron present below 900 °C. Deposition of C was enhanced by the effect of metallic iron as a catalyser.

While carbon monoxide is a more powerful reducing agent than hydrogen below 800 °C, it is generally accepted that ilmenite reduction proceeds faster with H_2 than with CO (Jones, 1975). An investigation by Sun et al. (1992) confirmed that the ilmenite reduction with H_2 followed a shrinking core model. Hydrogen diffused into the core and reacted to produce metallic iron and rutile (TiO_2). Surface analysis indicated that iron migrated through the TiO_2 layers and formed iron nuclei on the grain boundaries. As these nuclei grew they finally covered the entire surface of the particle. Similar results were obtained with CO by Zhao and Shadman (1990).

Another important aspect of ilmenite reduction is that it often proceeded topochemically, which is closely linked to impurities like Mn and Mg (Jones, 1973; Sun et al., 1992). First a rapid reduction of Fe^{3+} to Fe^{2+} followed by a much slower reduction of Fe^{2+} to Fe^0. This is described more thoroughly in Section 2.5. Reduction of trivalent iron can proceed through the entire pellet

before a significant amount of divalent iron is reduced down to metallic iron. The initial stage involves Equation (2.6), (2.9) and (2.10) in addition to reduction of hematite to wüstite. The latter stage is described by Equation (2.7) and (2.11) together with final reduction of wüstite to metallic iron (Jones, 1973; Sun et al., 1992). This was also confirmed by Tangstad (1988*b*) and Johnsen (2005) with their reduction of Titania ilmenite.

Although reduction of iron is the desired reaction, some degree of titanium reduction, Equation (2.8), and (2.13), will also occur. With carbon as reducing agent, Welham and Williams (1999) found that Ti_3O_5 was the highest reduced titanium oxide. Further reduction was enhanced by iron present from the ilmenite reduction. The proposed mechanism for this was increased transport of C to the oxide surface by dissolution into iron. Welham (2002); Wang et al. (2009) also confirmed that Ti_3O_5 was the most reduced titanium oxide obtainable with reduction by pure H_2. For one single pellet of Bama ilmenite, the formation of Ti_3O_5 required 120 minutes of reduction at 950 °C (Wang et al., 2009). By combining the use of both H_2 and CO through the water shift reaction, Equation (2.17) (Kolbeinsen, 2010), high reaction rate and degree of reduction could be obtained. Gas composition in equilibrium with ilmenite as a function of temperature is shown in Figure 2.4b.

$$CO(g) + H_2O(g) = CO_2(g) + H_2(g) \tag{2.17}$$

2.3.3 Reduction of green pellets

Tangstad (1988*b*) reported that green pellets mainly consisted of Fe_2O_3 and $FeTiO_3$ both with mutual solid solution. The main reduction reactions are described by Equation (2.5),(2.7),(2.11) and (2.12).

2.4 Kinetics of ilmenite reduction

Considering the general heterogeneous reaction Equation (2.18), there are several possible rate determining steps.

$$aA(s) + bB(g) = cC(s) + dD(g) \tag{2.18}$$

If the shrinking core model is applied to a spherical pellet, Figure 2.5, the general steps are (Szekely et al., 1976):

1. Transport of gas B from the bulk gas phase through a stagnant gas film to the outer surface of the solid phase

2. Diffusion of gas B through the porous product layer, or through areas of partly reacted product towards the reaction interface of the unreacted product

3. Chemical reaction at the interface

4. Diffusion of gas D through the porous product layer, or through areas of partly reacted product back towards the outer surface of the solid

5. Transport of gas D through the gas film away from the surface of the solid phase to the bulk phase

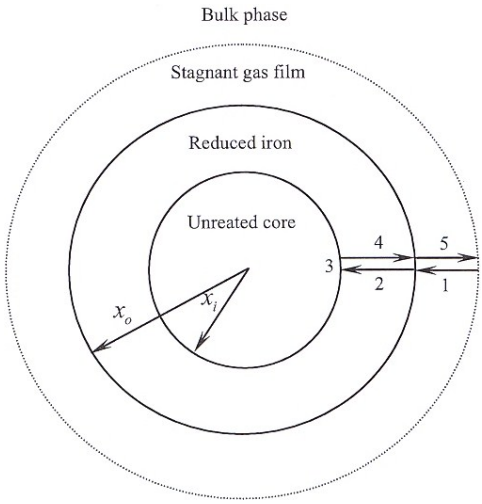

Figure 2.5: Illustrative shrinking core model for reduction of dense pellets under mixed control. The Figure is taken from Spitzer et al. (1966).

In addition to these steps chemical absorption of gas B to the surface of reaction and desorption of gas D from the surface of reaction can be rate determining steps. For ilmenite reactions the system is simplified by neglecting these terms. Because step 1 and 5 and 2 and 4 are of same type, the system can be simplified by only looking at step 1 to 3. Even in this simplified system the rate determining step can be altered by changing variables as temperature, gas flow, pellet size and the pellet porousity. In order to find the Equations describing the basic kinetics some further assumptions are required. One perfect spherical pellet is assumed to consist of many spherical grains. And all reaction mechanisms are assumed to be of first order (Szekely et al., 1976).

2.5 Parameters affecting the ilmenite reduction

This section will mainly focus on aspects important for reduction on both a macro scale and on the scale of individual grains. Impurities and iron nucleation is important on a micro scale, while changing parameters like pre-oxidation, gas composition and amount, temperature and grain size will determine the total extent of reduction.

Impurities that hamper the ilmenite reduction

During reduction of ilmenite ore Wang and Yuan (2006); Wang et al. (2009); Gupta et al. (1987, 1989) and Merk and Pickles (1988) found that Mn^{2+} replaced Fe^{2+} in the ilmenite phase at the reaction interface. As the Mn^{2+} enriched zone increased, this baffled carbon monoxide diffusion and the activity of Fe^{2+} decreased. This can be referred to as the barrier effect visualized in Figure 2.6a (Jones, 1974; Wang and Yuan, 2006; Wang et al., 2009). According to thermodynamic data of ilmenite reduction, Mn in titanate lattice is very stable. It is neither possible to reduce Mn in the lattice to manganese oxide or manganese metal, nor could Mn be found in solid solution with rutile (Wang and Yuan, 2006). Eventually the activity of Mn became so high, and the corresponding activity of iron so low, that the reduction of divalent iron to metallic iron ceased (Wang and Yuan, 2006; Wang et al., 2009; Zhang and Ostrovski, 2001).

Gupta et al. (1989) found that M_2O_3 (α-oxide) often was surrounded by M_3O_5 (pseudobrookite), where Mg, in spite low concentration, tied up and stopped iron oxide from further reduction. Even though the mechanisms of delaying reduction by Mn^{2+} and Mg^{2+} are about the same, Wang et al. (2009) reported larger influence by magnesium oxide. The suggested explanation was that Mg, compared to Mn, formed a more stable solid solution with titanium and iron oxide (Wang et al., 2009; Merk and Pickles, 1988).

Calcium oxide may also segregate and form a barrier towards carbon monoxide diffusion, leading to decreased kinetics of ilmenite reduction (Merk and Pickles, 1988). Due to formation of fayalite ($FeOSiO_2$), silicon oxide also inhibited reaction since the activity of iron oxide was decreased (Wang and Yuan, 2006; Wang et al., 2009; Merk and Pickles, 1988).

Merk and Pickles (1988) found that addition of small amount of impurities reduces both degree of reduction and rate quite substantially, see Figure 2.6b and 2.6c. Addition of MgO had larger impact on reduction than SiO_2, and the effect of further increasing the amount of SiO_2 above 0.75 wt.% was limited.

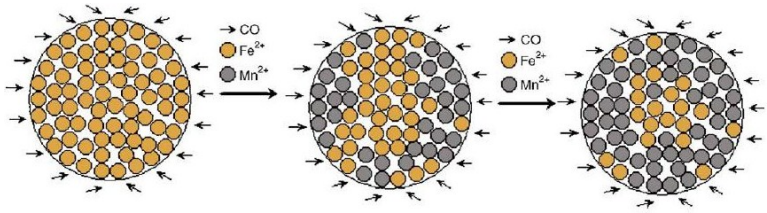

(a) The barrier effect, taken from Wang and Yuan (2006).

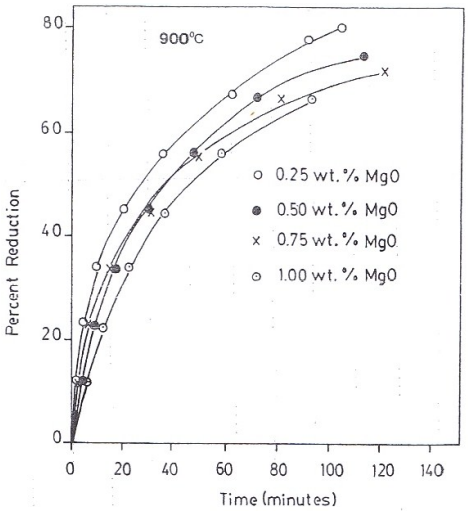

(b) Influence of MgO. Figure taken from Merk and Pickles (1988).

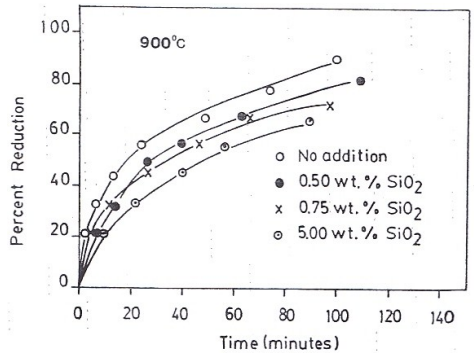

(c) Influence of SiO_2. Figure taken from Merk and Pickles (1988).

Figure 2.6: The barriere effect and impact of impurities on reduction at 900 °C for single briquette Q.I.T. ilmenite sintered in air for 12 hours at 865 °C.

Iron nucleation

Iron will nucleate on grain boundaries, in small pores and other places where the lattice is affected by defects and missorientations. These nucleation spots are generated during weathering and oxidation of the ilmenite. Crystalline materials naturally contain few nucleation spots. Ilmenite is trigonal and if the lattice is dense few spots for nucleation are present inside the grains (Johnsen, 2002). Nucleation of iron will therefore occur on grain boundaries. If the ilmenite structure is more open, nucleation spots are also found inside the grains. A larger fraction of the iron will then form on these nuclei in the grains. These nuclei will grow, and iron might migrate towards the surface of the grains if temperature increases. Too much iron at the grain boundaries might lead to encapsulation of the grain, which reduces the diffusivity of reactant and product gas (Jones, 1974).

Grain size

Decreased grain size will increase surface area and reduce the gas diffusion path from surface to reaction interface. Structural defects will also appear more frequently as the mechanical treatment is increased. Generally this will increase the reaction rate as can be seen in Figure 2.7. Welham (2002) reported that the reduction rate increased more than the surface area after extended milling and H_2 as reducing agent. In addition, increased milling time led to a decrease in reduction temperature.

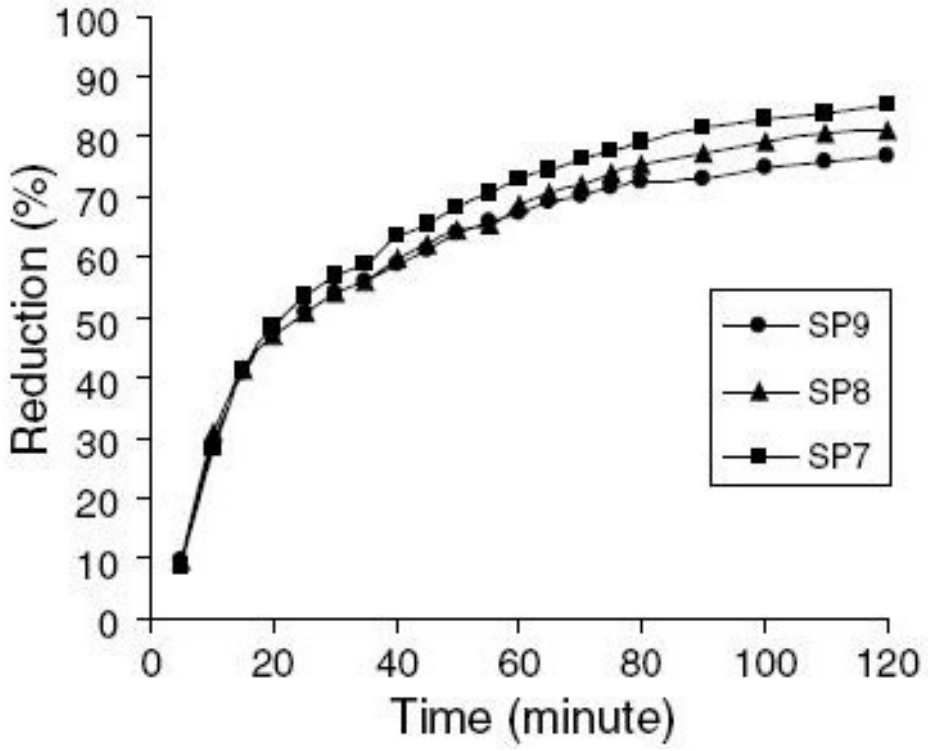

Figure 2.7: Effect of grain size on reduction with graphite at 1350 °C. SP7: -90 + 75 μm, SP8: -106 + 90 μm, SP9: -125 + 106 μm. Figure from Kucukkaragoz and Eric (2006).

Gas flow

If the gas consumption is larger than the provided gas flow, this will limit the reduction. Increasing the gas flow will reduce the contribution from gas diffusion resistance. Finally, the gas flow is higher than the limiting value (Bardi et al., 1987), then reduction is determined by other parameters. For 15 gram of Titania ilmenite the limiting value was 200 Nl H_2/h (Øye, 1990).

From the chemical analysis in Table 3.2 16.5 gram of oxygen is bound to iron assuming pre-oxidized pellets from 2010. In the initial stage, 0.5 to 1.5 minutes after reduction began, the oxygen removal rate with 9 Nl of CO/min was 0.13 moles/min. With this rate the value of conversion would have reached unity within 8.2 minutes. For pre-oxidized pellets from 2011 reduced with 9 Nl/min of CO gas the initial removal rate of oxygen was 0.10 moles/min. By assuming this reduction rate during the whole experiment a complete conversion would have been obtained within 9.09 minutes. The oxygen removal rate is high compared to the rate of CO at 0.37 moles/min

2.5.1 Effect of pre-oxidation on reduction rate

From the literature there is general agreement that pre-oxidation improves the subsequent reduction. In natural ilmenite, Mg and Mn enriched zones tend to hamper the reduction under 1000 °C (Jones, 1974; Merk and Pickles, 1988). Merk and Pickles (1988) found that single crystals of ilmenite transformed into arrays of pseudobrookite with fine dispersion of rutile during oxidation above 800 °C. Under the following reduction metallic iron segregated to the sub grains where shells of iron formed. The influence on reduction rate was therefore less pronounced (Merk and Pickles, 1988), this is in agreement with the results obtained by Jones (1974).

Merk and Pickles (1988) and Tangstad (1988*b*) reported that pre-oxidation increased the reduction rate with the use of CO. According to Tangstad (1988*b*) Tyssedal ilmenite obtained a peak reducibility at pre-oxidation between 850 and 950 °C. For the similar Titania ilmenite, Hussein et al. (1967) reported an increased extent of reduction with the use of H_2. Sun et al. (1992) found that reduction rate, but not the extent of reduction, increased with pre-oxidation followed by H_2 reduction, Figure 2.8a. This is in contradiction to the results by Jones (1975) who reported decreased reduction rate, while the extent of reduction slightly increased. Vijay et al. (1996) on the other hand reported higher extent of reduction, Figure 2.8b. Zhang and Ostrovski (2002) discovered that pre-oxidized ilmenite could be reduced at lower temperature than natural ilmenite. This disagreement can be explained by different factors affecting pre-oxidation such as: Initial porousity, nature of the reducing agent, chemical composition, and whether any solid state transformation occurs.

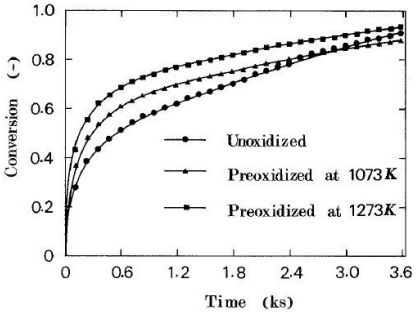

(a) H_2 reduction of Australian cement bonded pellets, pre-oxidized with pure O_2. Figure from Sun et al. (1992).

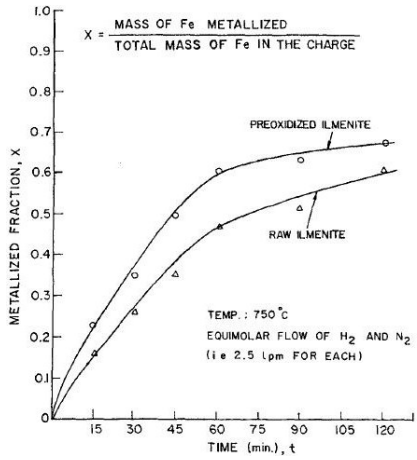

(b) H_2 reduction of Quilon beach sand pellets pre-oxidized with air. Figure taken from Vijay et al. (1996).

Figure 2.8: Effect of 2 hour pre-oxidation on reduction rate.

2.5.2 Effect of gas composition on reduction rate

It is generally accepted in the literature that reduction with H_2 is faster than with CO (Jones, 1975). From Figure 2.9, by Wang et al. (2009), both reduction rate and degree increases with H_2 content. As the temperature increased from 800 to 900 °C this effect was more pronounced.

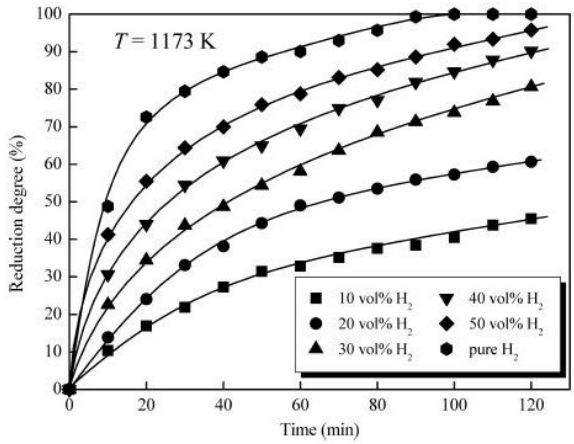

Figure 2.9: Reduction of single pellet Bama ilmenite versus time in H_2-Ar mixture at 900 °C. Figure from Wang et al. (2009).

2.5.3 Effect of temperature on reduction rate

It is generally accepted that reduction rate and extent of reduction increases with temperature (Merk and Pickles, 1988; Zhao and Shadman, 1990; Wang et al., 2009; Wang and Yuan, 2006; Zhao, 2010; Jones, 1975; Wang et al., 2009; Gupta et al., 1987, 1989). The lowest temperature possible for ilmenite reduction with H_2 was 650 °C according to Jones (1975). If the reduction is controlled by chemical reactions it can be described by the Arrhenius relation, Equation 2.19:

$$\text{Reduction rate} \sim \exp(\frac{-1}{\mathrm{T}}) = \frac{1}{\exp(\frac{1}{\mathrm{T}})} \tag{2.19}$$

Increased temperature will therefore imply enhanced reduction rate. This can be seen in Figure 2.10, (a) by Wang et al. (2009) and (b) Gupta et al. (1989). The study by Merk and Pickles (1988) showed that reduction rate increased linearly with temperature up to 1000 °C. At higher temperature metallic iron segregated to the ilmenite grain boundaries. As metallic iron covered most of the grain surface, this inhibited diffusion of carbon monoxide and hence reduction.

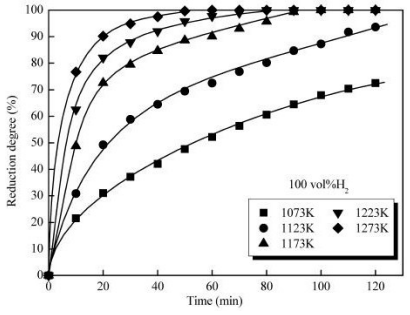

(a) Single pellet Bama ilmenite. Figure taken from Wang et al. (2009).

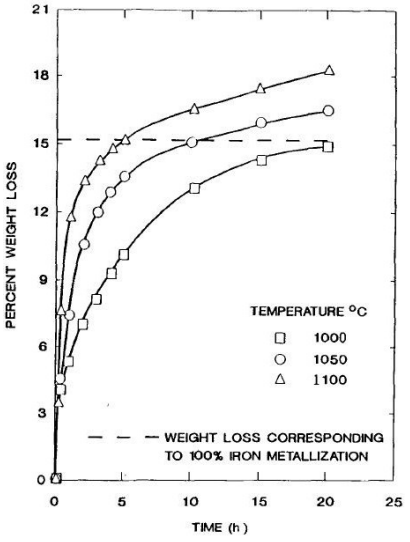

(b) Western sand ilmenite compressed with coal. Figure taken from Gupta et al. (1989).

Figure 2.10: Reduction degree at various temperatures.

3 EXPERIMENTAL WORK

This section describes the apparatus and how it was used. An overview of the raw material and the four analytical methods used to examine the reduced pellets are also included.

3.1 Experimental setup

All experiments were performed with a thermogravimetric furnace (TGA) apparatus. Apparatus and principles of gas flow into the crucible are given in Figure 3.1. The crucible is made of high temperature resistant stainless steel. From Figure 3.1 it can be seen that gas is heated before it reaches the ilmenite pellets. The inner diameter of the off gas tube is larger than the tube at the inlet to prevent pressure from building up inside the crucible. At the centre of the radiation sheet, and surrounding the thermocouple is a high temperature resistant alumina tube. The inner and outer diameters are 4 and 6 mm, respectively. Three stainless steel wires are used to ensure that the crucible is placed in the centre of the furnace. The same wires are connected to a weight with an accuracy of 1 mg. Manufacturer is Mettle Toledo and the type is PR2003 Delta Range (Hlady and Gaal, 2004). More pictures of the TGA furnace with equipment is given in Figure A.2 and A.3 in the Appendix.

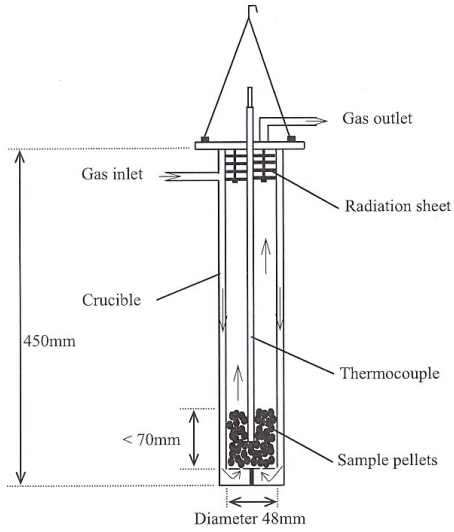

Figure 3.1: Principle sketch visualizing both pellets and gas flow in the crucible. Figure taken from Zhao (2010).

A schematic drawing of the piping and instrumentation diagram is given in Figure 3.2 (Hlady and Gaal, 2004; Zhao, 2010). This Figure explains the gas flow from gas containers, through flow cells and into the crucible. One flow meter is used for each type of gas. Configurations of flow cells and connections between flow cells, weight, crucible and computer are also given in Figure 3.2 (Hlady and Gaal, 2004; Zhao, 2010).

All gas flow, temperatures and weights are recorded in Labview 8.6 version 24 made by National Instruments. FLOWDDE2 version 4.35 is used to communicate and provide data to flow cells, manufactured by Bronkhorst. HI-TEC ELFLOW Mass flow meters were used. Full opening equals 10 Nl/min, for further details see Hlady and Gaal (2004). To ensure that gas tubes are light and compliant they are based on silicone. Temperature is measured in the centre of the crucible and halfway up the pellet bed by a thermocouple of type-S-Platinum. A similar thermocouple to measure the set temperature is placed inside the furnace. The furnace is of type VTF 80/15, delivered by ENTECH Energiteknik AB. If the measured temperature is lower than the programmed set point temperature, resistance in wires will increase rising the effect and temperature in the furnace (Hlady and Gaal, 2004).

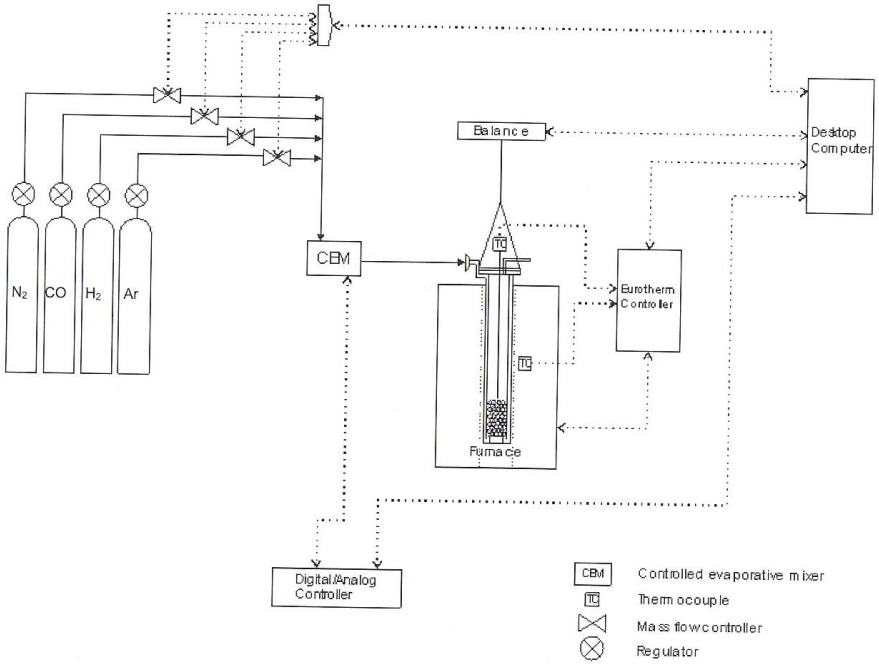

Figure 3.2: Diagram showing piping and instrumentation. Taken from Hlady and Gaal (2004).

3.2 Experimental procedures

This subsection explains the experimental procedure. Chemical analysis of the material used is given.

3.2.1 Raw materials

Pellets used in these experiments are taken from the pre-reduction plant at ETI Tyssedal. Pellets referred to as pre-oxidized are taken after pre-oxidation, just before entering the pre-reduction zone of the rotary kiln. These pellets are heated with air and exhaust from the pre-reduction in order to increase strength and possibly enhance later reduction. The other pellets used in the experiments, named green pellets are taken just after pelletizing, they remained unoxidized. Chemical composition is given in Table 3.1 and 3.2. The 3-6 wt.% not accounted for are due to moisture, extra oxygen and other elements in addition to experimental errors. The content of moisture in the green pellets are measured from the weight difference before and after heating at 150 °C for 5 hours. The results can be found in Table A.1 in the Appendix. CO($\geq$99 %), H_2 (99.99 %) are used to control reduction, while Ar (99.9999 %) was used to prevent oxidation during heating and cooling. All the technical industry gasses are delivered by AGA.

Table 3.1: Chemical composition of pre-oxidized and green Tyssedal ilmenite based on XRF-analysis, all values in wt.%. Composition of pre-oxidized 2010 is taken from Jørstad (2010).

Sample	S	MnO	CaO	MgO	SiO_2	Al_2O_3	Cr_2O_3	V_2O_5	Nb	P_2O_5	ZrO_2
pre-oxidized 2011	0.02	0.38	0.27	3.4	2.7	0.86	0.09	0.20	0.01	0.018	0.04
Green 2011	0.08	0.38	0.27	3.3	2.6	0.81	0.09	0.19	0.01	0.016	0.04
pre-oxidized 2010	0.1	0.45	0.30	3.4	2.5	0.75	0.09	0.19	0.01	0.016	0.04

Table 3.2: Overview of valence of iron and content of TiO_2, water and carbon for different Tyssedal ilmenite, measured by XRF-analysis and wet-chemical analysis. The sum of all elements and oxides in wt.% is below 100 %. Composition of pre-oxidized 2010 is taken from Jørstad (2010).

Sample	FeO	Fe_2O_3	Total Fe	TiO_2	C	H_2O
pre-oxidized 2011	17.7	28.7	33.8	41.9	0.4	-
Green 2011	26.7	17.9	33.3	40.9	1.5	9.9
pre-oxidized 2010	8.0	39.6	33.9	41.9	1.2	-

3.2.2 Reduction in TGA furnace

In total 18 experiments have been carried out during the work of this master thesis. Some general information about these experiments can be found in Table 3.3.

Table 3.3: Overview of the experiments.

Name	Pellet size [mm]	Temperature [°C]	Pre-treatment	Gas flow [Nl/min]	Gas Composition	Time [min]
b4.8CO	8-10	900	pre-oxidized	4.8	CO	45
b7CO	8-10	900	pre-oxidized	7	CO	45
b9CO	8-10	900	pre-oxidized	9	CO	45
b4.8H2	8-10	900	pre-oxidized	4.8	H_2	45
b7H2	8-10	900	pre-oxidized	7	H_2	45
b9H2	8-10	900	pre-oxidized	9	H_2	45
Alumina	10-12.5	900	No	9	H_2	45
b9CO3	8-10	900	pre-oxidized	9	CO	3
b9CO10	8-10	900	pre-oxidized	9	CO	10
b9CO10-12.5	10-12.5	900	pre-oxidized	9	CO	6
b4.8CO10-12.5	10-12.5	900	pre-oxidized	4.8	CO	45
b4.8CO12.5+	12.5+	900	pre-oxidized	4.8	CO	3
b5CO12.5+	12.5+	900	pre-oxidized	5	CO or H_2	45 + 45
g4.8CO	8-10	900	Green	4.8	CO	45
g7CO	8-10	900	Green	7	CO	45
g9CO	8-10	900	Green	9	CO	45
b3.183d	8-10	900	pre-oxidized	1 +3	CO and H_2	135
b9CO.old	8-10	900	pre-oxidized	9	CO	45

Experimental procedure varied slightly depending on pre-oxidation condition. All pellets are sieved and 150 gram of pre-oxidized pellets and 167.7 gram of green pellets. The normal size fraction is between 8 and 10 mm. The weight was of the type CP324S with an accuracy of 0.1 mg, delivered by Sartorius AG Göttingen. The alumina sample consists of 152.6 g of spherical alumina pellets of type AD 90 delivered by CoorsTek, for more detail see Table A.3 in the Appendix.

The samples are given names according to pre-treatment, gas flow, gas composition, pellet size and time for reduction. The sample prefix ”b” or ”g” for burned and green pellets, respectively, the gas flow in Nl/min and size for larger pellets in mm. Sample b9CO3 and b9CO10 are reduced under the same conditions as sample b9CO except that reduction lasted only 3 and 10 minutes respectively. Sample b9CO.old is pre-oxidized pellets from 2010 reduced with 9 Nl CO/min. The four samples b9CO10-12.5, b4.8CO10-12.5, b4.8CO12.5+ and b5CO12.5+ are reduced under same conditions as the samples b4.8CO and b9CO, the difference is related to size range of the pellets in the sample surfix, numbers in mm. Sample b5CO12.5+ consist of pre-oxidized pellets from 2011, where pellets are larger than 12.5 mm. This sample was first reduced with 5 Nl CO/min for 45 minutes. Then the CO was replaced with 4 Nl H_2/min. The crucible was cooled under Ar according to normal procedure. Sample b3.183d consists of

pre-oxidized pellets from 2010, this sample was reduced 183 days after the pellets were pre-oxidized. Reduction occurred with 1 Nl CO/min together with 3 Nl H_2/min.

After sieving,the pellets were filled into the crucible while an alumina tube was held at the centre of a grate at the bottom of the crucible. The radiation sheet was tightened at the top and the alumina tube was raised until the thermocouple inside could measure the temperature halfway up the pellet bed. Finally the alumina tube were fastened according to Figure 3.1 (Zhao, 2010; Hlady and Gaal, 2004).

The wires were connected to the weight above the furnace, and gas tubes tightened to the apparatus. The furnace was raised up to around the crucible, and heating began simultaneously as 1 Nl/min of Ar was purged in. Pre-oxidized pellets were heated for 45 minutes and held at the set temperature of 900 °C for 15 minutes. This was done to ensure that reduction began at equal temperature for all samples. Reduction began when hydrogen or carbon monoxide replaced argon. The gas flow was 4.8 (5), 7 or 9 Nl/min. The temperature in centre of the pellet bed dropped from 950 °C to 930 °C during reduction with CO and H_2. Changes in temperature, weight and gas flow were logged once per second. After reduction for 3 to 143 minutes the gas mixture was changed back to argon, heating shut off and the furnace lowered. 45 minutes later the flow of argon was stopped and the crucible could be removed and emptied. Weight of the samples before and after reduction was measured by use of a SAUTER RL 1200 with an error of 0.01 gram. Sample b4.8CO, b7CO and b9CO were not weighted afterwards.

3.2.3 Experimental analysis

After finishing reduction in TGA three pellets per sample were crushed down for XRD-analysis, while two other pellets per sample were studied in EPMA, type JEOL JXA-8500F. The EPMA was adjusted to analyze the elements Fe, Ti, O, Mn, Mg, Ca, Si and Al as metals, not oxides. 50 gram pellets from each sample were sent to Eramet Titanium and Iron in Tyssedal for XRF-analysis and to test degree of metalization.

As preparation for XRD analysis pellets from each sample were crushed down to 10 μm. The powder was put into a sample container, and a glass slide was used to ensure perfect filling of the holder. When the powder surface was smooth and aligned with the container it was placed inside the XRD analyzer.

Prior to the EPMA analysis sample preparation was carried out, all equipment were delivered by Struers. First 2 pellets per sample were cast in ClaroCit in a

cylindrical mould with 25 mm diameter and height of 20 mm. Samples were then ground down by the use of RotoPol-31 and RotoForce-4 with silicon carbide paper (P80, P500, P1200, P2400 and P4000 for 25, 10, 10, 10 and 20 minutes respectively). The applied force was 50N at a rotating speed of 300 rpm. Polishing were carried out by using TegraPol-31, TegraForce-5 and TegraDoser-5. First with 3 μm plate (MD Dur) and 3 μm polishing fluid (DiaPro Dac 3) for 3 minutes, followed by 3 minutes with 1 μm plate (MD Nap) and 1 μm polishing fluid (DiaPro Nap B 1 μm). After polishing the samples were placed in a drying cabinet at 69 °C until examination, in order to avoid oxidation. Finally, carbon was deposited on the specimen surface and aluminum foil were wrapped around the remaining area of the samples. This was done both to increase conductivity and to avoid charging of the specimen surface.

3.3 Analytical methodes

This section is included to explain the analytical methods: XRF, XRD, wet-chemical and EPMA.

3.3.1 X-ray fluorescence (XRF)

The XRF analysis was performed at the laboratory of ETI in Tyssedal. From the XRF machine of type Philips PW2404 amount of TiO_2, FeO, MnO, CaO, MgO, SiO_2, Cr_2O_3, V_2O_5, Al_2O_3 and Nb from bulk samples are obtained. Wet chemical analysis, see Section 3.3.2, are used to correct for the valence state of iron ($^{3+}$, $^{2+}$ and ^{0}).

The analysis is based on wavelength dispersive spectroscopic principles, which also the probe micro analyzer (EPMA) is based upon, see Section 3.3.4. An X-ray beam is illuminating the sample, while a fraction is scattered and absorbed the remaining X-ray will interact with the atoms in the sample. The beam is often produced by Rh, although W, Mo and Cr also have been used. If an electron is hit by an X-ray the energy can be transferred from the wave to the electron. This increase in energy will dislodge the electron from its shell. Depending on beam properties and energy connected to the electron, this energy release can excite the electron to an outer shell and even ionize the atom. Removal of an electron causes destabilizing of the atom. To restore balance an electron from an outer shell needs to fall down, emitting energy that can be detected. Binding energy is larger for electrons far from the proton, like M shell, than for electrons in the K shell. Because binding energy for electrons varies with atomic number and between

shells this will generate X-rays with characteristic wavelength (SERC at Carleton College, 2010).

To detect intensity of the X-rays and translate it into elemental analysis both gas flow proportional and scintillation can be used. Flow counter is utilized for measuring long wavelength X-rays (>0.15 nm), while shorter wavelengths in the X-ray spectra is detected by scintillation. Intermediate wavelengths are measured by the use of both detectors. Amount of elements in the sample are proportional to the detected X-ray intensity. Exact value of proportionalities between intensity and amount of elements are derived from analysis of samples with known composition (SERC at Carleton College, 2010).

The technology is limited to analyze samples heavier than 1 gram, elements with atomic number (Z) exceeding 10 and concentration above 1 ppm. In addition the samples need to be crushed into a homogeneous powder. Another limitation for XRF is that it can not distinguish either isotopes or valence state for elements (SERC at Carleton College, 2010).

3.3.2 Wet-chemical analysis

The Wet-chemical analysis was carried out at the laboratory of ETI in Tyssedal. This analysis reveals the content of trivalent and metallic iron when the amount of divalent iron is known.

The content of metallic iron in the sample is determined by first adding HgCl and water to the crushed sample. Then metallic iron will be oxidized to divalent iron. By filtrating the solid sample from the solution and mixing the solid with Zimmerman-Reinhardt solution a new solution is obtained. This solution is titrated with $KMnO_4$ from which the content of metallic iron can be calculated (Seim, 2011).

To obtain the content of trivalent iron the sample is dissolved in a solution with H_2SO_4, H_2O and $NH_4Fe(SO_4)_2$. The trivalent titanium and metallic iron from the sample will react with the trivalent iron from the solution and form divalent iron and tetravalent titanium. Divalent iron from the sample will also be dissolved by the sulphuric acid. HF is added to the solution which then is boiled for 10 minutes. After cooling boric and sulphuric acid are added to the solution. Finally titration with $KMnO_4$ will reveal the total iron content in the solution. From this the amount of trivalent iron can be calculated (Seim, 2011).

3.3.3 X-ray powder diffraction (XRD)

The XRD investigations have been performed at the department of Material Science and Engineering (NTNU) by the use of Siemens D5005 and D8focus from Bruker axs. The former is slow but cuts away fluorescence and is better for samples with high iron content. D8focus is faster and can be programmed to analyze 9 samples in a row, the drawback is weaker analysis for samples containing iron. Each scan was performed by increasing the angle from 15 to 90 degrees with a step length of 0.02 degrees per 16 seconds for D5005 and 1.8 seconds for D8focus. The different spectra were evaluated and the phases determined by the use of DIFFRACplus EVA software. The samples b9CO.old, B9CO3, b48CO10-12.5 (core) and pre-oxidized pellets from 2010 and 2011 were analyzed with D5005. D8focus was used to analyze green pellets and the samples g7CO, b7H_2, b4.8CO (core and shell), g7CO and b4.8CO10-12.5 (shell).

XRD is a fast qualitative technique used to determine phase compositions of homogenized and finely ground crystalline material. This technique is based on constructive interference between monochromatic X-rays and a crystalline sample. X-rays are generated by a cathode ray tube, filtered to obtain a monochromatic ray and then concentrated and directed towards the sample surface. The wanted wavelengths Kα_1, Kα_2 and Kβ of the X-ray depend on the target material (Cu, Fe, Mo and Cr) inside the cathode ray tube (SERC at Carleton College, 2011).

The X-ray will interact with the crystalline structure of the sample. When Bragg's condition is fulfilled, $n\lambda = 2d\sin\theta$, this gives both constructive interference and a diffracted X-ray. This law relates the wavelength(s) of the X-ray with lattice spacing in the sample and half the angle between scattered and transmitted X-ray. Under constant illumination by the X-ray beam, the sample is tilted and the scattered X-ray is collected and counted. Each phase will have a unique lattice spacing and a set of θ's that fulfills the Bragg condition. By comparing the peaks in the intensity versus 2θ values for the sample with standard reference patterns, the phases can be identified. Usually the value of 2θ ranges from 5 to 70 $^\circ$ (SERC at Carleton College, 2011).

Advantages with XRD are related to straight forward data interpretation together with minimal sample preparation. For most samples all crystalline phases can be revealed within a 20 minute analysis. The material must be homogeneous and grained into a fine powder. Although only a tenth of a gram of sample might be enough, this technique will only reveal what phases are present, not where they are located inside the pellets. At high angle reflections overlapping peaks may occur, making interpretation more challenging (SERC at Carleton College, 2011).

3.3.4 Electron probe micro analyzer (EPMA)

The EPMA investigations were done at the department of Material Science and Engineering (NTNU) and JEOL JXA-8500F was used in the analysis. Sample b4.8CO, b7CO, b9CO, b9CO.old, b9CO3, b9CO10, b4.8CO10-12.5, b5CO12.5+, b4.8H_2, b7H_2, b9H_2, g4.8CO, g7CO and g9CO were investigated in EPMA.

Elements from Be (Z=4) to U (Z=92) are detectable from electrons with acceleration voltage between 1 and 30 kV. Probe current can be chosen in the interval: $1x10^{-11}$ to $5x10^{-7}$ A. Wavelengths between 0.087 to 9.3 nm are detected by 5 wavelength dispersive X-ray spectrometers (WDS). The equipment also includes an energy dispersive X-ray spectrometer (EDS). At optimum conditions the resolution on the SE image is 3 nm and the maximum resolution is 300 000X. In total, 9 samples of cylindrical shape (r = 12.5 mm, h = 20 mm) can be analyzed simultaneously (NTNU, 2010).

EPMA is an analytic technique used to find composition of small areas on the specimen. Electrons are accelerated and concentrated by lenses towards a small volume of the specimen surface, typically 1 to 9 cubic micrometers. These electrons will generate detectable characteristic X-rays. Since intensity is proportional to concentration, composition of the sample can be found. Advantages with this technique is high spatial resolution and sensitivity, this analysis is also quite fast, 1-2 minutes for each analysis (University of Minnesota, 2010; NTNU, 2010).

It is also possible to use EPMA as an ordinary scanning electron microscope (SEM). Detection of secondary electrons (SE) gives topographical information with a resolution of 100-200 nm, depending on beam current, accelerating voltage and other operating conditions. A fraction of the electron beam is scattered back after interactions with atoms on the specimen surface. More back scattered electrons (BSE) are detected from areas with high average atomic number, compared to areas with low atomic number. Based on BSE an image is created where areas with high atomic number will appear bright. Another useful application is mapping, where the electron beam is scanned over an area generating numerous of point analysis. This will generate maps representing concentrations as colours. Thus mapping gives a qualitatively representation of element distribution across the surface (University of Minnesota, 2010).

4 RESULTS

This section is included to present the most important features of the reduction of ilmenite pellets. Conversion is calculated and visualized in graphs. Degree of metalization and XRF-analysis from the reduced pellets are presented in tables. Reduced pellets are also studied in EPMA. By the use of mapping, line scan and images the elemental distribution within the pellet are revealed. Finally XRD-analysis is presented to give further knowledge of phase relation in the pellets. XRD-analysis is used to explain differences in reduction behaviour when the gas composition and flow are changed.

4.1 Conversion

Graphical representation of conversion gives information about changes in the rate of reduction as a function of time. The final conversion at the end of the experiments gives information about the total extent of reduction. In the following subsections all samples are divided in 5 groups.

4.1.1 Pre-oxidized pellets from 2011 reduced with CO

Figure 4.1 shows conversion as a function of time for pre-oxidized pellets from 2011 and has two distinct regions.

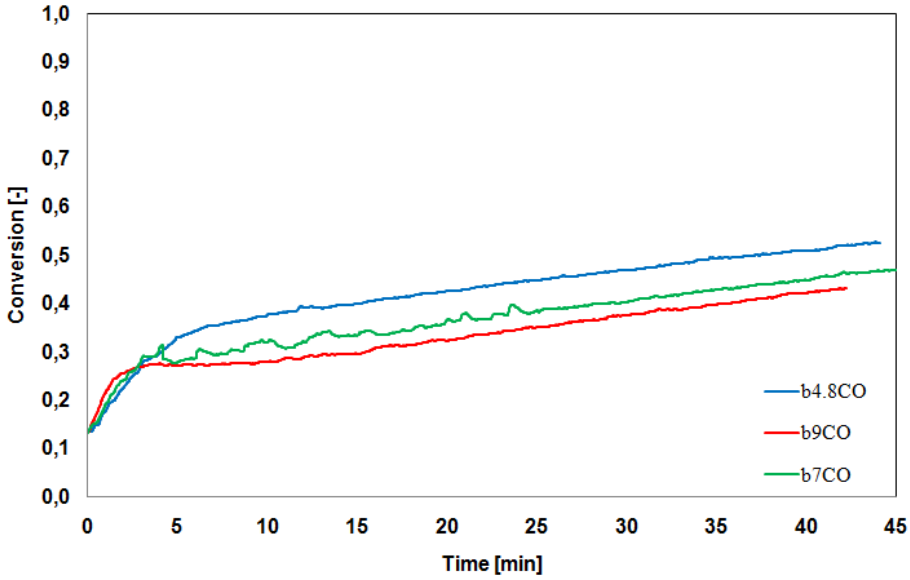

Figure 4.1: Conversion as a function of time for pre-oxidized pellets from 2011 reduced with CO for 45 minutes. Values of conversion are not corrected for weight loss from carbon.

The initial stage where values of conversion increases rapidly as time proceeds and a final stage starting 10 to 15 minutes after reduction began. For sample b4.8CO this shift in reduction rate is observed close to a value of conversion of 0.33. The initial stage last for about 5 minutes. With Sample b9CO the initial stage end with a value of conversion of 0.24 after 1.5 minutes of reduction. The slope of the initial stage, that is the oxygen removal rate, is steeper for reduction with 9 Nl CO/min, compared to lower gas flow of CO. In spite this lower value of conversion is obtained due to the limited time of the fast initial stage. Changes in conversion during reduction for sample b7CO are more similar to sample b4.8CO.

After reduction for 45 minutes the highest value of conversion is 0.53, observed for sample b4.8CO. This value is 0.06 and 0.10 higher than for samples b7CO and b9CO, respectively. Since the slopes of the final stage of reduction are almost equal for the three samples the difference in values of conversion develops within the first 15 minutes of reduction. For sample b9CO values of conversion are

unaltered between 4 and 10 minutes, From then on oxygen removal rate slowly increases and reaches a final value after 15 minutes. Sample b7CO also deviates from normal behaviour and large scattering are observed from the end of the initial stage until 25 minutes after reduction began.

4.1.2 Comparison of pre-oxidized pellets reduced with CO

Figure 4.2 is based on Figure 4.1 but the samples b9CO3, 9CO10 and b9CO.old are also added.

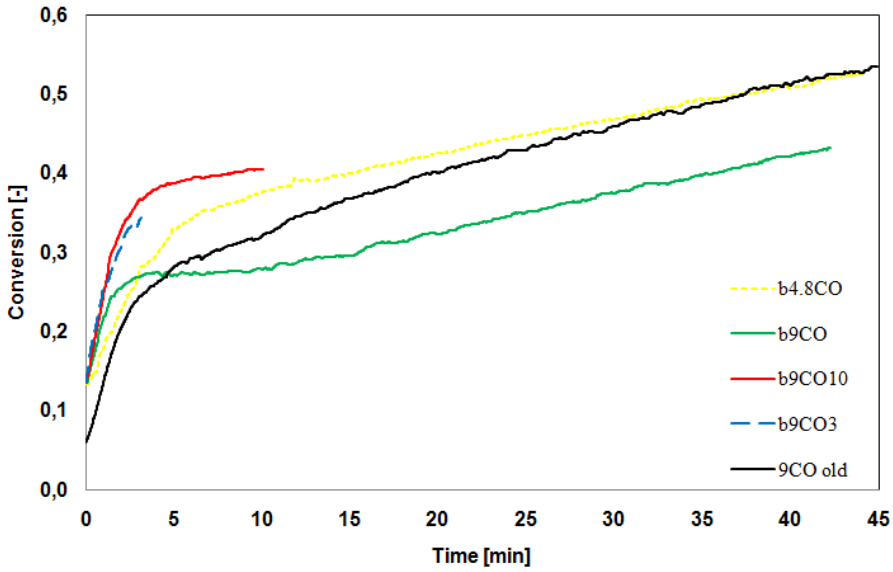

Figure 4.2: Conversion as a function of time for pre-oxidized pellets from 2010 and 2011 reduced with CO for 3, 10 and 45 minutes. Values of conversion are not corrected for weight loss from carbon.

For the samples b9CO3 and b9CO10 the initial stage ends after 3 minutes of reduction with a value of conversion of 0.33. After the initial reduction the slope of the conversion curve for sample b9CO10 declines, and approaches a lower value compared to the other samples reduced with CO. The changes in conversion as a function of time for the samples b9CO10 and b9CO are similar but the values of conversion are 0.12 higher for sample b9CO10. When sample b9CO.old is reduced the initial stage is finished within 3 minutes with a final value of conversion equal to 0.24. The difference in conversion compared to pre-oxidized samples from 2010 is related to a steeper slope in the final stage. The final value

of conversion is 0.52 which is similar to the value obtained in sample b4.8CO. In addition the starting value of conversion is 0.06 compared to 0.13.

4.1.3 Pre-oxidized pellets from 2011 reduced with H_2

In Figure 4.3 conversion as a function of time for pre-oxidized pellets from 2011 reduced with H_2 is given.

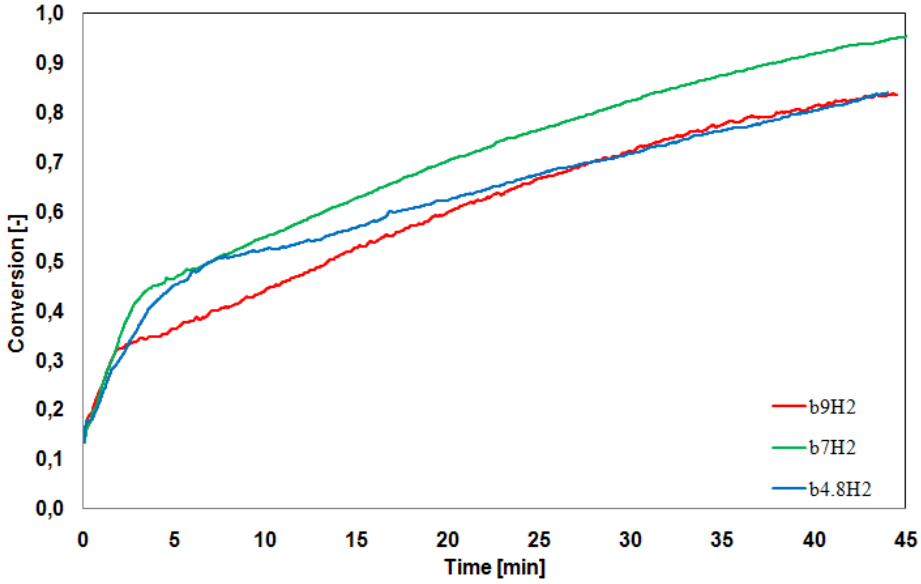

Figure 4.3: Conversion as a function of time for pre-oxidized pellets from 2011 reduced with H_2 for 45 minutes. Values of conversion are not corrected for weight loss from carbon.

The slope of the initial stage is steeper compared to the slope for pellets reduced with CO. Reduction for 3 minutes with 7 Nl H_2/min and 4 minutes with 4.8 Nl H_2/min gives a value of conversion of 0.40. For sample b9H_2 this stage ends after 2 minutes with a value of conversion of 0.32. Both for sample b7H_2 and sample b9H_2 the final stage begins immediate after the first stage is finished, this change is seen as a clear bend in the curve. The slope of the final stage is the same for those two samples, thus the difference in final degree of conversion is due to the initial reduction. The final value of conversion is 0.11 higher for sample b7H_2. With Sample b4.8H_2 reduction rate gradually slows down between the two stages, and the slope of the final stage is lower compared to sample b7H_2 and sample

b9H_2. After final reduction a value of conversion of 0.84 is obtained both for sample b4.8H_2 and sample b9H_2.

4.1.4 Green pellets from 2011 reduced with CO

Changes in conversion for green pellets from 2011 are found in Figure 4.4.

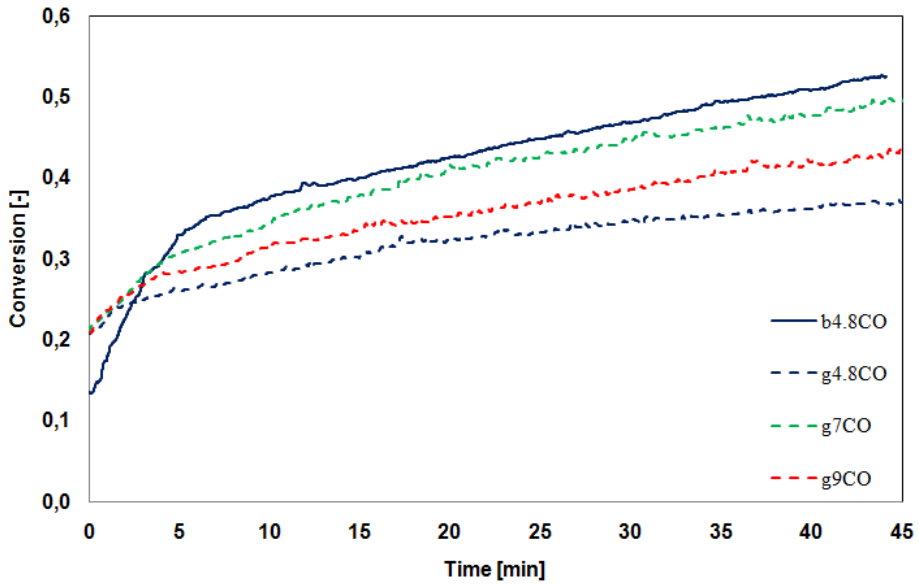

Figure 4.4: Conversion as a function of time for green pellets from 2011 reduced with CO for 45 minutes. The most reduced pre-oxidized sample from 2011, sample b4.8CO is added for comparison. Values of conversion are not corrected for weight loss from carbon.

Sample b4.8CO is added for comparison. For all samples with green pellets, the slope of the line for conversion is steadily decreasing. It therefore makes no sense to separate these curves into two stages. Although green pellets begin with a value of conversion of 0.21 compared to 0.13 for pre-oxidized pellets, the latter has higher values of conversion after more than 4 minutes of reduction. Towards the end of reduction the slope of the line with pre-oxidized pellets is steeper compared to all samples based on green pellets. The most obvious difference between the samples based on green pellets is related to reduction rate. The difference between the conversion curves is visible from 2 minutes and on. From then sample g7CO is more reduced than sample g9CO. Sample g4.8CO has lowest value of conversion at all times. This is the opposite of the situation with pre-oxidized pellets, where the lowest gas flow gives the highest value of

conversion. The final conversion for sample b4.8CO is 0.52 compared to 0.49 for sample g7CO, 0.44 for sample g9CO and 0.37 for sample g4.8CO.

4.1.5 Reduction of larger pellets from 2011, effect of size

Oversized pellets are also reduced, curves of conversion as a function of time for these pellets are found in Figure 4.5.

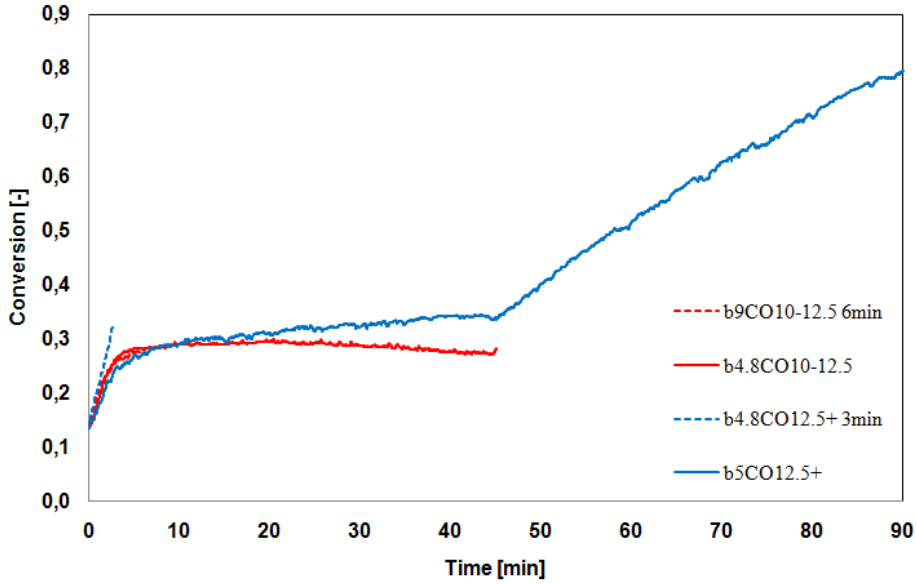

Figure 4.5: Conversion as a function of time for pre-oxidized pellets from 2011 reduced with H_2 for 45 minutes. Values of conversion are not corrected for weight loss from carbon.

For the two samples b9CO10-12.5 and sample b4.8CO12.5+ reduction stopped after 6 and 3 minutes, the former sample is therefore hidden behind sample b4.8CO10-12.5. The initial stage was finished after 3 minutes with a value of conversion of 0.25 and 0.32, respectively. For the sample with pellet size between 10 and 12.5 mm the reduction rate slows down after the initial stage and the value of conversion reaches a maximum value of 0.31 after 19 minutes. From then, values of conversion declines. For reduction of pellets larger than 12.5 mm reduction rate approaches a constant value after 15 minutes. The slope of this stage is limited though. After 45 minutes of reduction the final value of conversion reaches 0.34. In the next 45 minutes of reduction the values of

conversion increases at a constant rate with a steeper slope than the second stage for the same sample. The final conversion is 0.79.

4.1.6 Reduction of pre-oxidized pellets from 2010, effect of aging

Figure 4.6 visualize the changes in conversion as a function of time for the three samples made with pre-oxidized pellets from 2010.

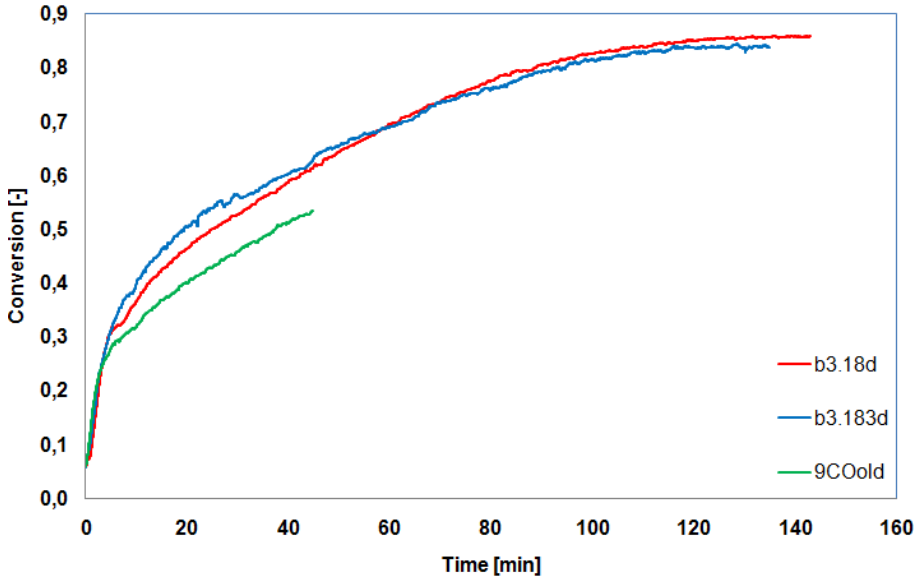

Figure 4.6: Conversion as a function of time for pre-oxidized pellets from 2010 reduced with CO and H_2 for 143 minutes. Pellets reduced with 9 Nl/min of CO are included for comparison. Sample b3.183d is taken from Jørstad (2010). Values of conversion are not corrected for weight loss from carbon.

As mentioned previously reduction of sample b9CO.old proceeds in two stages. For the two samples b3.183d and b3.18d a more gradually decrease in reduction rate are observed. In the first hour of reduction values of conversion for sample b3.183d are higher than for sample b3.18d. From then on the latter sample is most reduced, and finally values of conversion reaches 0.84 and 0.86. When comparing changes in conversion for the samples b3.18d and b3.183d with sample b9CO.old, no difference is observed before the initial stage ends at a value of conversion of 0.24. Then the reduction rate for the sample b9CO.old drops and the difference in values of conversion between sample b9CO.old and the samples b3.18d and b3.183d increases to 0.09-0.10, the latter is more reduced.

4.2 Rate of reduction

The conversion curves visualize the differences in oxygen removal rate during reduction. Figure 4.7 is added to quantify the variation between the initial and final stage and express the difference between the 5 groups of pellets.

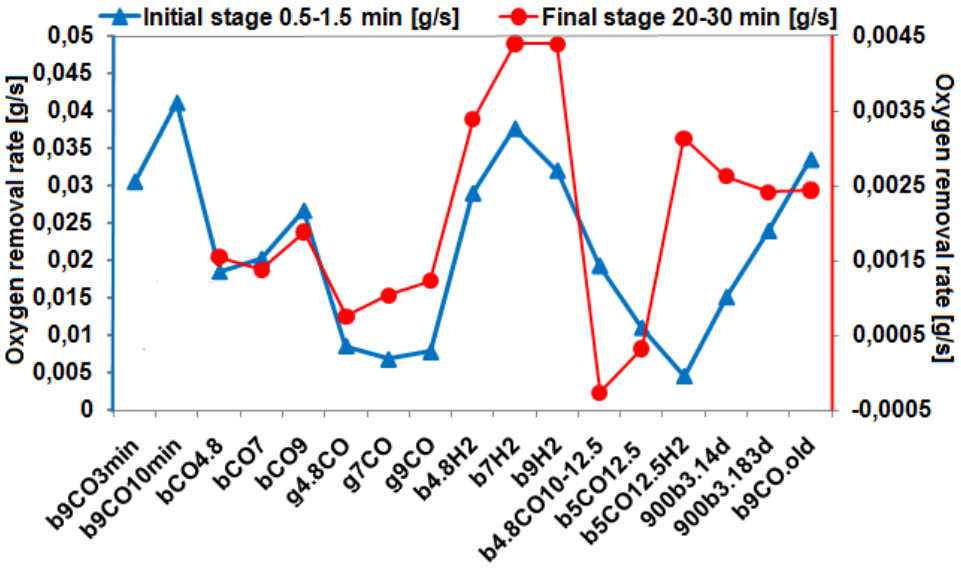

Figure 4.7: Oxygen removal rate in the initial stage (left y-axis) and final stage (right y-axis) [g/s].

From Figure 4.7 the oxygen removal rate in the initial stage from 0.5 to 1.5 minutes is about 10 times the rate in the final stage between 20 and 30 minutes. Apart from the samples b4.8CO10-12.5 and b5CO12.5H2 there is a clear correlation between the initial and final stage among different samples. Deviation is caused by a negative oxygen removal rate for sample b4.8CO10-12.5 and a slow initial oxygen removal rate for sample b5CO12.5, reduced with H_2 after 45 minutes of CO reduction. Despite the same conditions initially for the samples b9CO3, b9CO10 and b9CO the initial reduction rate is changing from 0.027 to 0.041. The final stage is only measured for sample b9CO.

Figure 4.7 also illustrates how the oxygen removal rate is affected by pellet treatment, pellet size and composition and amount of the reduction gas. The oxygen removal rate is higher for pre-oxidized pellets compared to green pellets, and the reduction rate is greater with pellets from 2010 than for pellets made in 2011. H_2 results in faster oxygen removal rate than CO and larger pellets obtains

the lowest oxygen removal rate. Reduction rate for green pellets from 2011 is barely higher compared to samples with oversized pellets.

4.3 Physical observations and measurements

The weight of each sample before and after reduction is measured. These data together with metalization and two different calculations for conversion are given in Table 4.1. Conversion is calculated both from the weight connected to the TGA and weight difference between unreduced and reduced pellets. Degree of metalization was analyzed at the laboratory at Eramet Tyssedal. Both values of conversion are corrected for carbon content in the pellets. The values in parenthesis for sample 5CO12.5+ are found after reduction with H_2 in addition to CO.

Table 4.1: Weight changes, metalization and final values of conversion for reduced samples of Tyssedal ilmenite. The analysis was done at the ETI laboratory in Tyssedal. Values are corrected for carbon content.

Sample	Weight before [g]	Weight after [g]	Final conversion TGA [-]	Conversion from weight loss [-]	Delta conversion [-]	Metalization [%]
b4.8CO	150.03	-	0.50	-	-	24.4
b7CO	149.95	-	0.44	-	-	29.4
b9CO	150.10	-	0.41	-	-	27.0
b4.8H2	149.86	133.41	0.87	0.87	0.00	51.2
b7H2	150.11	132.18	0.93	0.93	0.00	85.0
b9H2	150.07	131.10	0.81	0.98	-0.17	91.5
b9CO3	150.09	146.65	0.32	0.27	0.05	6.1
b9CO10	150.07	145.27	0.38	0.33	0.05	7.4
Alumina	152.60	152.59	-	-	-	-
b9CO10-12.5	150.13	146.30	0.25	0.28	-0.03	5.3
b4.8CO10-12.5	150.53	143.48	0.26	0.43	-0.17	20.2
b4.8CO12.5+	150.55	147.03	0.30	0.27	0.03	2.4
b5CO12.5+	150.36	134.44	0.31 (0.76)	(0.84)	-0.08	82.1
g4.8CO	168.12	141.66	0.47	0.53	-0.06	31.0
g7CO	168.12	141.89	0.41	0.52	-0.11	36.5
g9CO	167.18	141.18	0.38	0.52	-0.14	34.4
b3.183d	170.12	146.13	0.76	0.96	-0.20	93.6
b3.18d	170.38	147.07	0.78	0.93	-0.15	98.9
b9CO.old	170.04	155.40	0.64	0.58	0.06	51.7

4.3.1 Weight change and observation

Weight after reduction for the samples b4.8CO, b7CO and b9CO are not recorded. For the samples made by pre-oxidized pellets from 2011, 149.86 to 150.55 gram was used. Between 170.04 and 170.38 gram per sample were used for the three samples with pre-oxidized pellets from 2010. When green pellets from 2011 were reduced, the initial amount was between 167.18 and 168.12 gram.

For the alumina sample nothing happened with the 152.6 gram of white spheres, except that the colour changed to grey. After reduction of ilmenite pellets a weight loss up to 23.99 gram was measured. On the outside of the pellets no significant difference between the samples was observed except for the variation in amount of soot. In samples made by green pellets and samples reduced with pure H_2 or 3 Nl/min of H_2 in addition to 1 Nl/min of CO little or no soot were observed. For the other samples the amount of soot increased with reduction time, and sample b4.8CO10-12.5 contained most soot.

During sample preparation for EPMA examinations it became possible to study the core of the pellets. For all pellets the outer 2-3 mm of each pellet was shinier compared to the core. In addition the amount and size of cracks varied. Pre-oxidized pellets from 2010 contains many smaller cracks all the way into the core, while few, but large cracks are found in the pre-oxidized pellets from 2011. These cracks separate the pellet in many shells. This is also found in sample b9CO3 which is only reduced for 3 minutes. No cracks are observed in green pellets from 2011. A picture of different pellets are given in Figure A.4 in the Appendix.

4.3.2 Final conversion from TGA

From Table 4.1 it can be seen that the final values of conversion measured by the TGA is higher when the gas flow is lower. When pre-oxidized and green pellets from 2011 are reduced with CO and H_2 conversion is higher with 7 Nl/min compared to the use of 9 Nl/min. Final conversion for pre-oxidized pellets from 2011 is higher after reduction with 4.8 Nl CO/min compared to 7 and 9 Nl/min. The effect of increasing gas flow is less significant when pre-oxidized pellets were reduced with CO compared to reduction with H_2 or other pellet types. Among all samples the highest values of conversion are observed for pre-oxidized pellets reduced with H_2.

For pre-oxidized pellets from 2011 reduced with 9 Nl CO gas/min most of the possible reduction finishes within 3 minutes. Reduction for 7 more minutes

barely increases value of conversion. Compared to reduction for 45 minutes with 9 Nl/min of CO on pre-oxidized pellets from autumn 2010, final conversion of pre-oxidized pellets from 2011 are significant lower.

Another observation for pre-oxidized pellets from autumn 2010 is that values of conversion remains the same even if the experiment is repeated after 165 days.

Pre-oxidized pellets from 2011 with a diameter ranging from 10 mm to 12.5 mm obtains the lowest values of conversion compared to all experiments in this study. No significant difference in conversion is observed between reduction for 3-5 and 45 minutes. The larger pellets obtained a final conversion which was 0.19-0.24 lower than for the 8-10 mm pellets. For sample b5CO12.5+ the conversion values in brackets are obtained after additional 45 minutes of reduction under H_2. This value of conversion is 0.11 lower than with normal sized pre-oxidized pellets from 2010 reduced for 145 minutes with 4 Nl H_2 and CO/min.

4.3.3 Final conversion from weight measurements

Compared to the values of conversion based on TGA for samples reduced more than 10 minutes, most values of conversion from weight measurements are at least as high or higher, the only exception is sample b9CO.old which is 0.06 lower. For the four samples reduced 10 minutes or less conversion values from TGA are higher, with the exception for sample b9CO10-12.5 which is 0.03 lower. Although the highest value of conversion is obtained for sample b9H2, values of conversion are about the same for the three samples reduced with pure H_2 and the two samples based on pre-oxidized pellets from 2010. Another important difference compared to conversion based on TGA is that reduction of pre-oxidized pellets from 2011 is enhanced by increasing gas flow of H_2. For green pellets from 2011 conversion is almost unaffected by increasing gas flow.

4.3.4 Degree of metalization

Degree of metalization is also affected by gas flow. For reduction with CO it increases by c. 5 % points when the gas flow is changed from 4.8 to 7 Nl/min. A further increase in the gas flow up to 9 Nl/min results in c. 2 % points lower degree of metalization. For pre-oxidized pellets from 2011 degree of metalization increases from 51.2 to 91.5 % when the flow of H_2 is altered from 4.8 to 9 Nl/min. Degree of metalization is highest for pellets from 2010 compared to the ones from 2011, degree of metallization is c. 25 % points higher when 9 Nl CO/min is used. Sample b9CO.old and sample b4.8H2 therefore obtain the same

degree of metalization. The maximal value of degree of metalization is 98.9 % and is found after reduction of sample b3.18d.

The lowest value of degree of metalization are found in the samples reduced for less than 10 minutes, the highest value among these is 7.4 % and is obtained after reduction of sample b9CO10. An important observation is that pellets reduced only 3 minutes under the same conditions obtained a degree of metalization of 6.1 %.

If the samples are sorted in groups by pre-treatment and composition of reduction gas, the lowest values of degree of metalization are obtained for samples with pellets larger than 10 mm. Sample b4.8CO12.5+ is the exception with a degree of metalization of 82.1. Reduction of normal sized pellets from 2011 with CO results in higher degree of metalization. When CO is used, green pellets obtained higher degrees of metalization than pre-oxidized pellets. With the exception of pre-oxidized pellets from 2010 highest degree of metalization is obtained after reduction with H_2.

4.4 XRF-analysis

To give more information about the extent of reduction XRF-analysis were done. The results for all reduced samples are found in Table 4.2.

Table 4.2: XRF-analysis of reduced samples of Tyssedal ilmenite. The analysis is carried out at ETI laboratory in Tyssedal. Al values in wt.%.

XRF-Analysis													
Sample	TiO_2	Fe total	MnO	CaO	MgO	SiO_2	Al_2O_3	Cr_2O_3	V_2O_5	Nb	P_2O_5	ZrO_2	Sum XRF
b4.8CO	44.5	35.7	0.42	0.28	3.50	2.80	0.87	0.10	0.20	0.01	0.02	0.04	88.4
b7CO	44.8	36.0	0.41	0.28	3.60	2.80	0.88	0.10	0.20	0.01	0.02	0.04	89.1
b9CO	44.6	35.9	0.41	0.28	3.60	2.80	0.87	0.10	0.20	0.01	0.02	0.04	88.8
b4.8H2	46.7	37.5	0.42	0.30	3.70	2.90	0.91	0.11	0.21	0.01	0.01	0.04	92.8
b7H2	46.6	37.0	0.43	0.31	3.80	3.10	0.97	0.11	0.22	0.01	0.02	0.04	92.6
b9H2	47.1	37.1	0.43	0.31	3.80	3.00	0.93	0.11	0.22	0.01	0.02	0.04	93.0
b9CO3	43.3	34.7	0.40	0.27	3.50	2.70	0.84	0.10	0.20	0.01	0.02	0.04	86.0
b9CO10	43.3	34.6	0.40	0.27	3.50	2.70	0.84	0.10	0.20	0.01	0.02	0.04	86.0
9CO10-12.5	43.3	34.4	0.40	0.28	3.50	2.70	0.86	0.10	0.20	0.01	0.02	-	85.8
4.8CO10-12.5	44.2	35.1	0.40	0.28	3.50	2.80	0.88	0.10	0.20	0.01	0.02	-	87.5
4.8CO12.5+	43.0	34.4	0.40	0.27	3.50	2.70	0.85	0.10	0.20	0.01	0.02	-	85.5
5CO12.5+	46.6	36.9	0.43	0.30	3.70	2.90	0.91	0.10	0.22	0.01	0.02	-	92.1
g4.8CO	44.2	35.4	0.41	0.28	3.50	2.70	0.85	0.10	0.20	0.01	0.02	-	87.7
g7CO	44.2	35.9	0.41	0.28	3.60	2.80	0.87	0.10	0.20	0.01	0.02	-	88.4
g9CO	44.5	35.4	0.41	0.28	3.60	2.80	0.87	0.10	0.20	0.01	0.02	-	88.2
b3.183d	47.7	36.2	0.48	0.33	3.70	2.70	0.83	0.11	0.21	0.01	0.02	0.04	92.2
b3.18d	47.8	36.5	0.49	0.33	3.74	2.60	0.83	0.10	0.21	0.01	-	-	92.6
b9CO.old	45.7	36.3	0.46	0.32	3.60	2.60	0.77	0.11	0.21	0.01	0.02	0.04	90.1

In Table 4.2 the amount of the oxides and elements Cr_2O_3, Nb, P_2O_5 and ZrO_2 remains the same for all samples. Out of these Cr_2O_3 has the highest content with 0.11 wt.%. Amount of oxides like MnO, CaO, MgO, SiO_2, V_2O_5 and Al_2O_3 are affected by reduction. The content of these oxides increases with higher gas flow and time for reduction. All values are at least as high or higher for samples reduced with 7 Nl compared to 9 Nl of reduction gas/min. For pellets from 2011 maximal values are 8 to 16 % higher than the lowest values. For all oxides except MnO and CaO the highest contents are obtained in sample b7H2. The content of MnO and CaO is highest in sample b3.18d. While pellets from 2010 contains more MnO and CaO, the content of SiO_2 and Al_2O_3 are higher in pellets from 2011.

The amount of TiO_2, total iron and the sum of the XRF-analysis is affected by reduction. Changing gas flow has almost no effect. Reduction time for normal pellets influence these values less compared to the effect on the other oxides. For larger pellets, the increased time for reduction are followed by a significant increase in metal and oxide content. The amount of these elements varies between different gas and pellet types. The highest TiO_2 content is found in pre-oxidized pellets from 2010. Amount of iron and the sum of all oxides is highest for pre-oxidized pellets from 2011 reduced with H_2. Almost equally high values are obtained with pre-oxidized pellets from 2010, while lower values are found with pellets from 2011 reduced with CO. Normal pellets contains more iron and TiO_2 after reduction than green pellets, but the lowest values are found in pellets larger than 10 mm.

4.5 EPMA

The investigations in EPMA are carried out to reveal the difference between the pellet types and how reduction parameters affect the following reduction and phase composition. In addition to images of the microstructure this technique gives information about phase compositions. Point analysis, mapping and line scan gives quantitative information about element distribution in points, for an area and across a line, respectively.

4.5.1 Microstructure

Figure 4.8 reveals the impact of changing reduction time on the extent of reduction by the use of 9 Nl CO/min.

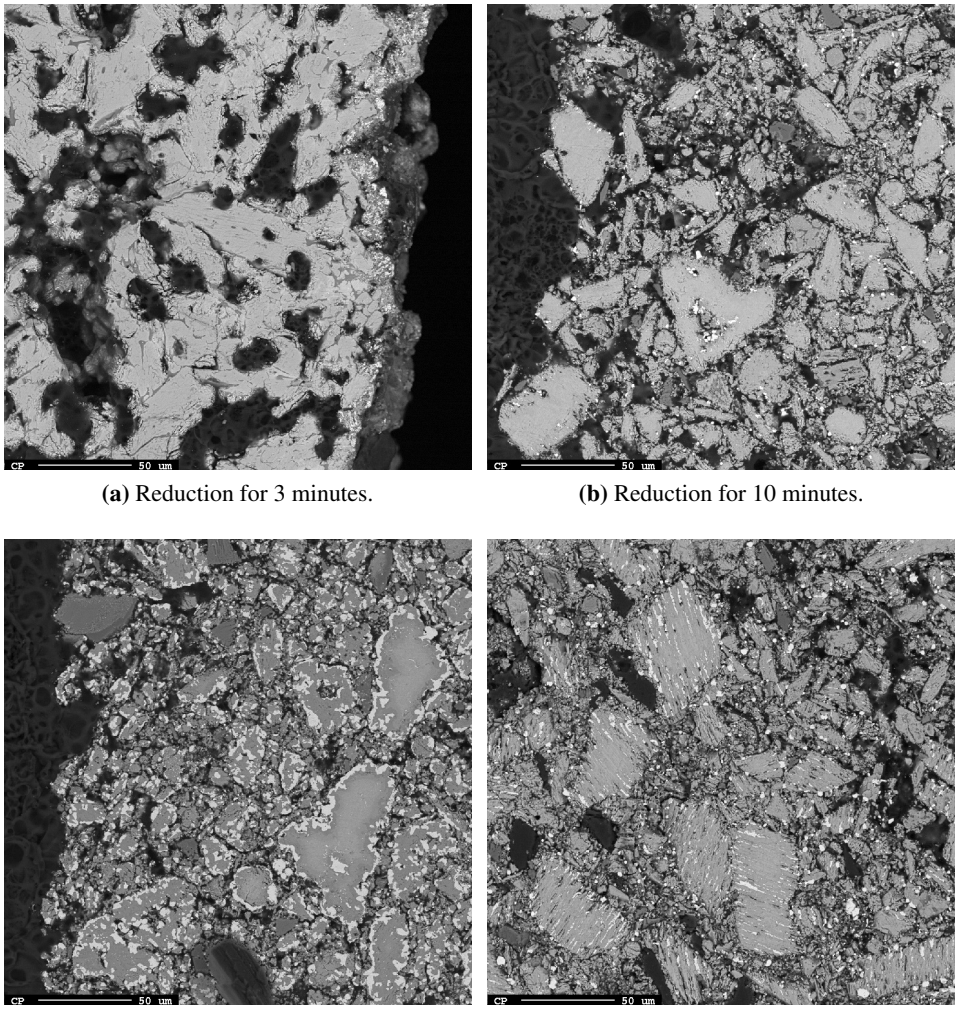

(a) Reduction for 3 minutes.

(b) Reduction for 10 minutes.

(c) Reduction for 45 minutes.

(d) Green pellet reduced with 7 Nl/min.

Figure 4.8: Microstructure of pre-oxidized pellets from 2011 reduced with 9 Nl CO/min for 3 to 45 minutes, a green pellet reduced with 7 Nl CO/min for 45 minutes is added for comparison. The image is taken at the surface at 400 times magnification.

Despite many differences between the 4 pellet types in figure 4.8, they have one thing in common; no white areas representing metallic iron is present at the center

of the grain. The pellet in Figure 4.8a is reduced for only 3 minutes. Iron is only found in a narrow area at the surface of the pellet. These numerous iron nuclei with spherical form are very small. Further away from the surface than 10 μm no iron nuclei are found.

By increasing the reduction time to 10 minutes, small spherical iron nuclei are found from the surface and 300-400 μm into the core of the pellet. These iron nuclei are evenly distributed on the surface of the grain and between various grains, but rarely found inside grains. The probability of finding an iron particle is the same 200 μm from the surface as close to the surface.

After reduction for 45 minutes, the amount of reduced iron is much higher. The iron nuclei have both become more numerous and the size has grown. Inside the grains with size above 20 μm, few iron nuclei are observed. For these grains most of the surface is covered with a several μm thick layer of iron. The colour of the grains reduced for only 10 minutes is grey. Most of the core of the larger grains reduced for 45 minutes appears in a light grey colour. Closer to the surface the phase appears grey. This indicates two different phases, where the inner phase probably is an unreduced grain, referred to as ”unreduced ilmenite”.

When these pellets are compared with the images of pellets from the samples b4.8CO and b7CO, both the amount and shape of metallic iron remains the same. The difference is related to the fraction of metallic iron present inside the grains and on the grain boundaries. While few iron nuclei are observed in pellets from sample b9CO, more are observed inside the pellets from sample b4.8CO. In the pellets from sample b7CO most of the grains contains small iron nuclei with size close to 1 μm. Both in pellets from the samples b7CO and b9CO many grains were almost completely covered with an iron phase, the largest fraction within this layer is often light grey. This was not observed at the grains in pellets from sample b4.8CO.

Pellets from sample b9CO.old are also examined. These were similar to the pre-oxidized pellets from 2011. The only difference is that no unreduced grains are observed in the pre-oxidized pellets from 2010. In addition more iron nuclei are observed inside the grains. Another important observation is that some spherical iron particles are found at the pellet center. Most of them are observed at the grain surface but one grain also contains lamella like iron particles inside.

In Figure 4.8d a reduced green pellet can be seen. Less iron is formed compared to the pre-oxidized pellets. Although the number of nuclei is about the same the average size is much smaller. In addition more of the iron is present inside the grains. No grains are covered with an iron layer. The shape of the outer iron particles is spherical, while iron nuclei formed inside the grains are more lamella

shaped. An unreduced core is also found within the largest grains of green pellets. No significant difference is observed among pellets from the samples g4.8CO, g7CO and g9CO.

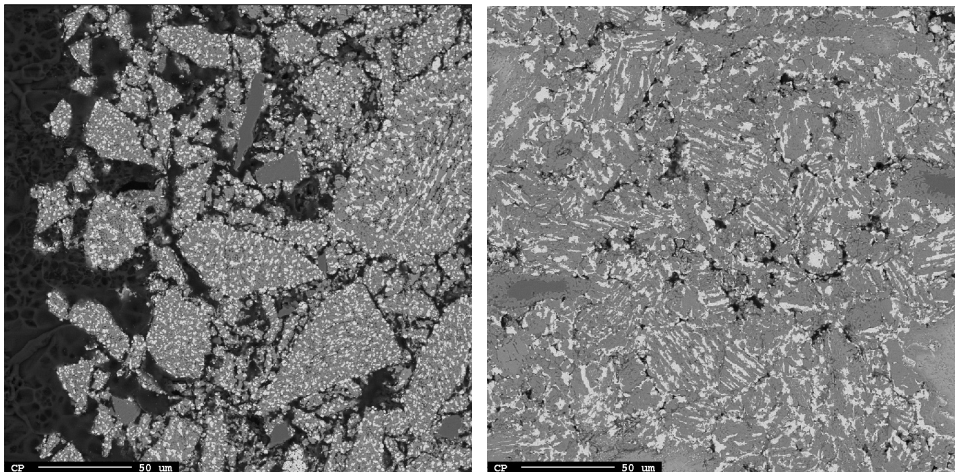

(a) Close to the surface. **(b)** At the pellet center.

Figure 4.9: Microstructure of pre-oxidized pellets from 2011 reduced with H_2 for 45 minutes. The image is taken at the surface with 400 times magnification.

A comparison between an area at the surface and at the center for pre-oxidized pellets reduced with H_2 is given in Figure 4.9. At the surface all grains are completely reduced with small spherical shaped iron nuclei both at the surface and in the grains. No coherent layer of iron is found on the grain surface. Inside the largest grains some of the iron nuclei are lamella shaped.

Another observation is that equal amount of iron is present in the center of the pellets reduced with H_2 compared to the surface of pre-oxidized pellets from 2011 reduced with CO. These iron nuclei found at the pellet center is larger and a higher fraction are lamella shaped, compared to the nuclei on the surface of the pellet. Many of the grains are also partly covered with an iron layer. It is hard to determine where one grain ends and the next begins, which indicates that sintering may occur. In the periphery of the image two grains with a grey and a dark grey phase are found. The dark colour indicates impurities, for instance silicate. Down to the right another grey coloured phase in a large grain is found, which is most likely ”unreduced ilmenite”.

When the gas flow of H_2 increases some changes occur. The size of the iron nuclei grows bigger as the gas flow rises from 7 to 9 Nl/min, while nothing

happens by increasing from 4.8 to 7 Nl/min. At the center of the pellet the amount of iron increases when the gas flow is changed from 4.8 to 7 Nl/min, while the effect of purging even more gas through is limited.

For larger pellets the microstructure for sample b4.8CO10-12.5 was similar to the normal sized pellets reduced with CO. Compared to those pellets reduction of sample b4.8CO10-12.5 ended closer to the surface. Towards the core less metallic iron is found. The microstructure at the core for sample b5CO12.5+ after finalized reduction are similar to the samples reduced with H_2. At the surface much of the grain boundaries are covered with iron. Compared to samples reduced with only CO, lamella shaped iron is also present in the core of the grains. The iron nuclei formed in the bigger pellets are larger compared to the samples reduced with H_2.

4.5.2 Point analysis

The chemical distribution within the iron nuclei close to the surface of two pellets from sample b7H2 is given in Table 4.3. It can be seen that the iron phase is capable of dissolving from 4.5 to 4.9 at.% Ti and 0.2 at.% Mg. Minor amount of other oxides are also dissolved into the iron lattice. The analysis also indicates that 5-6 at.% O is found in the iron phase. From the extreme values most scattering is found with O, where the values range from 3 to 9 at.%, the Ti content also varies between 3.7 and 5.8 at.%. Values of Fe are stable with the exception for one low value.

Table 4.3: Average and extreme values based on 7 point analysis from the surface of two pellets from sample b7H2. Values in at.%. The sum of all elements normalized to 100 %.

Grain	Si	O	Mn	Ti	Mg	Fe
1	0.10	5.13	0.03	4.92	0.22	89.60
2	0.01	6.14	0.01	4.46	0.22	89.15
Minimum	0.00	3.12	0.00	3.74	0.01	85.93
Maximum	0.29	9.07	0.06	5.81	0.39	92.36

4.5.3 Line scan

Line scans are presented to give information about the relative change in content of O across the pellet. This gives information about the extent of reduction, from the surface to the core.

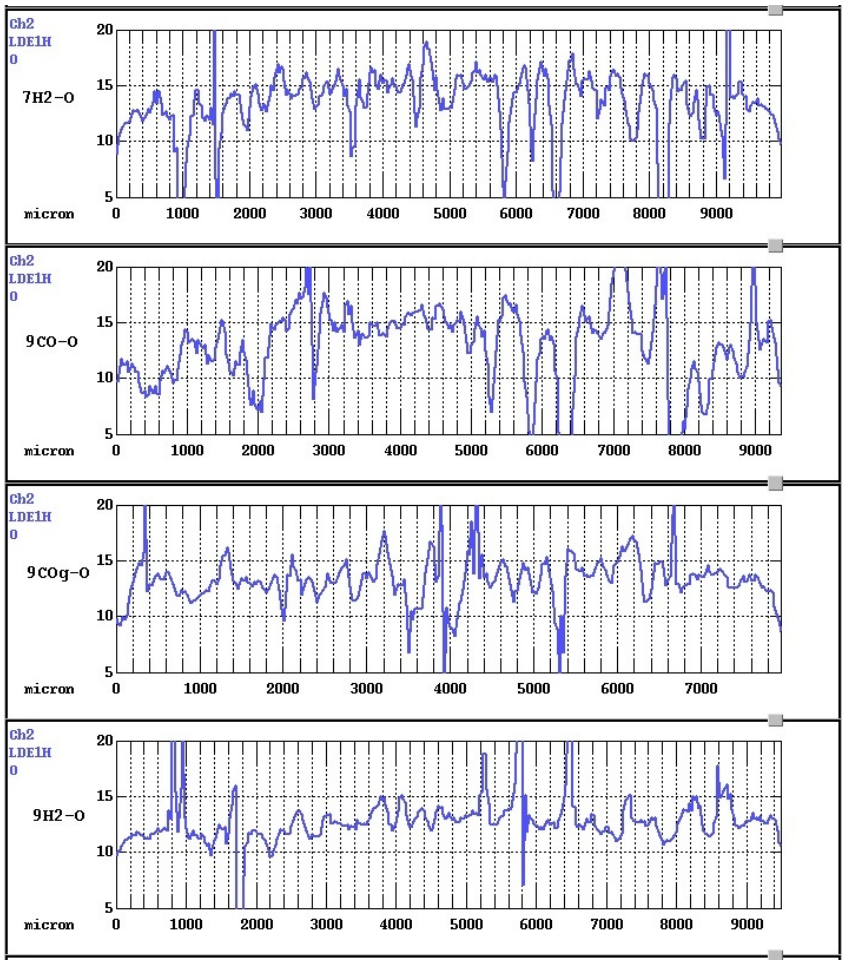

Figure 4.10: Line scan across the pellet, from surface to surface for the samples b7H_2, b9CO, b9CO.old and b9H_2. The scan indicates changes in amount of O. The y axes only indicates relative amount of oxygen.

The length of the line scan is the same as the pellet diameter. From the line scan in figure 4.10 it can be seen that the amount of O increases from the surface towards the core of the pellets. This trend is more visible with the use of H_2 compared to

CO. For all pellets the change in content O is largest close to the surface, but peaks and drops in the scans makes it difficult to decide which of the samples is more reduced. Information about extent of reduction is hard to interpret.

4.5.4 Mapping

This subsection gives information about the element distribution on both macro scale and on the scale of individual grains. This can further be used to understand the difference in conversion for the various samples. Element distribution on macro scale is affected by the chemical composition within the grains. This subsection will therefore begin with mapping of grains.

Unreduced grains

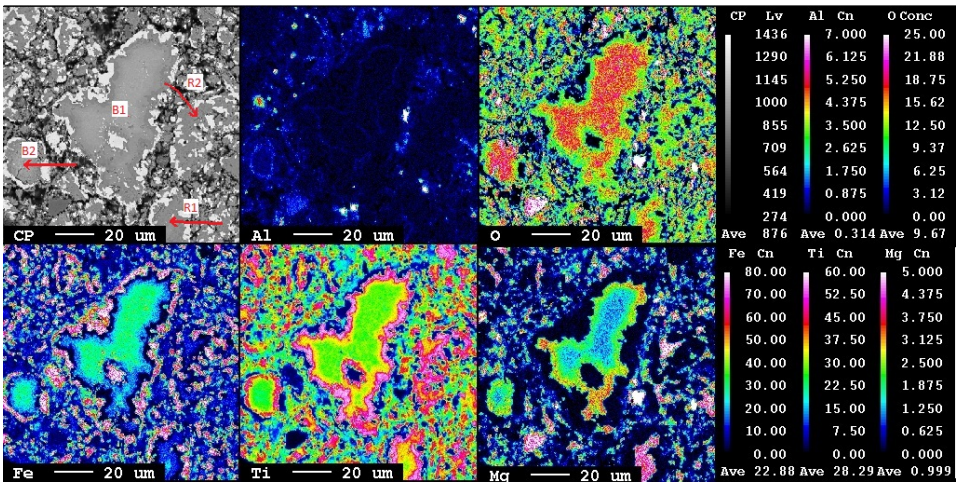

Figure 4.11: Mapping of a pellet from sample b9CO, revealing the barrier effect. The image is taken close to the surface at 200 times magnification.

The mapping in Figure 4.11 covers several grains of various sizes in a pellet from sample b9CO. The Focus is on the 4 grains which are marked. For the similar grains B1 and B2 the surface is almost covered with a thick layer of iron. Holes in the iron layer are observed especially for grain B2. At the core of grain B1 a large iron particle is observed. Underneath the outer iron layer, an equally thick titania shell is revealed. The rest of the grain consists of mediocre values of Fe and Ti and high O content. This indicates that reduction has halted and the core consists of ”unreduced ilmenite”. Another observation is that the outer part of this unreduced layer is enriched in Mg and Al, while the concentration decreases

towards the core. For both of these grains almost all of the Al is concentrated in a thin layer where the reduction of ilmenite ceases. This was not observed in the study by Jørstad (2010), where no Al was observed in the reduced grains halted by the barrier effect.

From the image generated from back scattered electrons up to the left, grain B2 and R1 look the same. Metallic iron is covering most of the outer surface, followed by an inner shell of titania and a thin layer of aluminum. Compared to B2, almost no Fe is present inside the titania layer for grain R1. Only minor amount is left at the center of the grain. The amount of O is lower while amount of Mg is higher inside R1 and all of the Mg is evenly distributed within the titania layer.

Grain R2 is different compared to the other grains. Iron is present in many spherical nuclei outside and some smaller nuclei inside the grain instead of as a thick shell. The rest of the grain is divided between areas of titania and some areas with oxides based on Ti and Mg. The total content of Al and O, and amount of ”unreduced ilmenite” in R2 is lower compared to the other grains.

Similar grains are also observed close to the surface for the samples b4.8CO, b7CO and b5CO10-12.5.

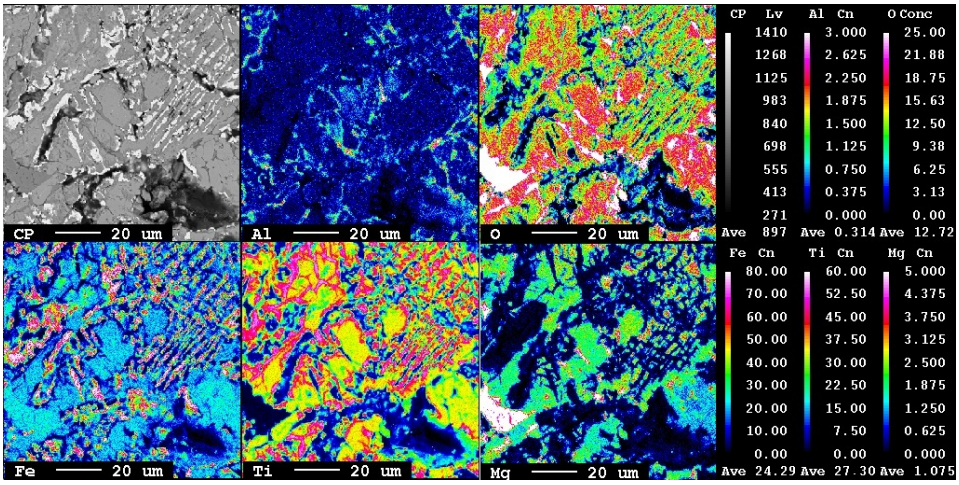

Figure 4.12: Mapping of pellets from sample b7H2. The image is taken 2 mm from the surface at 200 times magnification.

Figure 4.12 visualizes the element distribution within a pellet from sample b7H_2. The image based on backscattered electrons indicates that all grains more or less are in direct connection to each other. In this figure 5 different phases are present.

The white areas close to the surface of the grains are iron nuclei. Grey areas are present within the layer of iron and in the upper left part of the figure. This phase consists of high values of Ti with very little Fe, Al and Mg, also the O content is relatively low. The composition indicates that this is titanium oxide. The largest fraction of the grains are coloured light grey, they consists of mediocre values of Ti, Fe and Mg, and a large fraction of O. This is most likely ”unreduced ilmenite”. Grey areas also exist inside the grain in the lower right part of the backscatter image. The content of Mg and O is high, some Al and Fe is present while the amount of Ti is very low. This is therefore not titanium oxide, but probably agglomeration of impurities. Down to the left in the backscatter image a dark grey grain is found. This phase contains average values of Fe, no Ti and high amount of both Mg and O. This is most likely an impurity grain with high amount of Fe.

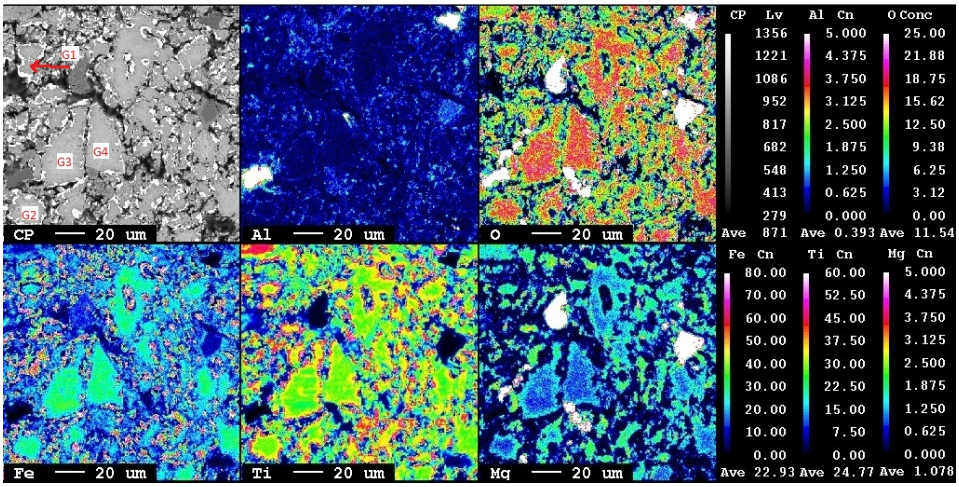

Figure 4.13: Mapping of pellets from sample b9CO. The image is taken 0.6 mm from the surface at 200 times magnification.

Figure 4.13 is a mapping of a pellet from sample b9CO. A general observation is that this area of the pellet is less reduced compared to the area in Figure 4.11, and the focus is given to the grains G1 to G4. The most highly reduced grain among these is G1. The surface of the grain is covered with a layer of metallic iron. Within a layer of titanium oxide is found. Small amount of Mg, but no Fe, is also present within this layer. In the core of the grain medium values of Fe, Ti and Mg are found, and the phase is high in O. This is therefore most likely ”unreduced ilmenite”.

For the three grains G2, G3 and G4 smaller amount of Fe is found on the surface compared to grain G1. The precipitated iron is found as separate nuclei stretched

along the pellet surface. Within the iron phase a thin and non coherent titania layer without Fe is present. The rest of the grain consist of average values of Fe and Ti, high amount of O and small amounts of Mg are concentrated in a shell towards the outer part of the unreduced core. The core of the grain is almost depleted in Mg. Al is also enriched in the transition between the titania layer and the unreduced part of the grain, which by far is the largest fraction of the grain.

Concentration gradients on pellet scale

The element distribution on a macro scale is best visualized by mapping of larger parts of the pellet. This can be seen in Figure 4.14.

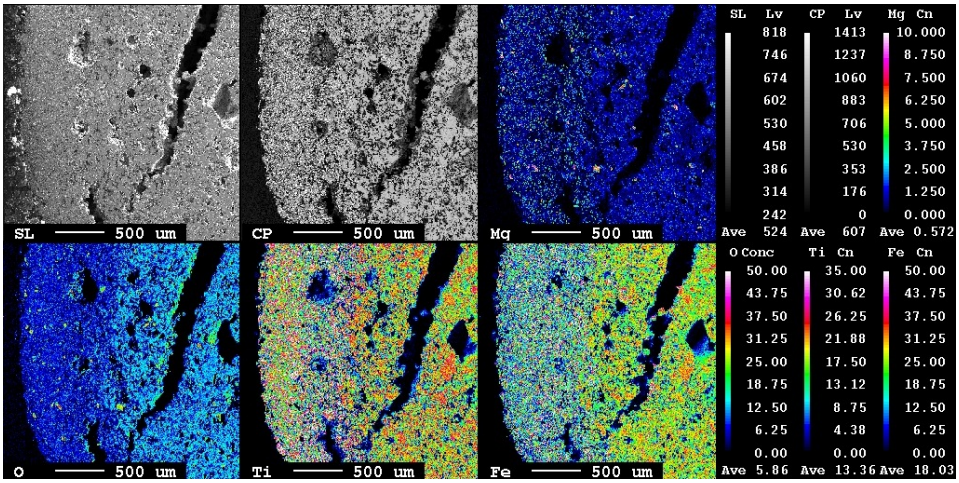

Figure 4.14: Mapping of a pellet from sample b9CO. The image is taken at the surface at 40 times magnification.

From this figure two general observations are made. Reduction stopped 0.8-1.0 mm from the surface and the pellet were full of flaws, holes and cracks. The fraction of white areas in the backscatter image diminishes gradually, and 1 mm from the surface few areas with Fe exists. The elemental distribution of O and Fe indicates an abrupt shift in reduction. The outer 0.8-1 mm of the pellet has a lower content of O and Fe, and then the amount of these elements element rises and remains constant towards the core of the pellet. From the mapping in Figure 4.14 no change in concentration is found in the outer part of the pellet. With regarding to titanium, the outer 0.4 mm of the pellet has a concentration slightly lower than what is found in the core, but the lowest concentration is found between these layers.

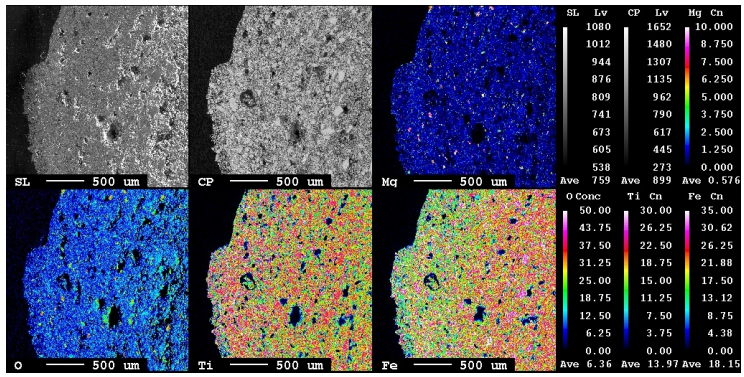

(a) Pellet from sample g7CO. No concentration gradient.

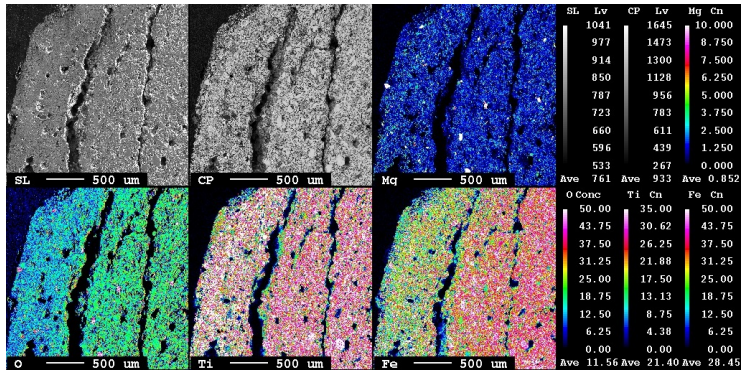

(b) Pellet from sample b4.8CO. Concentration gradient

Figure 4.15: Mapping of pellets, with emphasize on the elements Fe, O, Ti and Mg. The image is at the surface at 40 times magnification.

Figure 4.15 is given to visualize the difference between pellets without a concentration gradient and pellets were the concentration changes from the surface towards the center. Degree of porousity changes between the two pellets. Green pellets are dense, while the pre-oxidized pellets is turned into a multilayer pellet with cracks separating different shells. The outer shell is 0.6-0.7 mm thick, and contains less O and Fe compared to the next shell. Amount of O remains more or less the same throughout the second outer shell towards the center. This indicates that reduction stopped in the innermost part of the outer shell. Green pellets contain less O in all parts of the pellet compared to pre-oxidized pellets from 2011. Pellets without a concentration gradient are found in the samples g4.8CO, g7CO, g9CO and b9H2, while for the samples b4.8CO, b9CO and b4.8CO10-12.5 concentration of elements changes from the surface towards the core. No macro scale mapping has been done for the other samples.

4.6 XRD-analysis

Scans for all samples investigated by XRD are interpret and found in Figure 4.16.

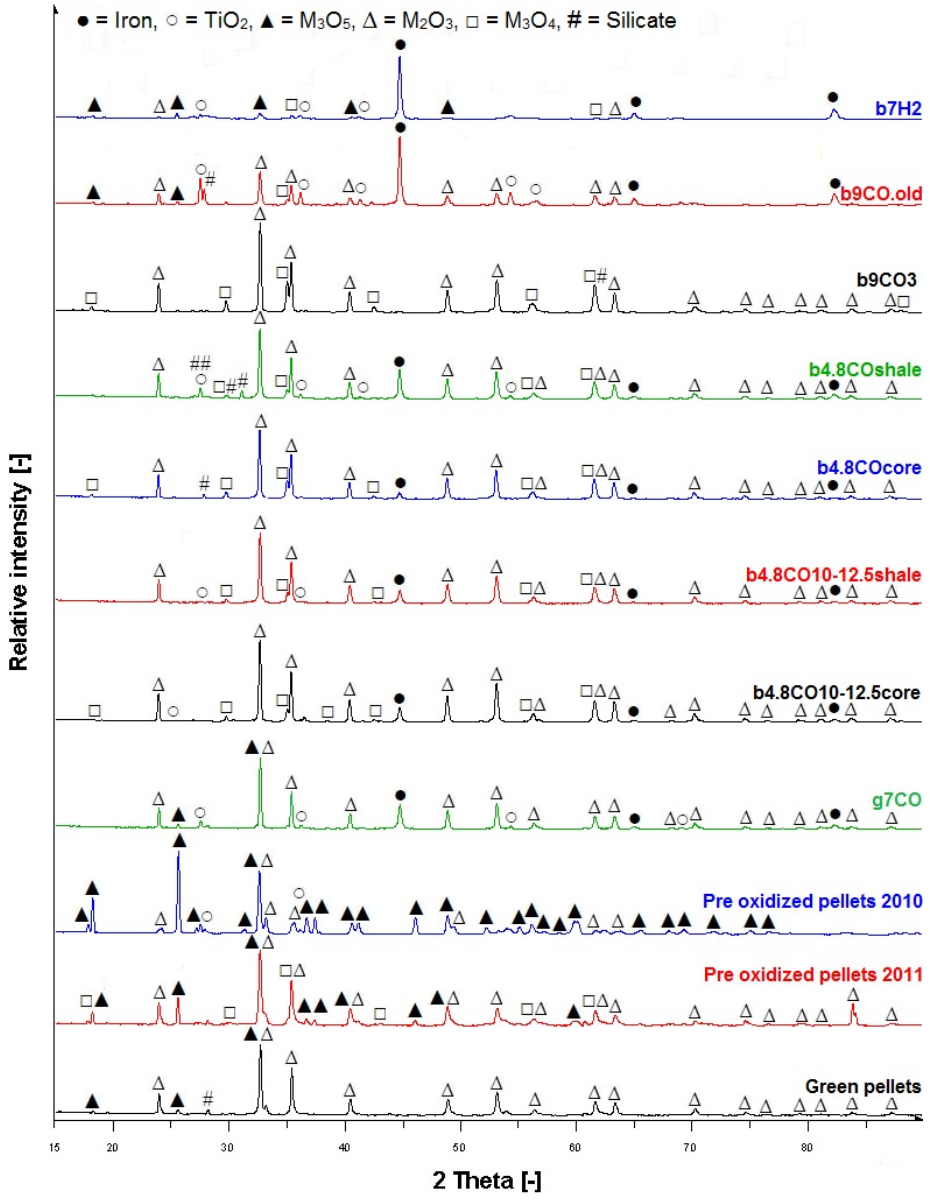

Figure 4.16: XRD scans for different samples in addition to green and pre-oxidized pellets. An interpretation is done to point out what phases are present and give some information about the relative amount in each sample. All peaks are normalized.

Complete scans are given in Figure A.6-A.16 in the Appendix. At the beginning, the raw material, referred to as green pellets, is a mixture of mostly M_2O_3 and some M_3O_5 phase, in addition $MgSiO_3$ might also be present.

When these green pellets are reduced with CO, the amount of M_2O_3 decreases, while more iron and TiO_2 is formed. Compared to the sample with green pellets, the amount of M_3O_5 is slightly decreased, while the phase composition of rutile is unaltered. The content of rutile is higher than the content of M_3O_5 phase.

From the theory the M_2O_3 structure in green pellets will transform into M_3O_5 during oxidizing, this is observed for the pre-oxidized pellets from 2010 which are dominated by a M_3O_5 phase with minor amounts of M_2O_3, in addition some TiO_2 is also present.

Within the normal sized pre-oxidized pellets from 2011 only some of the M_2O_3 phase is oxidized into M_3O_5 phase. A consequence less TiO_2 is present compared to the older pellets. In addition to these phases some M_3O_4 phase also occur. The major phases are M_2O_3 and M_3O_5.

The changes in phase composition after reduction with CO can be understood with the samples b9CO3, b4.8CO and b4.8CO10-12.5 with core and shell. The M_2O_3 phase, M_3O_4 phase, rutile and iron are present in all samples, except sample b9CO3 which lack iron. Within these samples no M_3O_5 phase is found. As more iron and rutile is formed during reduction of these samples, the content of the M_2O_3 phase decreases. Amount of the M_3O_4 phase is less influenced by reduction, but for the most reduced sample b4.8COshell almost no M_3O_4 phase is observed. These samples are best compared by looking at the iron content. Highest content is found in sample b4.8COshell and the lowest amount occurs in sample b4.8COcore, if sample b9CO3 is disregarded. Intermediate and almost equally high amount of iron are found in sample b4.8CO10-12.5, both for core and shell. The XRD scan for the samples b4.8CO, both for shell and core, indicates that protenstatite ($MgSiO_3$) is present.

When sample b7H2 is reduced only traces of the M_2O_3 phase is left. The scan is totally dominated by iron, with smaller and almost equal amount of the three phases M_3O_5, M_3O_4 and rutile. A part from the increase in iron and corresponding loss of M_2O_3 the major difference compared to the samples reduced with 4.8 Nl CO/min is the presence of the M_3O_5 phase. The relative amount of M_3O_4 phase is somewhat reduced and the peak height of rutile is halved compared to sample b4.8COcore.

Amount of iron is only slightly lower for sample b9CO.old than for sample b7H2. While the content of M_2O_3 and rutile is much higher, the relative peak height of

M_3O_5 and M_3O_4 is halved in sample b9CO.old. Wüstite ($Fe_{0.942}O$), Protenstatite ($MgSiO_3$) and aluminum oxide silicate (Al_2SiO_4O) are also likely to be present in this sample.

As mentioned in the theory all of the phases M_2O_3, M_3O_4 and M_3O_5 have a range of compositions caused by high solid solubility of Fe, Mg, Ti, and Mn. Based on the peaks and corresponding angles the M_2O_3 phase consist of ilmenite ($FeTiO_3$). Hematite (Fe_2O_3) is present in the green pellets and the pre-oxidized pellets from 2010 and 2011. The M_3O_5 phase has a composition ranging from ferric pseudobrookite (Fe_2TiO_5) to ferro pseudobrookite ($FeTi_2O_5$). If Mg is dissolved armalcolite ($MgFe_2Ti_3O_{10}$) is formed. The phase composition of the M_3O_4 is basically ulvöspinell ($Fe_{2.25}TiO_{0.75}O_4$) possibly with some additional dissolved Fe and Mg.

5 DISCUSSION

In this section unusual aspects of the experiments and results will be enlightened. The results are interpret in order to point out what the optimum conditions for reduction are. Based on analysis and knowledge from the theory effort will be put to answer what went wrong with the pellets where reduction halted. Recommendations for future work are found at the end.

5.1 Reducibility of ilmenite pellets

The major differences between reduction of green pellets and pre-oxidized pellets from 2010 and 2011 are explained. These pellet types are compared and the results based on values of conversion, degree of metalization and XRF-measurements are interpret. This section will also comment on the effect of changing the reducing atmosphere, pellet size and explain experimental errors.

Based on the results some important observations about the reducibility and reduction behaviour are made:

- Decreasing reduction with increasing pellet size
- Enhanced reduction with pre-oxidized pellets from 2010
- H_2 superior to CO as reducing agent
- Aging might have a minor negative effect on reduction

5.1.1 Decreasing reduction with increasing pellet size

Pre-oxidized pellets with size from 8-10 mm are more easily reduced than larger pellets.

Conversion

Besides the normal sized pellets, larger pellets are also reduced. Initially the values of conversion are the same. Due to lower oxygen removal rates both in the initial and final stage, values of conversion are lower compared to normal sized pellets. This can be explained by different phase composition close to the core of these pellets. Pre-oxidation conditions are similar for all pellets, but smaller pellets have a shorter mean diffusion path compared to larger pellets. This results in a higher degree of oxidation. The diffusion length from the surface towards the reaction interface increases with pellet size. As a result the rate of reaction is

expected to decrease. It can be assumed that the two pellet types have an average size of 9 and 11.25 mm. Therefore the number of pellets per sample is almost doubled for normal pellets. The volume deeper than 0.6 mm into the pellet is less reducible. This corresponds to 65% and 71% for the normal- and oversized samples, respectively. Because of this the oxygen removal rate in both stages are expected to decline. However only the formation of a diffusion impermeable layer on pellet scale can explain why reduction of sample **b4.8CO10-12.5** ceased after 20 minutes. This contradicts previous investigations, and is not found during reduction of pellets larger than 12.5 mm. However, when sample **b5CO12.5+** was reduced with H_2, fast oxygen removal rate was observed even at high values of conversion. The slope of the final stage was almost as steep as the samples reduced with only H_2. This indicates very slow diffusion of CO/CO_2 in these pellets. The rapid weight loss during reduction with H_2 suggest fast diffusion of H_2/H_2O.

Sample **b9CO10-12.5** and sample **b4.8CO12.5+** are also included in the graph with oversized pellets. These experiments were aborted due to gas leakage caused by overpressure after 6 and 3 minutes, respectively. No Ar was used under cooling and some oxidizing of the metallic iron might therefore occur. The influence on conversion and degree of metalization of oxidizing is assumed limited though. The leakage and oxidizing makes the recorded weight and corresponding conversion less reliable compared to the rest of the results. While sample **b4.8CO12.5+** ends with too high value of conversion the development in conversion for sample **b9CO10-12.5+** is similar to that of sample **b4.8CO10-12.5+**. The low value of conversion for sample **b4.8CO10-12.5+** is most likely caused by formation of soot.

Conversion from weight loss, degree of metalization and XRF-analysis

Conversion based on weight measurements, degree of metalization and the XRF-analysis indicates low reducibility with CO for oversized pellets. In order to confirm the trend with conversion, weight measurements should also have been done on the samples **b4.8CO**, **b7CO** and **b9CO**. Measured conversion is high for the sample **b4.8CO10-12.5** and suggest good reduction. By the XRF-analysis low values of iron, TiO_2 and the sum of oxides are found. These results, in addition to low degree of metalization and final conversion from the TGA furnace indicate that reduction stopped early.

The measured value of conversion for sample **b4.8CO12.5+** is lower than the one from the TGA furnace. This confirms the assumption of too high value of conversion based on TGA for this sample. It can also be seen by the low amount

of Iron, TiO_2 and sum of oxides in the XRF-analysis. These values will increase if oxygen is removed, as the total weight of the sample will decrease. XRF-analysis is therefore an indirect measure of reduction. While degree of metalization doubles when reduction time is increased from 3 to 6 minutes, values of conversion remains the same. This indicates that values of conversion for sample **b4.8CO12.5+** is too high. The fact that degree of metalization is doubled does not necessary imply that amount of iron is doubled. Degree of metalization is calibrated for values between 60 and 70 %. For values outside this range an increase in degree of metalization will only tell that amount of iron is higher (Seim, 2010).

5.1.2 Enhanced reduction with pre-oxidized pellets from 2010

Pre-oxidized pellets from 2010 are easier to reduce with CO than pellets from 2011. Green pellets from 2011 obtains higher degree of metalization, but lower values of conversion compared to pre-oxidized pellets from 2011.

Conversion

Pre-oxidation conditions also affects reduction. With 9 Nl CO/min pre-oxidized pellets from 2010 are more reducible than pre-oxidized pellets from 2011. Both initial and final oxygen removal rate are significantly higher for pre-oxidized pellets from 2010. The oxygen removal rate decreases slower for these pellets, as seen in Figure 4.2. Initially values of conversion are lower due to more oxidized pellets. Between 5 and 25 minutes of reduction values of conversion becomes higher for pre-oxidized pellets from 2010.

The two types of pre-oxidized pellets are only compared once, with reduction of 9 Nl CO/min. Lower gas flow of CO might result in better reducibility for pre-oxidized pellets from 2011. When these pellets are reduced with H_2 for 45 minutes values of conversion up to 0.95 are obtained. These are 0.09 higher than the maximal values obtained when pre-oxidized pellets from 2010 were reduced with 3Nl H_2 and 1 Nl CO until reduction stopped. Even with 4.8 NL H_2/min conversion reaches 0.84 at the end of reduction. This indicates that pre-oxidized pellets from 2011, which can be viewed as mildly oxidized green pellets, are easy to reduce with pure H_2. With the use of H_2 these pellets might be easier to reduce than pre-oxidized pellets from 2010. This agrees with Jørstad (2010), where green pellets were more reducible compared to pre-oxidized pellets when the H_2/CO gas ratio increased. Green pellets from 2011 reduced with pure CO results in a steadily decreasing reduction rate, and very low values of conversion compared to the other pellet types. This is probably due to changes in phase

composition and diffusivity of gas both towards and away from the reaction interface (Jørstad, 2010).

From Table 3.1 the chemical composition of the pellet types is about the same. Pre-oxidized pellets from 2011 contains 0.11 wt.% more Al_2O_3 and 0.07 and 0.08 wt.% less MnO and S respectively. Green pellets differ from the two other pellet types by intermediate values of S and Al_2O_3 compared to the two pre-oxidized pellet types. Despite the low amount of these elements, Mn and Al will incorporate into the titanium, iron and oxygen phases and possibly affect the reducibility of grains and pellets. Out of these elements the effect of Mn is most evident. This will therefore increase the reducibility of pre-oxidized pellets from 2011.

Although the iron content in the two pre-oxidized pellet types is the same, differences in degree of oxidation result in twice as much divalent iron present in pre-oxidized pellets from 2011. Less oxygen and more divalent iron will change the phase composition and influence the porousity and number of microcracks inside the pellets. Green pellets are dense, while pre-oxidized pellets from 2010 contain many small cracks without orientations. For pre-oxidized pellets from 2011 large cracks are separating different shells in the pellets. The difference in cracks and oxidation state are most likely caused by different temperatures during pre-oxidation. If the total time of the pre-oxidation is reduced this will also affect oxidation. This is an industrial process with various adjustments, changing flow of material and height of the pellet bed. As these parameters can be changed both temperature and time might be lower during the manufacture of pre-oxidized pellets from 2011 (Elstad et al., 1992).

Pre-oxidized pellets from 2011 contain one third of the amount of C found in pre-oxidized pellets from 2010. This will influence the weight reduction curves, and the graphs with conversion must be corrected for weight loss of carbon. Final values of conversion are 0.03 and 0.08 too high for pre-oxidized pellets from 2011 and 2010, respectively. C will also contribute to reduction, but compared to the flow of reduction gas this can be neglected. Green pellets contains the highest amount of C with 1.5 wt.%. Pre-oxidized pellets have been heated up to 1200 °C under air. The C content is therefore expected to increases towards the centre of the pellet as the most reactive carbon is removed from the surface. This might cause reaction between pellets and C under heating, and especially within the last 15 minutes where the pellets are kept at 900 °C under argon. With green pellets this might contribute to the low values of conversion since one gram of C reacts with 1.5 to 2.7 gram of O. This implies that some of the most accessible O already is removed before reduction begins. The weight measurements are also affected by unknown parameters during heating. This explains the observed

deviation in the weight versus time graph during heating, as can be seen in Figure A.5 in the Appendix. It is therefore impossible to quantify the possible reduction before reduction gas was added. Off gas analysis could have been preformed to quantify the amount of unwanted reduction. Since reduction with C is slower than with CO this is most likely a minor effect.

Conversion from weight loss, degree of metalization and XRF-analysis

The degree of metalization is twice as high for pre-oxidized pellets from 2010 compared the similar pellets from 2011. Values of conversion and the XRF-analysis indicate highest reduction for pre-oxidized pellets from 2011 reduced with H_2. Degree of metalization is highest for pre-oxidized pellets from 2010 reduced with 4 Nl/min of a gas mixture. Pellets from 2011 obtained higher values of conversion than degree of metalization. While the opposite is true for pre-oxidized pellets from 2010, with the exception of sample **b9C0.old**. One explanation for this is that the oxygen bound to titanium in pre-oxidized pellets from 2011 are more easily removed compared to the pellets from 2010. Even though a lot of oxygen is removed much of the iron can still be in the divalent state. Opposite to conversion and the amounts from the XRF-analysis, degree of metalization is higher for green pellets than for pre-oxidized pellets from 2011 reduced with CO. This supports the assumption of some reduction before CO was added.

Microstructure

When the images of microstructure from pre-oxidized pellets from 2010 and 2011 are compared, the amount of nucleated iron is the same close to the surface. Towards the core of the pellets the amount of iron is higher in the pellets from 2010. Close to the surface more iron is nucleated inside the grains for pre-oxidized pellets from 2010. In addition no ”unreduced ilmenite” grains are found in these pellets. Amount of iron close to the core is also higher. This indicates that pre-oxidized pellets from 2010 are more easily reduced with CO than pre-oxidized pellets from 2011 (Jørstad, 2010).

Larger differences are found between the two pellet types from 2011. In the green pellets smaller and more lamella like nuclei are found. The total amount of iron is lower compared to the pre-oxidized sample, and the grain surface is not covered with an iron shell. This indicates that green pellets are less reducible compared to pre-oxidized pellets. Based on the microstructure, reduction of green pellets is not inhibited by formation of a dense iron layer at the surface. The presence of

iron nuclei inside the grains indicates higher diffusion within green pellets than in pre-oxidized pellets. The fact that the total amount of iron is lower after reduction of green pellets indicate that these pellets contains less reducible phases, or that diffusion through these phases are more challenging than through the phases present in pre-oxidized pellets.

Iron lamellas were found in green pellets but rarely in pre-oxidized pellets. This can be explained by iron formation on previous hematite lamellas. The reason for this is probably because hematite is more rapidly reduced than ilmenite. In addition the migration of iron from the reaction interface towards the lamellas might be favourable. Green pellets is oversaturated with iron and therefore hematite lamellas are present between the ilmenite phases. During pre-oxidation most of the hematite is dissolved into new phases, and therefore a random nucleation of iron is observed.

Another difference between the pellet types is the cavities. This can be explained by pellet processing. Green pellets contain water and binder, when this evaporates and reacts during pre-oxidation cavities are created. These cavities are most likely created during oxidation, by thermal expansion caused by temperature gradients or phase transformations.

5.1.3 H_2 superior to CO as reducing agent

All analysis conclude that final reduction is enhanced by the use of H_2. Oxygen removal rate is higher through the whole experiment when H_2 is used compared to CO.

Conversion, degree of metalization and XRF-analysis

Values of conversion and degree of metalization are also affected by the gas composition used under reduction of pre-oxidized pellets from 2011. This can be seen in Figure 4.1 and 4.3. Final values of conversion are c. 0.4 higher for the samples reduced with H_2 compared to the samples reduced with CO, while the degree of metalization is 27- 64 % higher. The XRF-analysis confirms higher reducibility with H_2. The difference in values of conversion increases with time. The slopes of the initial and final stage under reduction with H_2 are about twice as steep compared to CO. Reduction of sample **b5CO12.5+** reveals the difference between H_2 and CO. Conversion from TGA reached 0.31 after 45 minutes of CO reduction. After additional 45 minutes with H_2 the value of conversion ended at 0.76. Even though the most accessible O was removed initially, the oxygen removal rates were higher with H_2. This means that under these conditions,

reduction are favoured by the use of H_2 compared to CO. This is in agreement with the theory that H_2 has higher reduction potential than CO above 812 °C. Diffusivities are also higher. Reduction with CO gives a higher number of active spots for reaction compared to H_2 (Kolbeinsen, 2011), but since reactions with CO generally are slower the total effect on reduction depends on grain properties.

Gas mixtures also proved more efficient than pure CO to reduce pre-oxidized pellets from 2010. When the initial stage ends values of conversion are higher after reduction with 4 Nl/min of a gas mixture compared to 9 Nl/min of pure CO. This agrees with the result on pre-oxidized pellets from 2011 where values of conversion almost doubled by the use of H_2 instead of CO. Data from degree of metalization and XRF-analysis points in the same direction. The high values of conversion obtained with low amount of reduction gas can be explained by the apparent high reactivity of H_2. There might also be synergy effects in relation to the water gas shift reaction that is enhancing the reaction.

Microstructure

The largest difference in microstructure is found between pellets reduced with CO and H_2. Iron is evenly distributed across grains after reduction with H_2. These iron nucleus are small, and do not cover the grain surface. Close to the centre of the pellet, larger iron nuclei are found, both at grain boundaries and inside the grains as lamellas. The amount of iron is the same across the whole pellet. This suggest that the pellets are much more reducible by the use of H_2 compared to CO. The phases present inside the pellets are the same and the reducing potential is high enough for the reduction of these phases. This means that the differences are related to gas diffusion towards both the pellet centre and reaction interface. These investigations can not tell whether the diffusivity of product or reactant gas is the limiting factor.

5.1.4 Aging might have a minor negative effect on reduction

Fresh pellets is easier to reduce than pellets stored for 165 more days, although the difference is limited.

Conversion and degree of metalization

In Figure 4.6 values of conversion remains the same if the experiment is repeated after 165 days. Degree of metalization is 5 % higher for the older sample. The experimental error is expected to be larger for the metalization testing than for the

values of conversion since only a fraction of the sample is tested. In the case where the tested part of the sample contains the most reduced pellets, higher degree of metalization will be obtained. If two different persons carried out the testing of sample **b3.18d** and sample **b3.183d**, this can also contribute to the general uncertainty. In addition phase transformation is slow at room temperature, much more than half a year is needed to change phase composition. In spite of the uncertainty and slow phase transformation, both conversion and degree of metalization are slightly higher for the older sample. The same trend is found in the XRF-analysis. This indicates that aging can result in a minor decrease in reducibility. However only one experiment is carried out to test this hypothesis, to conclude more samples needs to be tested.

5.2 Abnormal behaviour, what went wrong?

Based on interpretation of the results and some further observations this section will emphasize on explaining the abnormal behaviour during reduction. Two main observations are done:

- Decreasing reduction with increasing gas flow
- Two stage reduction with a sharp bend

5.2.1 Decreasing reduction with increasing gas flow

When pellets are reduced with CO, 7 Nl/min is the optimum gas flow. Higher gas flow result in lower reduction. Reduction with H_2 is enhanced by increasing the flow rate and highest reduction is obtained with a gas flow of 9 Nl H_2/min.

Conversion

For all pellet types lower values of conversion are obtained with 9 Nl/min compared to 4.8 and 7 Nl/min. For sample **b9CO** lower values of conversion are obtained because the initial stage ends to early compare to what is observed with lower gas flow. The slope of the final stage is more or less the same for 7 and 9 Nl/min and somewhat lower with 4.8 Nl/min. This indicates that gas diffusion controls the reaction at gas flows of 7 Nl/min or higher. With lower gas flow, reaction is slowed down by limited supply of reduction gas. When green pellets are reduced there is no final stage, but a gradual decreasing reaction rate. For these pellets higher values of conversion are obtained by the use of 7 Nl/min compared to the use of 9 Nl CO/min. The difference increases gradually with time. This has no natural cause and is left unexplained. For the calculated

conversion based on weight loss measurements this trend is more unclear. For green pellets, the values of conversion is almost unaffected by changing gas flow. Highest value is found with 4.8 Nl/min. With H_2 the two values of conversion based on TGA and weight measurements are the same for 4.8 and 7 Nl/min, but with 9 NL the value of conversion from weight measurements are 0.17 higher. The large deviation indicates that the values of conversion from TGA is too low and the corresponding values from weight measurements too high. For sample **b9H2** nothing unusual occurred during pre-heating and reduction, but the first 10 minutes of cooling proceeded without Ar. This will not affect the values of conversion from TGA furnace. Since H_2 is surrounding the pellets and not flushed away after the flow of H_2 ceased, some further reduction is possible. The volume and moles of H_2 are limited and reduction with H_2 is very temperature dependent. Only 9 mole% of the gas can be utilized at 900 °C. At 800 °C reduction stops if the off gass contains more than 5 % water. This can therefore only partly explain the higher values for conversion from weight loss measurements.

Metalization

Degree of metalization confirmed that 7 Nl CO/min is the optimum gas flow. Compared to the values of conversion higher gas flow resulted in better metalization than low gas flow. When H_2 was used as reducing agent degree of metalization grew with increasing gas flow. This contradicts the result based on values of conversion. The increase in degree of metalization was 34 % when the gas flow increased from 4.8 to 7 Nl/min, but only 6% when the gas flow was raised to 9 Nl/min. Even though the increase in metallic iron might be less than these numbers indicates, it is significant. This is also expected since reduction will proceed faster and at a higher extent when more reduction gas is added. The only demand is that the gas reaches the reaction interface.

XRF-analysis

The XRF-analysis confirms that a gas flow of 7 Nl CO/min is optimal. Higher values of iron, TiO_2 and the sum of all elements are present after a gas flow of 9 Nl/min compared to 4.8 Nl/min. When H_2 is the reducing agent highest values were obtained with 9 Nl H_2/min. These values are only slightly higher than the values obtained with 4.8 Nl H_2/min. Lowest values are obtained with a gas flow of 7 Nl/min. The latter result has no natural explanation, but some of it might be explained by uncertainties in the XRF-analysis. The XRF-analysis is similar for all the samples, making it harder to interpret the results. When comparing the

different ways of measuring reduction, the XRF-analysis is regarded as the most uncertain.

Microstructure

With increasing gas flow no change was observed with green pellets from 2011. This supports the previous results. The same amount of iron is present after reduction by CO on pre-oxidized pellets from 2011. With a gas flow of 4.8 or 7 Nl/min iron was nucleated within the grains. At the highest gas flow few iron nuclei were observed inside the grains. Only two pellets per sample were examined. These observations can be accounted for by the random choice of pellets and the fact that these results are based on a subjective interpretation, no other explanation is found. With a gas flow of 7 and 9 Nl/min most of the largest grains were almost covered with a layer of metallic iron. The rest of these grains mostly consist of a light grey phase. Few such grains were observed with the lowest gas flow. This light grey phase is identified as ”unreduced ilmenite”, see Section 5.3 Mapping. This indicates that the layer of iron is baffling the reduction, or that iron accumulates on the grain boundary after reduction ceased. Why this happened with the two highest gas flows can not be explained. If the amount of ”unreduced ilmenite” grains is largest with the highest gas flow this can explain the lower values of conversion and degree of metalization when the gas flow was increased from 7 Nl/min. This explanation fails to account for the increased reduction when gas flow was raised from 4.8 to 7 Nl/min. Unfortunately no better explanation is found.

Reduction with H_2 proceeded as expected. When the gas flow was raised from 4.8 to 7 Nl/min, the amount of iron at the centre of the pellet increased. A further increase from 7 to 9 Nl/min was followed by a growth of the iron nucleus close to the surface. Both can be explained by enhanced reduction which verifies the results based on degree of metalization, but disagrees with values of conversion and the XRF-analysis.

Line scan

To reveal variations in reducibility between different samples line scans were performed. A clear trend only occurred with the samples reduced with H_2. For the other samples too many peaks and drops made the result hard to interpret. These are most likely caused by cracks and cavities within the pellet. The trend for the two samples reduced with H_2 is that the lowest amount of oxygen was observed with a gas flow of 9 Nl/min compared to 7 Nl/min. The problem with this analysis

is related to large scattering in the results. It is also hard to choose a representative pellet and line to analyze. These results are therefore not very reliable.

5.2.2 Two stage reduction with a sharp bend

For all experiments with pre-oxidized pellets reduction proceeds in two stages separated by a sharp bend. The oxygen removal rate is constant within each stage. First an initial fast rate followed by a ten times slower final rate.

Conversion

For reduction of pre-oxidized pellets from 2011 a sharp bend in the conversion curves is observed both with CO, H_2 and regardless the pellet size. The same bend is also observed when pre-oxidized pellets from 2010 are reduced with 9 Nl/min of CO. No similar graphs are found in the literature. Typical behaviour is steadily decreasing oxygen removal rate as found with pre-oxidized pellets from 2010 (Jørstad, 2010). This abnormal behaviour can be explained by phase composition, gas diffusion and pellet properties as porousity and microcracks. This will be further enlightened below.

Reduction of pre-oxidized ilmenite pellets from 2011 results in two distinct oxygen removal rates. The initial stage of reduction finishes with a value of conversion around 0.33. This can be explained by the difference in valence state of iron. At the beginning iron is present as both Fe^{3+} and Fe^{2+}, then Fe^{3+} is reduced to Fe^{2+}. When all iron is reduced to Fe^{2+} the value of conversion will reach 0.33. This is based on the assumption that no metallic iron is formed before all trivalent iron is reduced to divalent iron. For all samples reduced during the work on this master thesis the first stage ends at a value of conversion between 0.24 and 0.40.

A value of conversion lower than 0.33 indicates that Fe^{3+} is trapped inside the pellets. Trivalent iron is most likely present in the core of grains or close to the pellet centre. Unreduced grains can be explained by the barrier effect, grain properties, like phase compositions and porousity, or formation of a dense layer of iron. Slow migration of gas is a more probable cause if the core of the pellet remains unreduced. This will be thoroughly commented on later.

Two of the values of conversion after the initial stage exceeds 0.33, and both from the samples reduced with H_2. This is probably caused by simultaneously reduction of divalent and trivalent iron. Because chemical reactions with divalent iron occur in the initial stage, this indicates that gas diffusion inside the pellet is limiting the reduction. Both for reduction with 4.8 and 7 Nl H_2/min the initial

value of conversion ends at 0.40. The reason oxygen removal rate slows down at this point can be explained by reaction products halting the gas diffusion or by completely reduction of the most easily reducible phases. Since the same pellets are used, only the former explanation can account for the low value of conversion obtained after reduction with 9 Nl/min. Still, the fact that higher flow of reduction gas gives lower values of conversion lack a natural explanation and contradicts what is generally accepted in the literature.

Degree of metalization

Degree of metalization increases only 1 % when reduction is extended for 7 additional minutes. A small increase in metalization is expected since the reduction rate in the initial stage is about ten times higher than in the next stage. But the degree of metalization after the initial stage is higher than expected. Ideally all iron is in the divalent state after the initial stage. Some iron will be reduced out, but the fact that 6 % of the iron is in metallic form can only be explained by an error in the metalization test.

XRF-analysis

While conversion and degree of metalization both increases with increased reduction from 3 to 10 minutes, the XRF-analysis reveal that the amount of all elements remains the same. Total amount of iron actually decreased. Some variation between the chemical compositions in different pellets will occur, and there are also uncertainties in the XRF-analysis. This can to some extent explain the low values from the XRF-analysis for sample **b9CO10** compared to sample **b9CO3**.

Microstructure

When CO was used as reducing agent the effect of increasing time was also studied. Only some iron occurred at the pellet surface after 3 minutes of reduction. This can be explained by the fact that trivalent iron is easier to reduce than divalent iron. If trivalent iron is present, this will be reduced first. The diffusivity and migration of CO varies within both pellets and grains. Depending on this, CO might reach the core of the pellet before it reaches the reaction interface of the largest grains close to the surface. Because the amount of CO is high at the surface some reduction of divalent iron is expected.

After 10 minutes of reduction more iron is observed evenly distributed within the area closest to the surface. The total amount of iron is higher, but not the content close to the surface. This confirms the increase in degree of metalization. Somewhere between 3 and 10 minutes of reduction values of conversion reaches 0.33. These values of conversion and the limited amount of iron present indicate that all trivalent iron is removed after 10 minutes. This requires CO migration towards the core. If the assumption of trivalent iron is wrong, then this implies that both values of conversion are wrong or that reduction of tetravalent titanium occurs.

Even though the amount of CO is high close to the surface, little iron is nucleated. This indicates that reduction of divalent iron is slow. One explanation for this is slow diffusion of CO from the grain boundary to the reaction interface or slow diffusion of CO_2 back towards the surface.

5.3 Mapping

The mapping of the pellets and grains give an overview of the element distribution. This may help to understand the limited reduction and why it halted. It must be kept in mind that these results are based on investigations of one or two pellets from each sample, therefore these pellets might deviate from the ideal pellet representing the sample.

5.3.1 Grains with barrier effect

The barrier effect is present in pre-oxidized pellets from 2011 and is one of the reasons for the low reducibility.

Some of the limited reduction can be explained by the unreduced grains observed in Figure 4.11 and 4.13. In the image generated from back scattered electrons the contrast depends on the mean atomic number. The mean atomic numbers and oxygen content for several phases and elements in the ilmenite system are given in table 5.1.

Table 5.1: Overview of mean Z values and oxygen content for different phases and element in the ilmenite system.

Phase	Mg	TiO_2	Ti_3O_5	Ti_2O_3	$FeTi_2O_5$	Fe_2TiO_5	$FeTiO_3$	$Fe_{2.25}Ti_{0.75}O_4$	Fe
Mean Z value [-]	12.0	12.7	13.3	13.6	13.8	14.3	14.4	15.3	26.0
O content [at.%]	-	33.3	62.5	60	62.5	62.5	60	57.1	-

Based on the table of average mean atomic number and the elemental mapping, white areas must contain the heaviest phase which is metallic iron. This is also confirmed by the high count rate of Fe and low or no signal of other elements. However this does not rule out the possibility for some solid solution of other elements. Within the iron layer, the area is coloured grey, while the innermost part of the largest grains are whiter, thus contain a phase with larger mean atomic number.

The darker phase contains no Fe, Mg and Al average values of O and high concentration of Ti. This is likely to be a titanium oxide. The relative low oxygen content indicates that it is TiO_2. Since no point analysis was carried out on this phase the possibility of some reduced rutile can not be ruled out.

The brighter phase closest to the core contains mediocre values of Fe, Ti and high values of O. Some Mg and Al are also present. This is therefore ”unreduced ilmenite”. Other possible phases are pseudobrookite or ulvöspinell. Within all phases impurities like Mg are dissolved as solid solution. To be able to reveal the exact composition of this phase point analysis is required.

Mapping can also be used to explain why some grains are completely reduced while large parts of other grains contain ”unreduced ilmenite”. Common for the grains with ”unreduced ilmenite” is the presence of an almost coherent shell of metallic iron and a shell of titanium oxide within. The rest of the grain is ”unreduced ilmenite”, but the outer part of this phase is enriched with some elements from the grain. Both Mg and Al have migrated towards the reaction interface where reduction halted. The grain size is typically 20 μm or larger. There is no reason for impurity elements to migrate from the outer part to the surface of the unreduced phase. These high values of impurities at the interface are therefore most likely due to accumulation in front of where the reaction take place. This will limit the reduction and the result is the barrier effect. Since the concentration of Al and Mg is highest where the reduction stopped this indicates that the unreduced grains are caused by the barrier effect.

Although some grains have higher amount of impurities, the barrier effect can be less pronounced. Grain R1 and B2 in Figure 4.11 are similar except for a higher amount of Mg in grain R1. In spite of this, a larger fraction of ”unreduced ilmenite” is present in grain B2. One possible explanation for this can be variations in phase composition between the grains. This suggests higher reactivity and diffusion of gas in grain R1 than in grain B2.

Common for completely reduced grains are the presence of more iron inside the grains than on the surface. One interesting issue regarding this is whether the presence of an iron shell is limiting the reduction or a result of baffled reduction.

If a large part of the surface is covered with iron this might limit diffusion and contribute to the low reducibility. Migration of iron towards the surface can also be viewed as an indication of hampered reduction. If the growth of iron nucleus inside the grains is stopped, this iron might migrate towards the surface if this is energetically favourable.

No barrier effect or grains covered with an iron shell were observed when H_2 replaced CO. In addition to iron, TiO_2 and ”unreduced ilmenite”, some grains with impurities are found. Concentration of Mg, O, Al is high and some Fe is also present. To reveal correct phase composition point analysis is required. The iron content entrapped inside the grains 2 mm from the surface is lower compared to grains at the surface reduced with CO. This also indicates that H_2 is better than CO for ilmenite reduction. It is also difficult to point out where one grain ends and the next one begins. This can be explained as early sintering. The temperature is similar, but it is harder to determine where grain boundaries are after reduction with H_2 compared to CO. This might be caused by more reduction with H_2 and some volume expansion during reduction. If this is true it indicates different phase composition closer to the core than on the surface since no expansion is observed closer to the surface.

No sintering was observed 0.6 mm from the surface after reduction with CO, and only small grains and the surface of larger grains are reduced. Total amount of iron is relatively low as the largest fraction of the grains remains unreduced. Also here iron agglomerates on the surface of the grains and the reaction interface is enriched in impurities. This looks like an early stage of the barrier effect. The large fraction of ”unreduced ilmenite” phases are most likely due to the limited diffusion of CO/CO_2.

5.3.2 Concentration gradients in the outer parts of the pellets

Reduction stopped 0.6-1.0 mm from the surface when pre-oxidized pellets from 2011 were reduced with CO. No iron metal was formed within this border. For green pellets and pellets reduced with H_2 the change in oxygen content is more gradual.

After reduction by CO on pre-oxidized pellets from 2011 mapping of the outer 2x2 mm^2 of the pellets was carried out. This was done to reveal differences in concentration between elements from the surface and towards the core of the pellets. An abrupt change is observed 0.6-1.0 mm from the surface. Closer to the core concentrations remain unchanged. Amount of O and Fe decreased while the content of Ti was higher close to the surface. The loss of oxygen will result in

increased values of Ti and Fe close to the surface, but there is no reason for decreased concentration of Fe close to the surface. This can partly be explained by bad interpretation of the mapping. Sample curvature, cavities and properties of the elements will also affect in what degree mapping gives representative data for the sample. Since the concentration remains the same in the unreduced part of the grain, migration of Fe from the surface towards the core also fails to explain the lower amount of Fe in the reduced zone near the surface.

The abrupt change in concentration and lack of iron nucleus closer to the core indicates that reduction stopped. The fact that only the outer 1 mm of the pellet is reduced after 45 minutes confirms the theory of slow diffusion of CO/CO_2. The thickness of this outer shell is not significant larger with a gas flow of 9 Nl/min compared to 4.8 Nl/min. This might explain why the effect of increasing the gas flow is limiting. There is sufficient gas present at the surface, but migration towards the reaction interface is too time consuming. Due to pre-oxidation conditions, phase composition might vary from the surface to the core of the pellet. This will also affect the porousity and how easy gas molecules can be transported towards the reaction interface. If the difference in concentration was due to pre-oxidation condition a more gradually decrease would have been expected.

Concentration gradients were also observed with mapping of a pellet from sample **b4.8CO**. Large cracks were found, the crack closest to the surface marks the border where reduction stopped. The O content started to increase before this crack, while the concentration of Fe and Ti rapidly changed on the inside of this crack. These cracks are probably caused by thermal expansion and phase transformation during the pre-oxidation.

For green pellets and sample **b9H2** no clear concentration gradients were observed. This indicates faster diffusion of gas through the pellets due to a more porous structure and gas species with higher diffusivities, respectively. The decreasing amount of iron from the surface towards the core of sample **g7CO** is an exception to the rule. Based on the latter result, higher degree of reduction is expected with the pellets without a concentration gradient. This is true for pellets reduced with H_2, but this can not explain the poor reducibility of green pellets.

5.4 XRD

There are differences in phase composition between the pellet types, and this affects the reduction. The presence of more M_3O_5 in pre-oxidized pellets from 2010 makes it easier to reduce these pellets. Pre-oxidized pellets from 2010 also

contains the less reducible M_3O_4. This phase is still present after 45 minutes of reduction.

Green pellets mainly consist of M_2O_3. Some M_3O_5 and $MgSiO_3$ are also found. These pellets are made of pure ilmenite with some impurities like $MgSiO_3$. M_3O_5 is therefore unexpected. Dust and unreduced material is recycled and fed into the pelletizing part of the plant. Especially dust from pre-oxidation might contain M_3O_5 and thus explain the presence of pseudobrookite (Elstad et al., 1992).

After reduction of green pellets some of the M_2O_3 and M_3O_5 are reduced into metallic iron and TiO_2. This is anticipated, but the degree of reduction is low and some M_3O_5 is still left. The M_3O_5 phase can be assumed evenly distributed inside the pellets. Even though this phase is more reducible than the M_2O_3 phase, slow diffusion of CO towards the core might limit the supply of gas for reduction. As a result, unreduced M_3O_5 and M_2O_3 can be found towards the core.

In pre-oxidized pellets from 2010 most of the M_2O_3 was oxidized into M_3O_5 and TiO_2. The TiO_2 peaks were less distinct than the M_3O_5 peaks. A part from the low values of TiO_2 this is expected. The low values of TiO_2 will be discussed in relation to sample **b7H2**.

Normal sized pre-oxidized pellets from 2011 contain less M_3O_5 and some M_3O_4 is present. A lower M_3O_5 content indicates that these pellets are less reduced compared to the similar pellets from 2011. This is also confirmed by the chemical analysis and valence state of iron. The pre-oxidation is determined by mass flow and thickness of the pellet-bed, water content of the green pellets and amount of binder. These variables will affect the temperature and a lower peak temperature will result in altered phase composition. The low degree of pre-oxidation is most likely caused by too low peak temperature. The presence of M_3O_4 is more difficult to explain. This phase can form during oxidizing of the M_2O_3 phase, but as can be seen from Figure 2.3 this phase is more reduced than the M_2O_3 phase.

Compared to the reduction of green pellets all M_3O_5 is gone after 3 minutes of reduction with CO on pre-oxidized pellets from 2011. Since no iron and TiO_2 is found, M_3O_5 is reduced into M_3O_4. Some formation of M_2O_3 is also possible, but then more TiO_2 would have been expected.

After reduction for 45 minutes with CO less M_2O_3 and M_3O_4 were found, but some iron and TiO_2 was present. The normal sized pellets were significantly more reduced in the outer shell compared to the core. Little difference is found between the core and outer shell for pellets with size from 10 to 12.5 mm. This indicates that the phase composition closer to the surface is more reducible in normal sized pellets than in the larger pellets. The opposite is true for the phase

composition in the core, where larger pellets are more reducible. This can be explained by the pre-oxidation conditions. It is also important to remember that only three pellets are crushed per sample, these pellets might deviate from the ideal pellet representing the sample. The presence of some M_3O_4 phase inside the shell of sample **b4.8CO** implies that this phase is hard to reduce.

The amount of iron is much higher after reduction for 45 minutes with CO on pre-oxidized pellets from 2010. Some M_2O_3 and TiO_2 is also present. In addition minor amount of M_3O_5 and M_3O_4 were also found. Based on the results for pre-oxidized pellets from 2011 the latter phase is hard to reduce. The presence of M_3O_5 is unexpected. This phase should have been reduced first. The presence of M_3O_5 can be caused by contamination of the sample or by some of it retained inside the pellets.

When H_2 is used to reduce the pre-oxidized pellets from 2011 only traces of M_3O_5, M_3O_4, M_2O_3 are left unreduced. The iron content is correspondingly high and in addition to this the amount of TiO_2 is low. Since H_2/H_2O migrates swiftly towards the core complete reduction is expected. Based on the XRD-analysis pre-oxidized pellets from 2011 reduced with H_2 are more reducible compared to pre-oxidized pellets from 2010 reduced with CO. In spite the sample is almost completely reduced some M_3O_5 and M_3O_4 remains. This can be due to contamination or enclosed phases.

Another observation is the low value of TiO_2. One explanation for this is that TiO_2 can appear in three different phases. Each compound has different angles related to the peaks. The different phases are therefore more difficult to separate from the background noise than if all TiO_2 was contained in one phase. Rutile and anatase are tetragonal and both are polymorphous with each other and with the orthorhombic brookite (Johnsen, 2002). TiO_2 might also be present as non crystalline remains in the ilmenite lattice after the removal of Fe and O. This will generate less significant peaks and more noise instead (Seim, 2011). Titanium metal can also dissolve into the iron phase and thus decrease the amount of TiO_2 present after ilmenite reduction. The XRD scan can not distinguish between the peaks of iron and $Fe_{0.9}Ti_{0.1}$ (Tolchard, 2011).

To investigate whether Ti was dissolved into the iron phase in sample **b7H2** 7 point analysis was done. They revealed that an average of 4.9 and 4.5 at.% Ti in addition to 5-6 at.% O were dissolved into the iron phase. Little O can dissolve into the iron phase, the high O value is therfore more likely caused by background noise from an ilmenite or a TiO_2 phase. If all this O is bound as TiO_2, MgO, SiO_2, and MnO 1.5-2.6 at.% Ti is dissolved into the iron phase. This value increases if the surface of the analysed phase is assumed oxidized and the

remaining value of Fe and corrected Ti content is normalized to 100 %. This can however only account for some of the low TiO_2 value from the XRD-analysis.

The correct phase composition of particularly M_2O_3 and M_3O_5, is hard to reveal since the peaks of the different variants of ilmenite and pseudobrookite overlaps. The exact composition might affect the reduction, but the difference in reducibility between Fe_2TiO_5, $FeTi_2O_5$ and $MgFe_2Ti_3O_{10}$ is unknown and not an aim for this master thesis.

5.5 Additional observations and remarks

In this subsection the results from the weight test of the TGA furnace are explained. A comparison of the reliability of the analysis is also given.

5.5.1 Test of the TGA furnace

The weight recorded by the TGA furnace is accurate and reliable, but changing gas flow will affect the recorded weight measurements.

In relation to the weight test one important observation was done. The conversion graphs indicate high reducibility immediately after reduction gas was switched on. This was also observed when 9 Nl/min of H_2 was added to the alumina sample, see Figure A.5 in the Appendix. This was unexpected since the sample should be inert. After 45 minutes of reduction 1 Nl/min with Ar replaced H_2 and the recorded weight loss was reversed. This weight change is affected by gas flow, gas compositions, amount and type of sample and actual temperature. This error can be quantified by reducing inert pellets at similar conditions. The two pellet types should be identical in shape and amount. The recorded initial weight loss from the change of gas flow and composition can then be corrected for. One alternative is to use the same gas flow of Ar and reduction gas in the minutes before reduction begins. The density difference and gas flow increase is highest for the test experiment with alumina spheres, 1.4 g weight loss during the first 1.7 minutes can be viewed as the maximum error.

Four objects were also placed on the weight connected to the TGA furnace, see Table A.4 in the Appendix. When these objects were removed a maximal difference in the recorded weight was 0.06g. A part from one object, the difference between the actual weight of the object and the weight recorded by the TGA furnace was less than 0.1g. The error is most likely due to placement and removal of the objects by hand.

5.5.2 Reliability of the analysis

The analysis is reliable and a part from some scattering they point in the same direction. The trend for degree of metalization is slightly different compared to the other analysis.

To be able to compare the different analysis and get some idea of the uncertainties these values are plotted in a graph. This can be seen in figure 5.1.

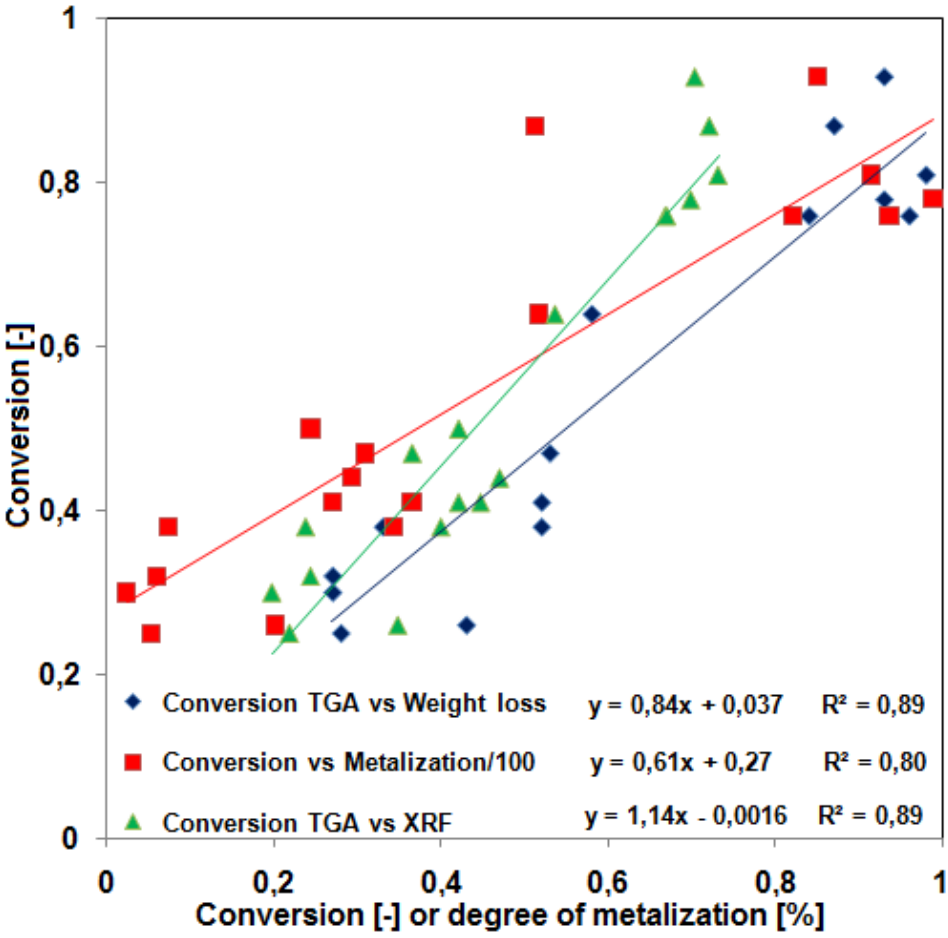

Figure 5.1: Test of the reliability of different analysis. Trend lines with equations are added for comparison.

If the pair of values is exactly the same this will give a trend line which intersects the origin with a slope of unity. When the slope is increasing this reveals that

conversion from the TGA is higher than the corresponding values along the x-axis. If the slope is less than unity, the values from the TGA furnace are lower compared to the values along the x-axis. A slope of 1.1 corresponds to a value on the x-axis of 10 and a value of 11 on the y-axis.

When the trend line intersects one of the axes far from the origin this tells that the pair of values are not directly comparable. The connection between the two analysis is less clear. The R^2 values indicates how well the trend line fits the set of data. A low value is followed by high scattering and poor consistency between the two pair of values. For these analysis the R^2 value of 0.89 indicates that the conversion data matches the model well. The lower R^2 value of 0.8 suggest that the linear relationship between conversion and degree of metalization is too simple.

Based on this, the values of conversion from weight measurements are a bit higher than the ones from the TGA furnace. These values of conversion both points in the same direction. The same is also true for the conversion from TGA and the calculated conversion based on XRF-analysis. However the values based on the XRF-analysis is lower compared to conversion from the TGA furnace. Conversion from the XRF-analysis is calculated based on the amount of oxygen. The oxygen content is the difference between 100 wt.% and the sum of oxides, metals, and a residue. When this oxygen is assumed bound to iron values of conversion can be calculated. If the residue is 0, the trend line intersects at 0.2. This indicates poor relation between the values of conversion from TGA and the XRF-measurements. Since pellets are exposed to air after reduction the pellets will contain some moisture. The XRF does not detect all elements in the sample and the sum of all oxides and metals is rarely 100 %. By trial and error a good relation between the values of conversion from TGA and XRF-analysis is found with a residue of 2.7 wt.%. This indicates that the maximum content of water in the redused samples are 2.7 wt.%.

Degree of metalization can not be directly compared to the conversion from the TGA since the intersection is at 0.27. This means that the values of conversion both are higher than the degree of metalization and that the value of degree of metalization increases more rapidly with extended reduction.

5.6 Future work

In order to simulate the conditions present in an industrial furnace it would have been interesting to reduce the pellets with alternating reduction potential. This can be done by stepwise changing both temperature and gas mixture. At the beginning both temperature and the reducing potential are low. To approach the situation in an industrial process where the pellets are reaching the bottom of the furnace, both temperature and reduction potential are increased. The reduction potential is altered by changing the ratio between CO/CO_2, H_2/H_2O or a mixture of both. Based on these experiments kinetic calculations can be done to get increased knowledge of the ilmenite reduction. To remove the effect of a stagnant gas film layer a gas flow of 1m/s is required, this corresponds to a gas flow of 27 Nl/min if the crucible designed for the TGA furnace is used. This can not be achieved since the maximal flow is 10 Nl /minute.

To avoid the uncertainties in the weight measurements in the beginning of the experiment no change in gas flow should occur during the last minutes of heating. This can be done by heating the furnace under 1 Nl/min of Ar and then increase the gas flow 2-4 minutes before reduction gas is introduced.

This investigation indicates that H_2 is a beneficial reducing agent for pre-oxidized pellets. To find out whether pre-oxidation is beneficial for reduction with H_2, green pellets should also be reduced.

As one of the conclusions from this master pre-oxidized pellets have poor reducibility with CO as reducing agent. For increased understanding of the effect of pre-oxidation the same pellets should have been tested with similar gas flows at temperatures up to 1200 °C. If results and analysis still indicate low reduction, this will be important knowledge for the industry.

6 CONCLUSION

Pelletized Tyssedal ilmenite are reduced for c. 45 minutes at 900 °C. Mainly three phases are present after reduction; metallic iron, titanium oxide and ”unreduced ilmenite”. The iron nuclei are circular, and often found close to grain boundaries. For pre-oxidized pellets from 2011 reduced with CO iron nuclei tend to encapsulate larger grains. This is not observed after reduction with H_2. Where the average size of the iron nuclei decreases, and approaches 1 μm. More lamella shaped iron nucleus are found both under reduction with H_2 and in green pellets reduced with CO. Besides Fe, this phase contains up to c. 5 at.% Ti and some impurities like O, Mg, Mn, and Si.

The titanium oxide phase can vary in shape from oval to a spherical shell. The latter is found within iron encapsulated grains. The chemical composition is most likely TiO_2, but reduction to Ti_3O_5 can not be ruled out. Close to the core of larger grains reduced with CO ”unreduced ilmenite” is found. The exact elemental composition is unknown and will vary, but based on the XRD-result both ilmenite, pseudobrookite and spinell are possible. The phase composition will vary depending on the Fe/Mg ratio.

- Normal sized pellets are more easily reduced than larger pellets. Final values of conversion from the TGA are 0.19-0.24 lower for oversized pellets. This can be explained by longer mean diffusion path. Pellets with a size between 10 and 12.5 mm were less reducible compared to pellets larger than 12.5 mm. This can be explained by different phase composition since it is harder to oxidize larger pellets in the pre-oxidation process. When pellets were reduced with H_2 instead of CO, more iron was formed in the centre of the pellets. Degree of metalization was 27-64% higher and final values of conversion were c. 0.4 higher. This can be explained by faster migration of H_2 and H_2O in the core of the pellet, and the fact that H_2 is a more powerful reducing agent at these temperatures.

- Pre-oxidized pellets from 2010 are more easily reduced by CO compared to pellets from 2011. Final values of conversion and degree of metalization are 0.23 and c. 24 % higher for pre-oxidized pellets from 2010. The reason for this is altered phase composition and degree of oxidation. This gives slower migration of gas towards the centre of the pellets and the grains. Green pellets from 2011 reduced with CO obtain higher degree of metalization, but lower final conversion than pre-oxidized pellets from 2011. This indicates more reduction of tetravalent iron in pre-oxidized pellets than in green pellets. The difference can be explained by phase

composition, cracks and porosity. Since the main objective for the pre-oxidation part at ETI Tyssedal is to enhance reduction, this indicates that the pre-oxidation conditions must be better controlled or modified.

- Aging can have a minor decreasing effect on reduction. Degree of metalization and final conversion are 5% and 0.02 higher for the sample reduced 18 days after pre-oxidation compared to the sample reduced 165 days later. This small difference can be explained by variation among the pellets and uncertainty in the analysis.

- For pre-oxidized pellets from 2011 an increased gas flow of CO resulted in decreased reduction. Pellets were slightly more reduced with a gas flow of 7Nl CO/min compared to 4.8 Nl CO/min. The fact that pellets were less reduced when the gas flow increased to 9 Nl/min contradicts previous knowledge and has no natural explanation known to the author. The limited effect of increasing the gas flow from 4.8 to 7 indicates that migration in the pellet, not the amount of gas, is limiting the reduction.

- Reduction of pre-oxidized pellets from 2011 occurs in two distinct stages, separated by a clear bend at a value of conversion of c. 0.33. The initial oxygen removal rate is about 10 times faster than the oxygen removal rate in the final stage. The increase in conversion as function of time is relatively constant for both stages. This deviates from the normal declining oxygen removal rate observed for green pellets. Because no concentration gradients are found after reduction with H_2, the shift in reduction rate can be explained by complete reduction of trivalent iron. For pellets reduced with CO, the centre of the pellets remains unreduced. The presence of trivalent iron implies that some of the shift in reduction rate can be explained by complete reduction of the most easily reduced phases. No other explanation is found.

- From mapping in EPMA two interesting observations were done. In pre-oxidized pellets reduced with CO some of the largest grains were almost covered by a layer of iron. Within this layer, titanium oxide was found encapsulating a unreduced core. The interface separating these two phases was enriched in Mg and Al. This is a strong indication of the barrier effect which hampers the reduction. These investigations can not tell whether the layer of iron is baffling reduction or if the limited reduction favours migration of iron towards the surface. After pre-oxidized pellets from 2011 were reduced with CO, concentration gradients was found. Especially a sharp increase in amount of O was observed 0.6-1.0 mm from the surface. Since the core of the pellets were unreduced, this indicates

limited migration of CO/CO_2.

- Based on the XRD-analysis, normal sized pre-oxidized pellets from 2010 consist of M_3O_5 and M_2O_3. In similar pellets from 2011, M_2O_3 is the main phase, but M_3O_5 and M_3O_4 are also found. The difference is due to the pre-oxidation at ETI Tyssedal. M_3O_5 is easy to reduce compared to M_2O_3 and particularly M_3O_4. After reduction with CO amount of iron is much higher in pellets with M_3O_5. Since oversized pellets contain more iron close to the core, this indicates more favourable pre-oxidation conditions than for normal sized pellets. Amount of TiO_2 is low. Because TiO_2 can be reduced and dissolved into other phases and the fact that TiO_2 has 3 polymorphs makes the composition hard to analyze.

The pre-oxidized pellets from 2010 and 2011 are supposedly two batches of the same material: They are produced in the same manner from the same raw materials. In spite of this, their behaviour during reduction is dramatically dissimilar. This fact should be remembered when comparing results from different sources.

References

Bardi, G., D. Gozzi and S. Stranges (1987), 'High Temperature Reduction kinetics of Ilmenite by Hydrogen', *Materials Chemistry and physics* **17**, 325–341.

Borowiec, K., A.E. Grau, M. Gueguin and J.F. Turgeon (1997), 'Method to Upgrade Titania Slag and Resulting Product'. Patent no: PCT/CA1996/000767.

Borowiec, Krzyszof and Terkel Rosenqvist (1981), 'Phase Relation and Oxidation Studies in the System Fe-Fe_2O_3-TiO_2 at 700-1100 °C.', *Scandinavian Journal of Metallurgy* **10**, 217–224.

Borowiec, Krzyszof and Terkel Rosenqvist (1982), 'On the Iron-Titanium-Oxygen System. Phase Relations During Reduction of Norwegian Ilmenite.'. Sintef report STF34 A82100, Trondheim.

Borowiec, Krzyszof and Terkel Rosenqvist (1985), 'Phase Relation and Oxidation Potentials in the Fe-Ti-Mg-O System.', *Scandinavian Journal of Metallurgy* **14**, 33–43.

Calphad (2010), 'Iron titanium phase diagram', `http://www.calphad.com/iron-titanium.html`. visited 7 October 2010.

CoorsTek (2011), 'Wear, Grinding Media', `http://www.coorstek.com/materials/ceramics/alumina/ad90.asp`. visited 3 may 2011.

Elstad, H., K. Ure and Ø. Tvedt (1992), *Elektrokjemifaget Karbotermiske Prosesser Ilmenitt*, TINFOS Titan and Iron KS, Tyssedal.

Gupta, S.K, V. Rajakumar and P. Grieveson (1987), 'Kinetics of Reduction of Ilmenite with Graphite at 1000 to 1100 °C', *Metallurgical Transactions B* **18B**, 713–718.

Gupta, S.K, V. Rajakumar and P. Grieveson (1989), 'The Influence of Weathering on the Reduction of Ilmenite with Carbon', *Metal Transition B* **20B**, 735–745.

Hlady, M. and S. Gaal (2004), 'Operating Manual for Thermal Gravimetric Analyzer for DISvaDRI'.

Hussein, M.K., R. Kammel and H. Winterhager (1967), 'A Study on the Reduction Mechanism of Ilmenite Ores', *Indian Journal of Technology* **5**(12), 369–377.

Jasna, B (1978), 'Phase Transformations in an Ilmenite Concentrate Roasted in the Temperature Range from 400 °C to 1200 °C ', *Proc. Conf. App. Crystallogr.* **2**, 776–787.

Johnsen, E.R. (2005), Redusibilitet av ilmenittpellets, Master thesis, Institute for material science, NTNU.

Johnsen, Ole (2002), *Photographic Guide to Minerals of the World*, Oxford university press. page 167-172.

Jones, D.G. (1973), 'Reduction sequences in the reduction of ilmenite: 2-gaseous reduction by carbon monoxide', *Transactions of the Institution of Mining and Metallurgy* **82C**, 186–192.

Jones, D.G. (1974), 'Optical Microscopy and Electron-probe Microanalysis Study of Ilmenite Reduction', *Transactions of the Institution of Mining and Metallurgy* **83C**(808), c1–c9.

Jones, D.G. (1975), 'Kinetics of Gaseous Reduction of Ilmenite', *Journal of Applied Chemistry and Biotechnology* **25(8)**, 561–582.

Jørstad, Steinar (2010), Reduction of pelletized Tyssedal ilmenite with excess amounts of CO and H_2., Experimental work, Institute for material science, NTNU.

Kolbeinsen, Leiv (2010), 'Personal communication'.

Kolbeinsen, Leiv (2011), 'Personal communication'.

Kucukkaragoz, C.S. and R.H. Eric (2006), 'Solid state reduction of a natural ilmenite', *Minerals Engineering* **19**, 334–337.

Merk, R. and C.A. Pickles (1988), 'Reduction of Ilmenite by Carbon Monoxide', *Canadian Metallurgical Quarterly* **27(3)**, 179–185.

NTNU (2010), 'JEOL JXA-8500F Electron Probe Micro analyzer (EPMA)', `http://www.material.ntnu.no/lab/material/equipment/ProdInfoEPMA.pdf`. visited 2 December 2010.

Øye, K. (1990), Reduksjon av Ilmenitt med Hydrogen, Experimental work, Metallurgisk institutt, NTH.

Seim, Stian (2010), 'Personal communication'.

Seim, Stian (2011), 'Personal communication'.

SERC at Carleton College (2010), 'Geochemical Instrumentation and Analysis, X-Ray Fluorescence (XRF)', `http://serc.carleton.edu/research_education/geochemsheets/techniques/XRF.html`. visited 3 December 2010.

SERC at Carleton College (2011), 'Geochemical Instrumentation and Analysis, X-ray Powder Diffraction (XRD)', `http://serc.carleton.edu/research_education/geochemsheets/techniques/XRD.html`. visited 15 March 2011.

Spitzer, R.H., F.S. Manning and W.O. Philbrook (1966), 'Mixed-Control Reaction Kinetics in the Gaseous Reduction of Hematite', *Transaction of the Metallurgical Society of AIME* **236**, 726–742.

Sun, K., R. Takahashi and J.I. Yagi (1992), 'Reduction Kinetics of Cement-bonded Natural Ilmenite Pellets with Hydrogen', *ISIJ International* **32**(4), 496–504.

Szekely, J., J.W. Evans and H.Y. Sohn (1976), *Gas - Solid Reactions*, Academic Press. page 125-132.

Tangstad, M (1988*a*), Oksidasjon av Ilmenitt Pellet, Experimental work, Metallurgisk Institutt, NTH.

Tangstad, M (1988*b*), Oksidasjon og Reduksjon av Ilmenittpellets, Master thesis, Metallurgisk institutt, NTH.

Tolchard, Julian (2011), 'Personal communication'.

Towhidi, N. and J. Szekely (1983), 'The Influence of Carbon Deposition on the Reduction of Commercial Grade Hematite Pellets with CO, H_2 and N_2', *Metallurgical Transactions B* **14**, 359–367.

University of Minnesota (2010), 'Electron Probe Microanalysis', `http://probelab.geo.umn.edu/electron_microprobe.html`. visited 2 December 2010.

Vijay, P.L., R. Venugopalan and D. Sathiyamoorthy (1996), 'Preoxidation and Hydrogen Reduction of Ilmenite in a Fluidized Bed Reactor', *Metallurgical and Materials Transactions B* **27B**, 731–738.

Wang, Y., Z. Yuan, H. Matsuura and F. Tsukihashi (2009), 'Reduction Extraction Kinetics of Titania and Iron from an Ilmenite by H_2-Ar Gas Mixtures', *ISIJ International* **49**(2), 164–170.

Wang, Yuming and Z. Yuan (2006), 'Reductive Kinetics of the Reaction Between a Natural Ilmenite and Carbon', *International Journal of Metal Processing* **81**, 133–140.

Welham, N. J. (2002), 'Enhancing Oxygen Recovery From Ilmenite by Extended Milling', *Materials Science and Engineering A* **336**(1-2), 7143 – 149.

Welham, N.J. and J.S. Williams (1999), 'Carbothermic Reduction of Ilmenite ($FeTiO_3$) and Rutile (TiO_2)', *Metallurgical and Materials Transactions B* **30B**, 1075–1081.

Zhang, Guangqing and O. Ostrovski (2001), 'Reduction of ilmenite concentrates by methane containing gas, Part II: Effects of preoxidation and sintering', *Canadian Metallurgical Quarterly* **40**(4), 489–497.

Zhang, Guangqing and O. Ostrovski (2002), 'Effect of preoxidation and sintering on properties of ilmenite concentrates', *International Journal of Mineral Processing* **64**(4), 201–218.

Zhao, Dongju (2010), Processing and Properties of Direct Reduced Iron Pellets Containing Material for Control of Steel Structure, Phd thesis, 2010:42, Norwegian University of Science and Technology.

Zhao, Y. and F. Shadman (1990), 'Kinetics and Mechanism of Ilmenite Reduction with Carbon Monoxide', *AIChE Journal* **36**(9), 1433–1438.

A APPENDIX

This section is included to give the reader extra information.

A.1 Degree of oxidation

From analysis of pre-oxidized ilmenite both total amount of iron and distribution between divalent (FeO) and trivalent iron (Fe_2O_3) can be found. Degree of oxidation is a measure of actual amount bound to oxygen compared to maximum amount of oxygen that can be bound to iron. The connection is shown in Equation (2.2), which is derived from assumption of one gram of pellet, and number of moles of iron given by Equation (A.1) (Elstad et al., 1992):

$$n_{Fe,tot} = \frac{\text{wt } \%Fe_{tot}}{M_{Fe}} \tag{A.1}$$

Here n is number of moles, and M is the molar weight. From stoichiometry one mole of divalent iron can bind the same amount of oxygen, while one mole of trivalent iron can bind 1.5 mole of oxygen. When every oxygen atom is bound to trivalent iron the total mass of oxygen is given by Equation (A.2) (Elstad et al., 1992):

$$m_{O,tot} = n_{O,tot} \times M_O = \frac{1,5 \times wt\%Fe_{tot} \times M_O}{M_{Fe}} \tag{A.2}$$

Where the total mass of Oxygen is $m_{O,tot}$. Actual amount of oxygen bound to iron can be calculated from Equation (A.3) when wt.% of FeO and Fe_2O_3 is known (Elstad et al., 1992):

$$m_O = \frac{3 \times wt\%Fe_2O_3 \times M_O}{M_{Fe_2O_3}} + \frac{wt\%FeO \times M_O}{M_{FeO}} \tag{A.3}$$

From this, Equation (A.4), degree of oxidation is defined as:

$$OX = \frac{m_O - \Delta_{Weight}}{m_{O,tot}} = \frac{(n_{Fe^{3+}} \times 1,5 + n_{Fe^{2+}} \times 1 + n_{Fe} \times 0) \times M_O - \Delta_{Weight}}{(n_{Fe^{3+}} + n_{Fe^{2+}} + n_{Fe}) \times 1,5 \times M_O} \tag{A.4}$$

Connection between degree of oxidation (OX) and conversion (X) is given in Equation (A.5):

$$X = 1 - OX \tag{A.5}$$

A.2 Additional tests and a program schedule

Before green pellets were used, 2 or 3 pellets per sample were weighted before and after 5 hour in a drying cabinet held at 150 °C. The result is found in Table A.1.

Table A.1: Weight reduction of green pellets after 5 hours of heating at 150 °C.

Sample	Weight before [g]	Weight after [g]	Weight loss [%]
Bag 1	4.6493	4.1890	9.9
Bag 2	4.1394	3.7476	9.5
Bag 3	8.5571	7.6736	10.3
Bag 4	6.1961	5.5837	9.9
Average			9.9

A temperature test of the DISvaDRI furnace is found in Figure A.1. This figure indicates the temperature deviation away from the pellet bed when set temperature was 800 °C.

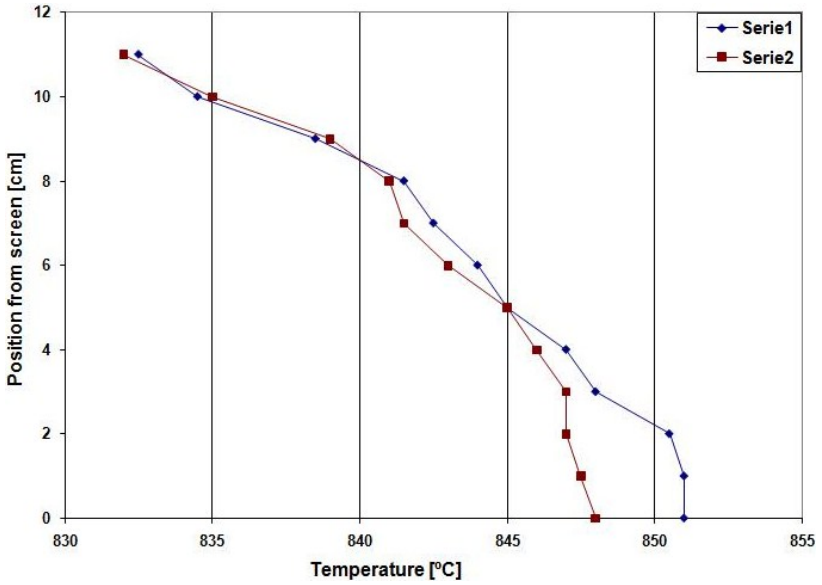

Figure A.1: Temperature test of the DISvaDRI furnace. Set temperature was 800 °C.

Example of program schedule for the DISvaDRI furnace is given in Table A.2.

Table A.2: The complete program schedule for sample 900b1 and 900u1.

Total time [HH:MM:SS]	Time interval [HH:MM:SS]	Set temperature ◦ C	CO [Nl/min]	CO_2 [Nl/min]	H_2 [Nl/min]	Ar [Nl/min	Furnace [up/down]	Cascade [on/off]	Sample rate [s]
00:00:10	00:00:10	900	0	0	0	1	up	off	5
00:45:10	00:45:00	900	0	0	0	1	up	off	5
00:60:10	00:15:00	900	0	0	0	1	up	off	5
01:00:20	00:00:10	900	9	0	0	0	up	off	1
01:45:20	00:45:00	900	9	0	0	0	up	off	1
01:45:30	00:00:10	25	0	0	0	1	down	off	5
02:30:30	00:45:00	25	0	0	0	1	down	off	5
02:30:40	00:00:10	25	0	0	0	0	down	off	5

In Table A.2 total time is the time used for all steps including the present. Time interval tells how long the step will last. Set temperature is the measured temperature inside the furnace. CO, CO_2, H_2 and Ar are gas flows into crucible. If the furnace is up, crucible is heated, while in position down, crucible remains cold. At a sample rate of 5, there are five seconds between each logging. Cascade on/off displays whether cascade control is being used or not (Hlady and Gaal, 2004).

A.3 Pictures of DISvaDRI furnace and crucible with equipment

(a) Overview of DISvaDRI furnace, crucible and gas tubes.

(b) Overview of crucible, gas sheet, thermocouple, alumina tube, bottom grating and tools (spanners and screwdriver).

Figure A.2: Overview of DISvaDRI furnace and crucible in addition to the tools used. Taken from Jørstad (2010).

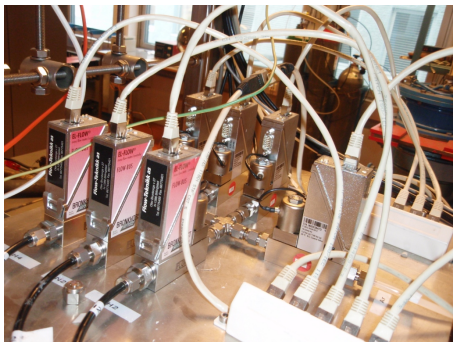

(a) Flow cells and gas tubes.

(b) Gas containers with gas tubes.

Figure A.3: Overview of flow cells and gas containers with connections to gas tubes. Taken from Jørstad (2010).

A.4 Ilmenite pellets after grinding and polishing and alumina pellets

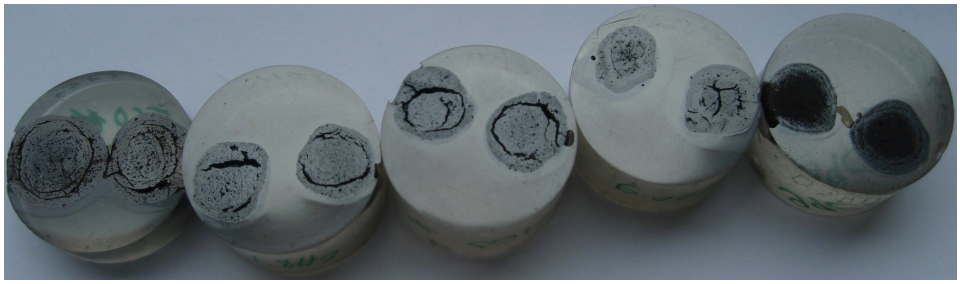

Figure A.4: Grinded pellets with a thin carbon layer deposited on the surface. Cracks and the outer shell are visible. From left side towards the right side the samples are b4.8CO10-12.5, b4.8H2, b9CO3, b9CO.old and g9CO.

In Table A.3 mechanical data for the alumina pellets is found. The chemical composition is unknown but the pellets contains at least 90 wt % Al_2O_3. Note 1: Data Measurements – All data measurements are typical and made at room temperature unless otherwise noted. Note 2: Composition Control – All CoorsTek ceramic compositions are controlled using modern chemical spectrographic and x-ray fluorescent methods. Note 3: Thermal shock resistance – Tests are run by quenching samples into water from various elevated temperatures. The change in temperature where a sharp decrease in flexural strength is observed is listed as (delta)Tc. Note 4: Wear resistance – Impingement tests are run by using a dry 240 grit fused alumina abrasive. The indices in the chart are calculated by dividing the material volume loss by the volume loss of an AD-85 alumina control. The lower in the index, the better the wear resistance (CoorsTek, 2011).

A.5 Weight test of the TGA furnace

Results from the weight test experiment with alumina spheres are given in Table A.4. The weight change are given in Figure A.5. From this figure the weight loss during reduction of these spheres are 0.51 from reduction began until argon was purged through. The measured weight difference from the pellets before and after reduction was zero.

Table A.4: Weight change measured by the PR2003 Delta Range weight connected to the TGA furnace. Measured values are found by the use of the SAUTER RL 1200 weight. Increase and decrease values are obtained when the objects were placed and removed from the PR2003 Delta Range weight connected to the TGA furnace. Delta W is the difference between these values. Delta TGA is measured values - the average of increase and decrease.

Object	Measured [g]	Increase [g]	Decrease [g]	Delta W [g]	Delta TGA [g]
Thin screw	5.41	5.423	5.361	0.062	0.018
Thick screw	7.175	7.746	7.796	-0.05	-0.596
Thin angle	40.01	39.928	39.945	-0.017	0.0735
Thick angle	79.97	79.862	79.897	-0.035	0.0905

A.6 XRD scans with peaks and interpretation

For further details in relation to the XRD scans, copies of the raw data with interpretations are given in Figure A.6-A.16.

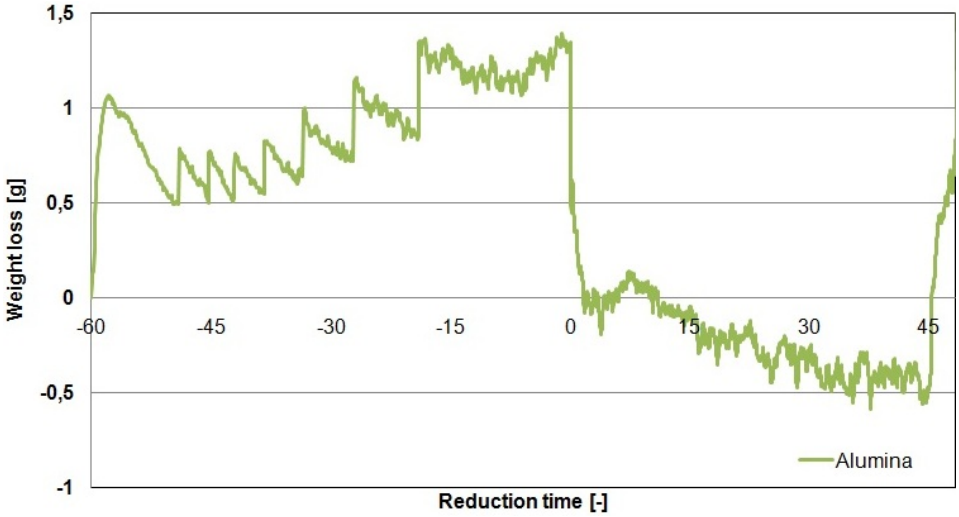

Figure A.5: Weight change during reduction of alumina spheres with the use of 9 Nl H_2/min.

Table A.3: Data certificate for alumina pellets delivered by CoorsTek. (CoorsTek, 2011).

AD-90 Alumina Material Properties				
Trade Name	AD-90			
Composition	Nominal 90% Al2O3			
Colour	White			
Property	Units	Test	Value	
Density	gm/cc	ASTM-C20	3.6	
Crystal Size	Microns	Thin-Section	4	
Water Absorption	%	ASTM-373	0	
Gas Permeability			0	
Flexural Strength (MOR), 20 degrees C	–	–	338 (49)	
Elastic Modulus, 20 degrees C	GPa (psi x 106)	ASTM-F417	276 (40)	
Poisson's Ratio, 20 degrees C	–	ASTM-C848	0.22	
Compressive Strength	MPa(psi x 103)	ASTM-C773	2482 (360)	
Hardness	GPa(kg/mm2)	KNOOP 1000 gm	10.4 (1058)	
		Rockwell 45 N	75	
Tensile Strength, 25 degrees C	MPa (psi x 103)	ACMA TEST #4	221 (32)	
Fracture Toughness K(Ic)	Mpa m1/2	NOTCHED BEAM	03.apr	
Thermal Conductivity, 20 degrees C	Wm degrees K	ASTM-C408	16.7	
Coefficient of Thermal Expansion, 25-1000 degrees C	1 x 10-6/degrees C	ASTM-C372	8.1	
Specific Heat, 100 degrees C	J/kg*K	ASTM-E1269	920	
Thermal Shock Resistance, (delta)Tc	degrees C	NOTE 3	250	
Maximum Use Temperature	degrees C	NO-LOAD COND.	1500	
Dielectric Strength	ac-kV/mm (acV/mil)	ASTM-D116	8.3 (210)	
Dielectric Constant, 1MHz	25 degrees C	ASTM-D150	8.8	
Dielectric Loss (tan delta) 1MHz	25 degrees C	ASTM-D2520	0.0004	
Volume Resistivity	25 degrees C	ohm-cm	ASTM-D1829	>1014
	500 degrees C	ohm-cm	ASTM-D1829	4 x 108
	1000 degrees C	ohm-cm	ASTM-D1829	5 x 105
Impingement	–	Note 4	0.45	
Rubbing	–	Note 4	0.36	

Green pellets from 2011

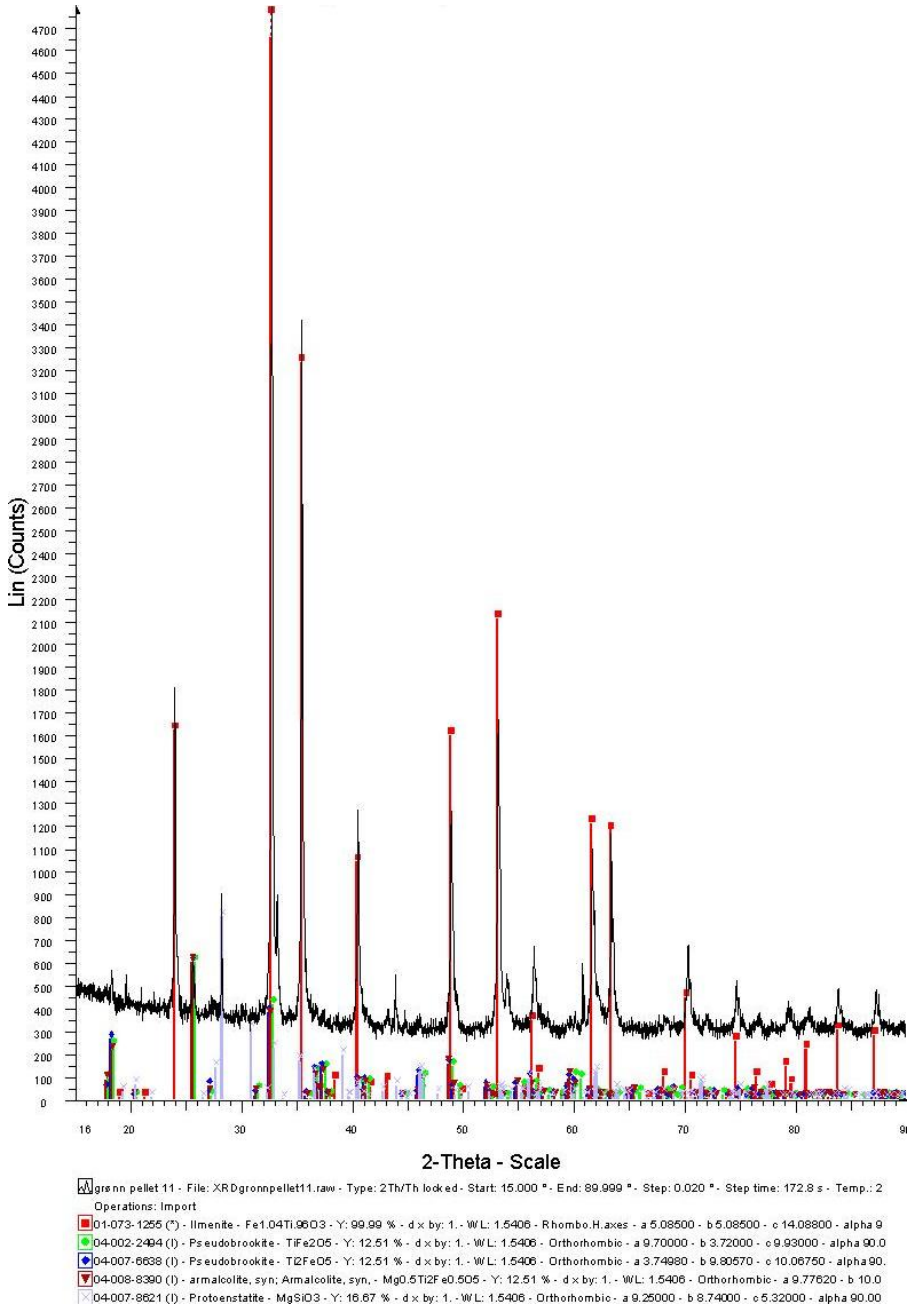

Figure A.6: XRD scan for green pellets from 2011 with interpretation and normalized peaks.

pre-oxidized pellets from 2011

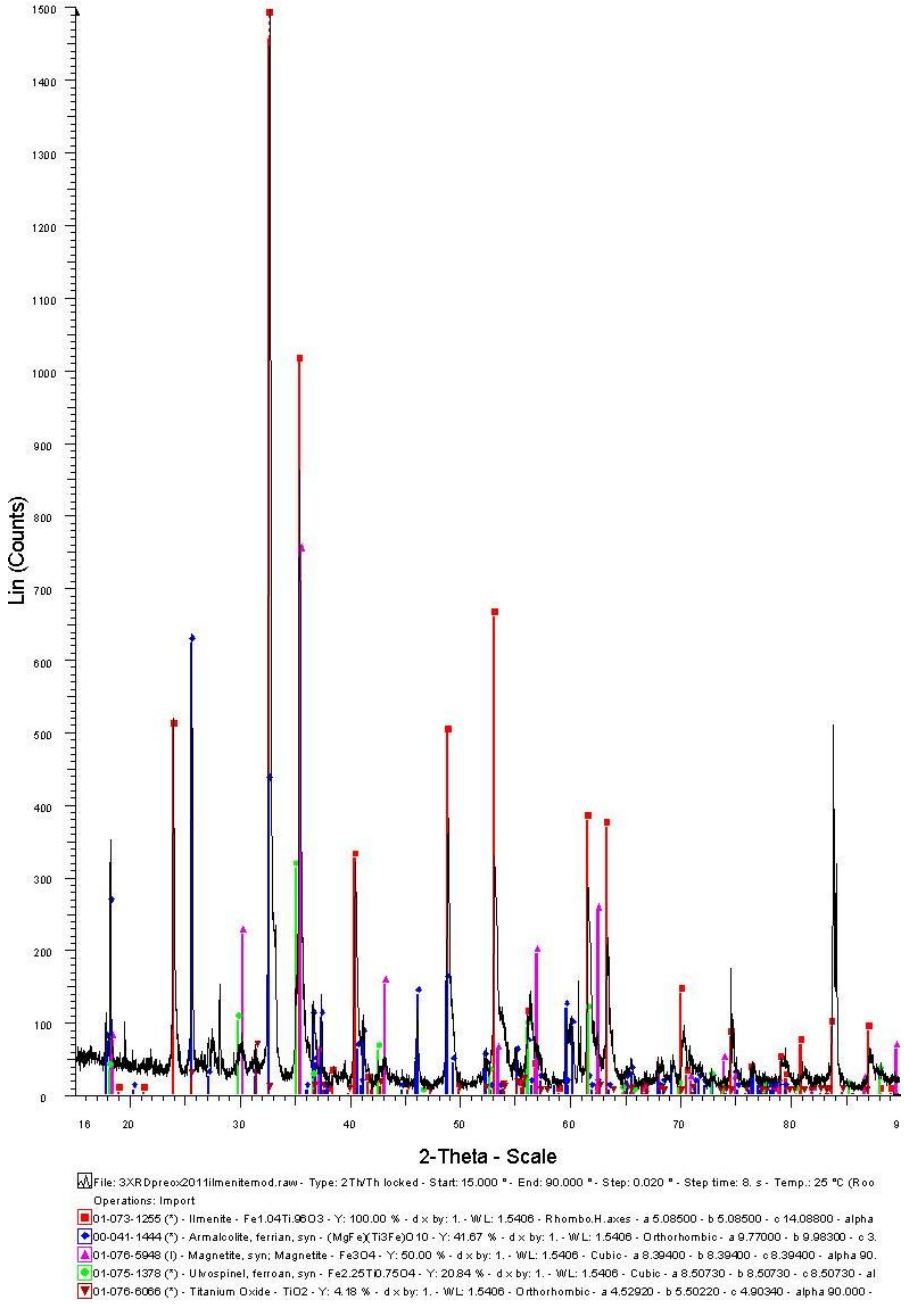

Figure A.7: XRD scan for pre-oxidized pellets from 2011 with interpretation and normalized peaks.

pre-oxidized pellets from 2010

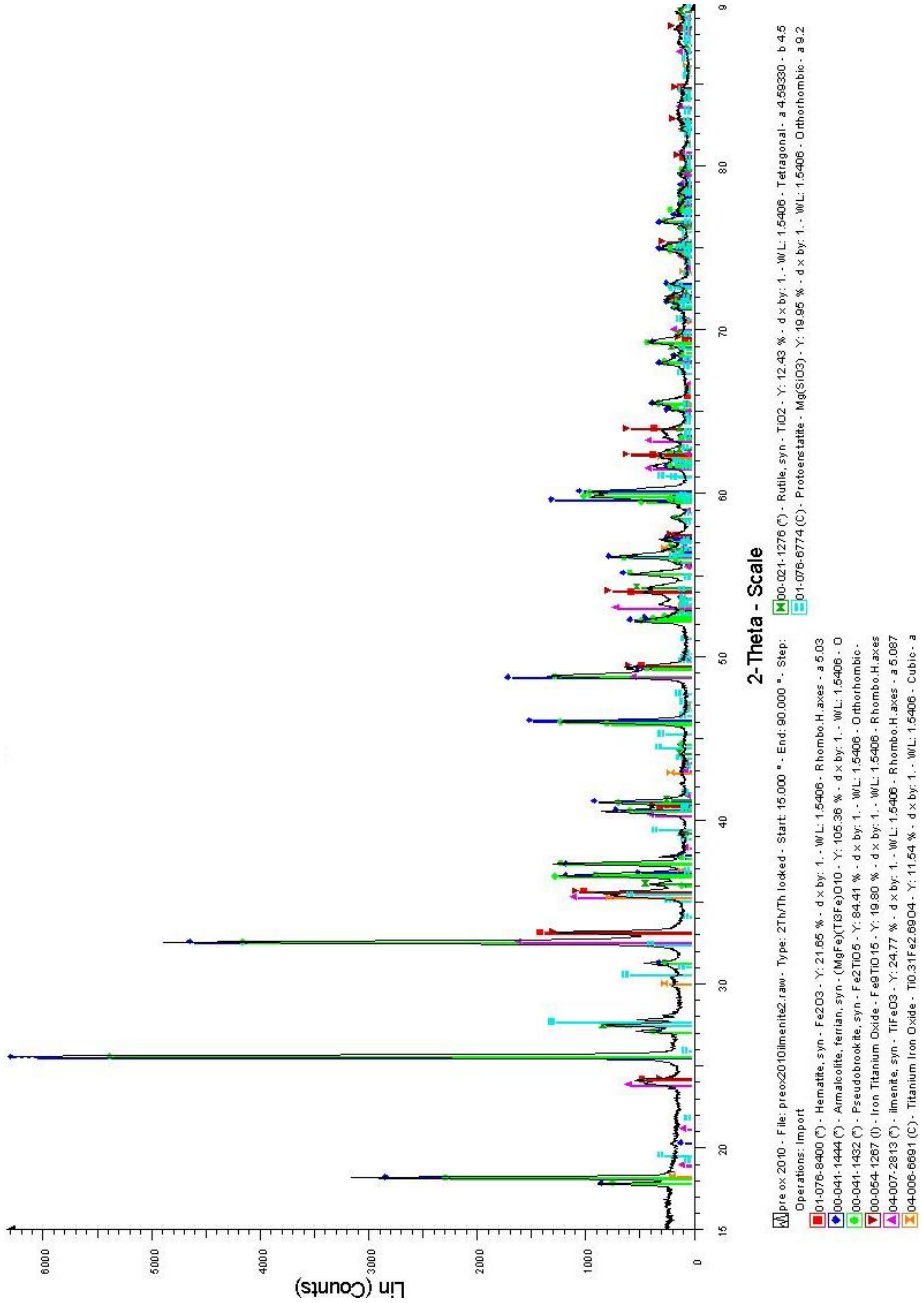

Figure A.8: XRD scan for pre-oxidized pellets from 2010 with interpretation and normalized peaks.

Sample g7CO

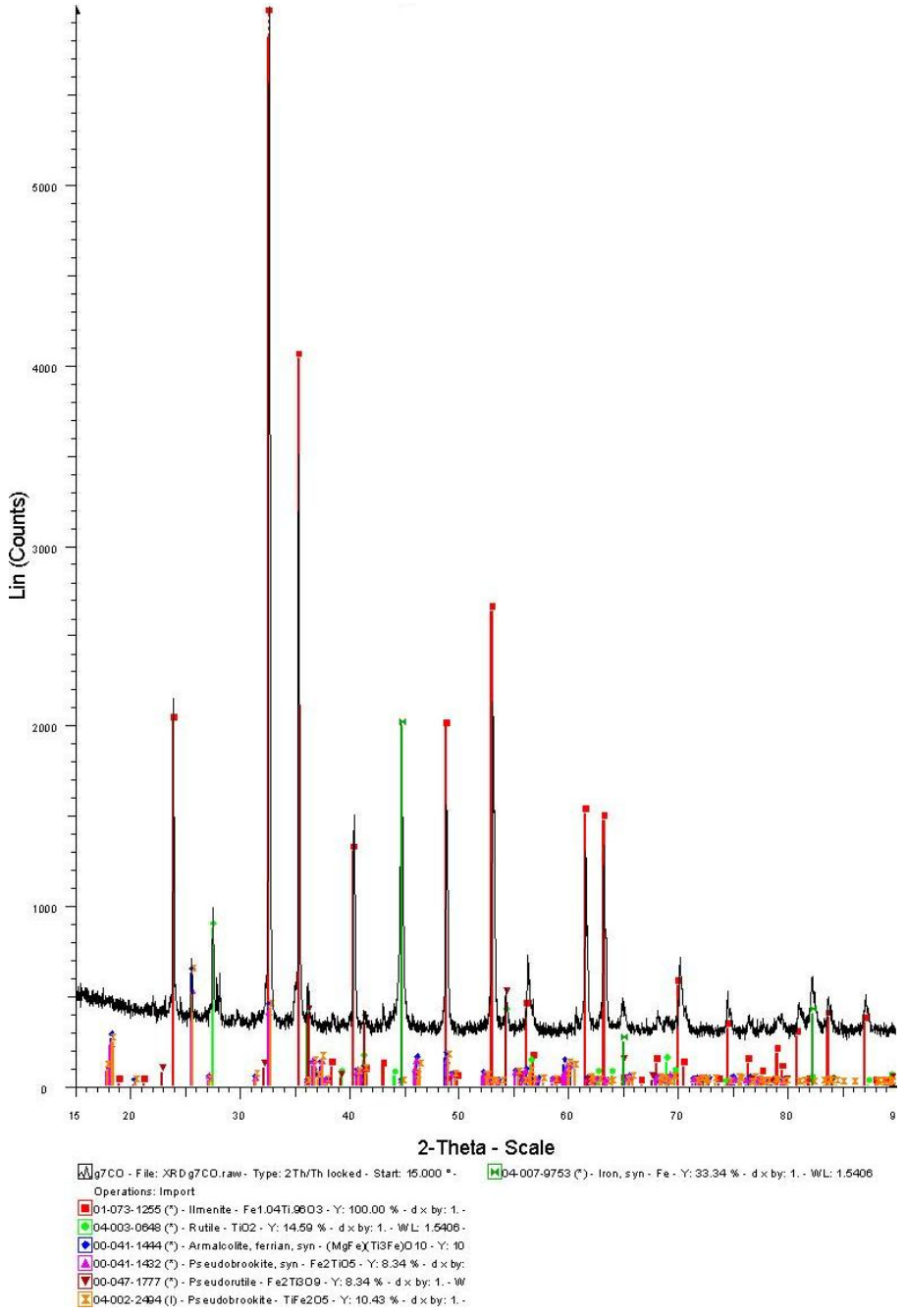

Figure A.9: XRD scan for sample g7CO with interpretation and normalized peaks.

Sample b4.8CO10-12.5core

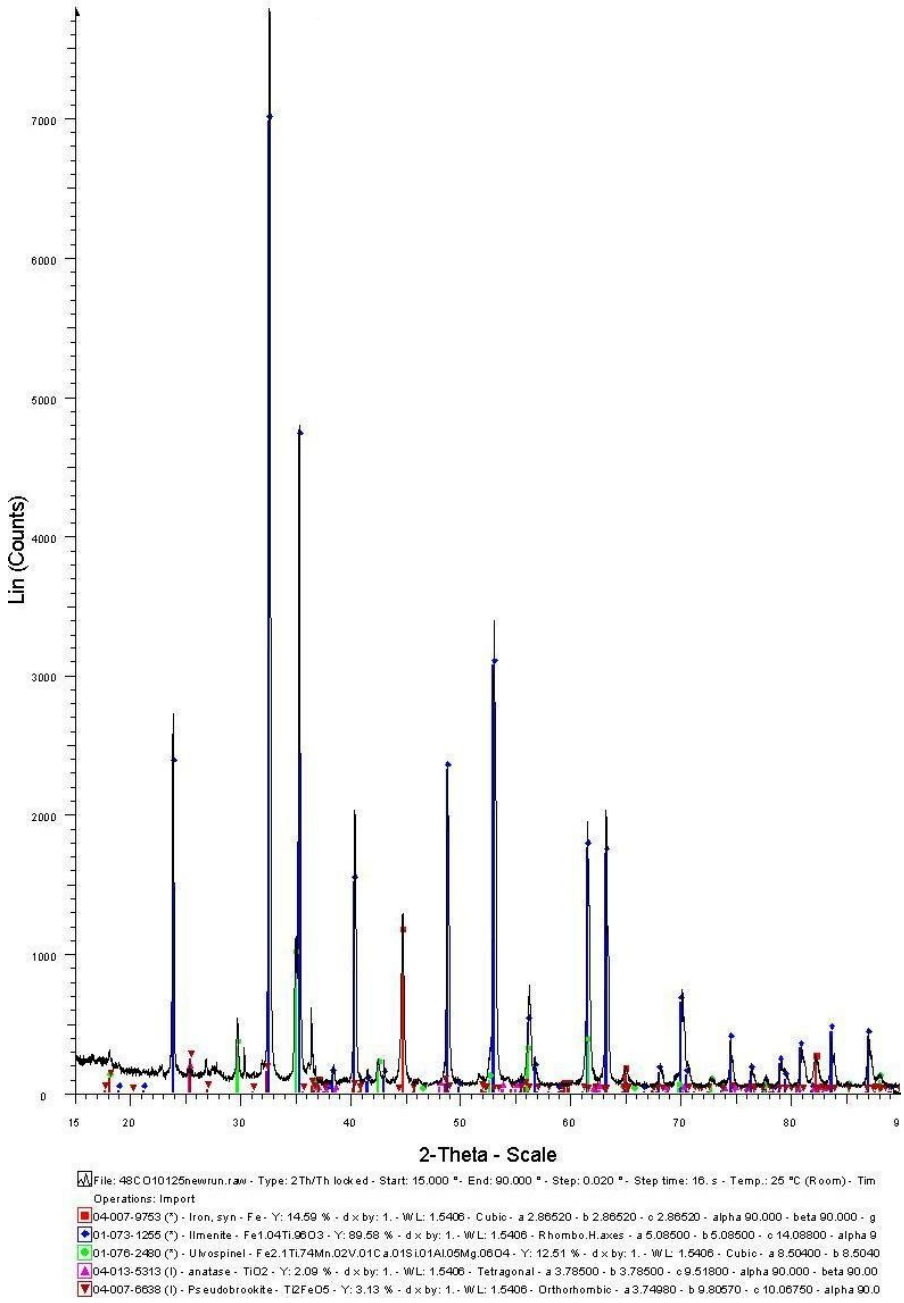

Figure A.10: XRD scan for sample b4.8CO10-12.5core with interpretation and normalized peaks.

Sample b4.8CO10-12.5shell

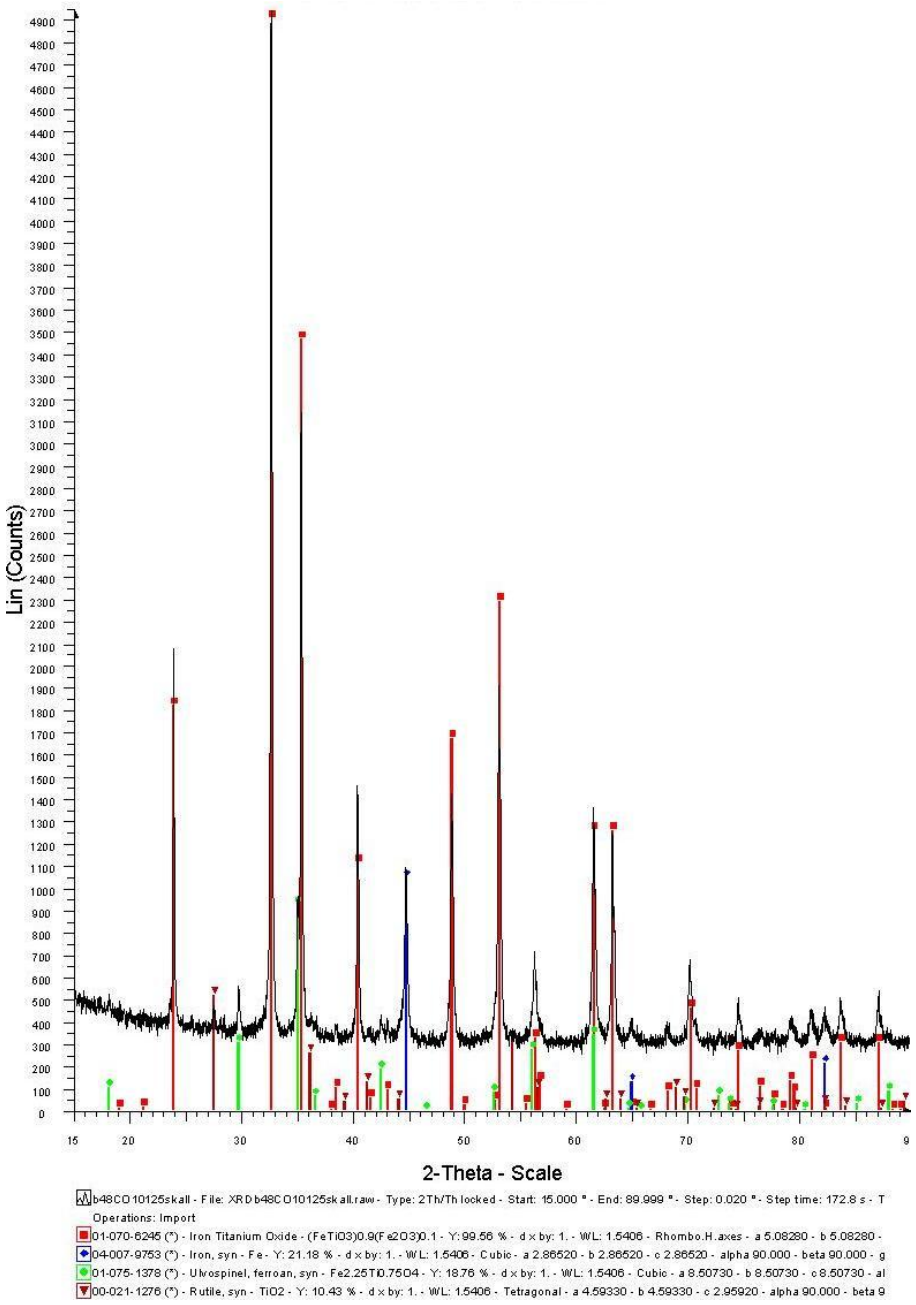

Figure A.11: XRD scan for sample b4.8CO10-12.5shell with interpretation and normalized peaks.

Sample b4.8COcore

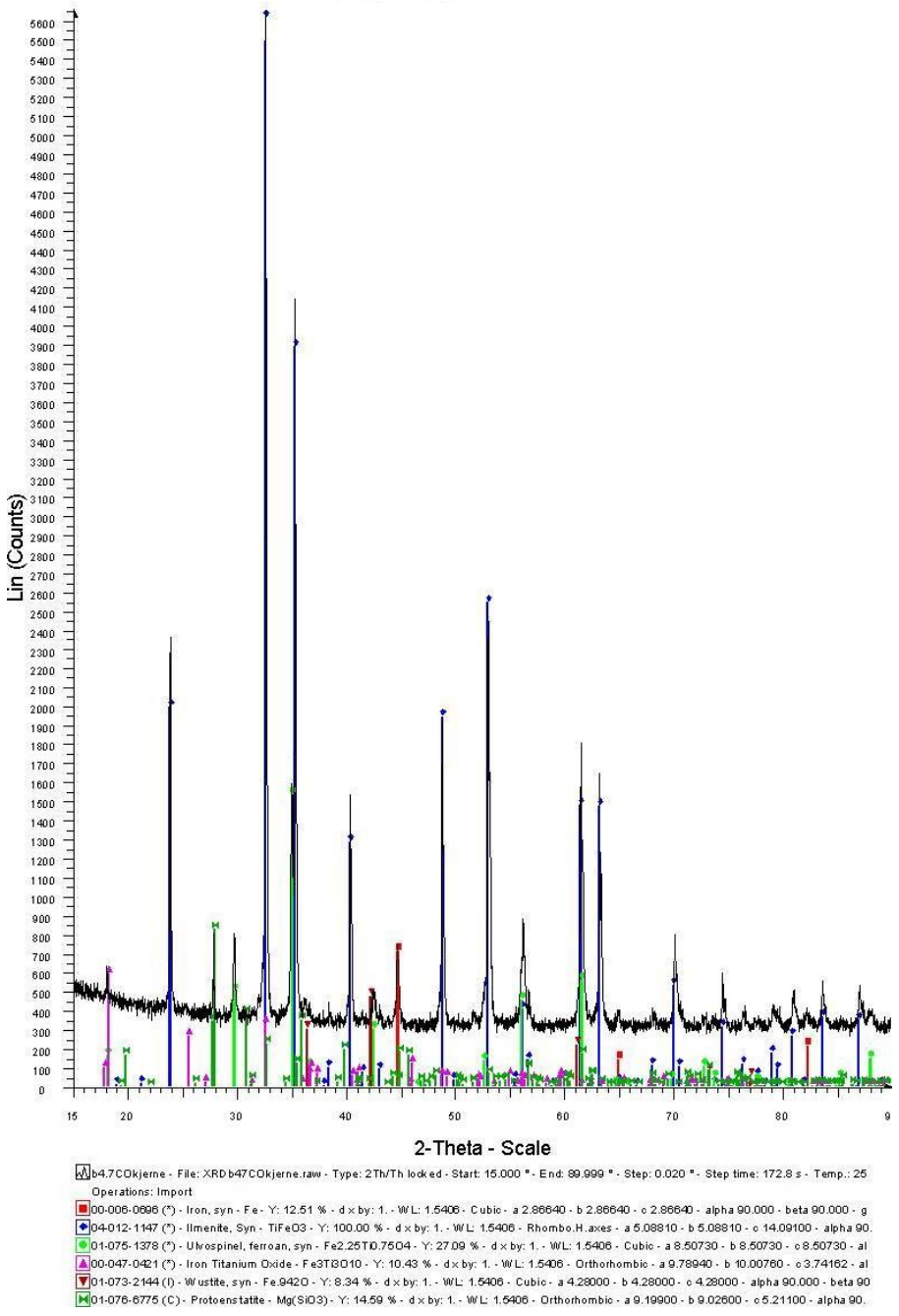

Figure A.12: XRD scan for sample b4.8COcore with interpretation and normalized peaks.

Sample b4.8COshell

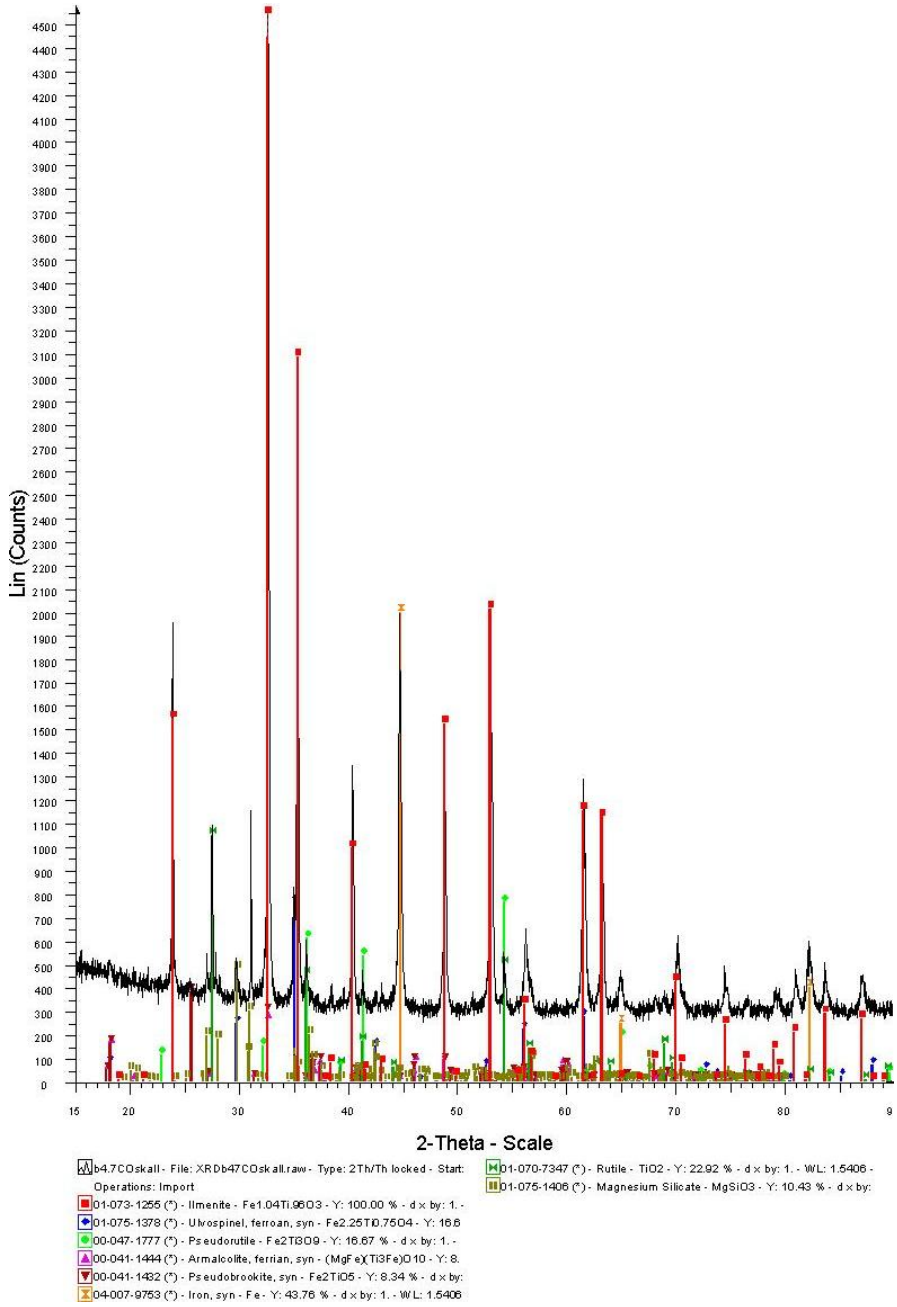

Figure A.13: XRD scan for sample b4.8COshell with interpretation and normalized peaks.

Sample b9CO3

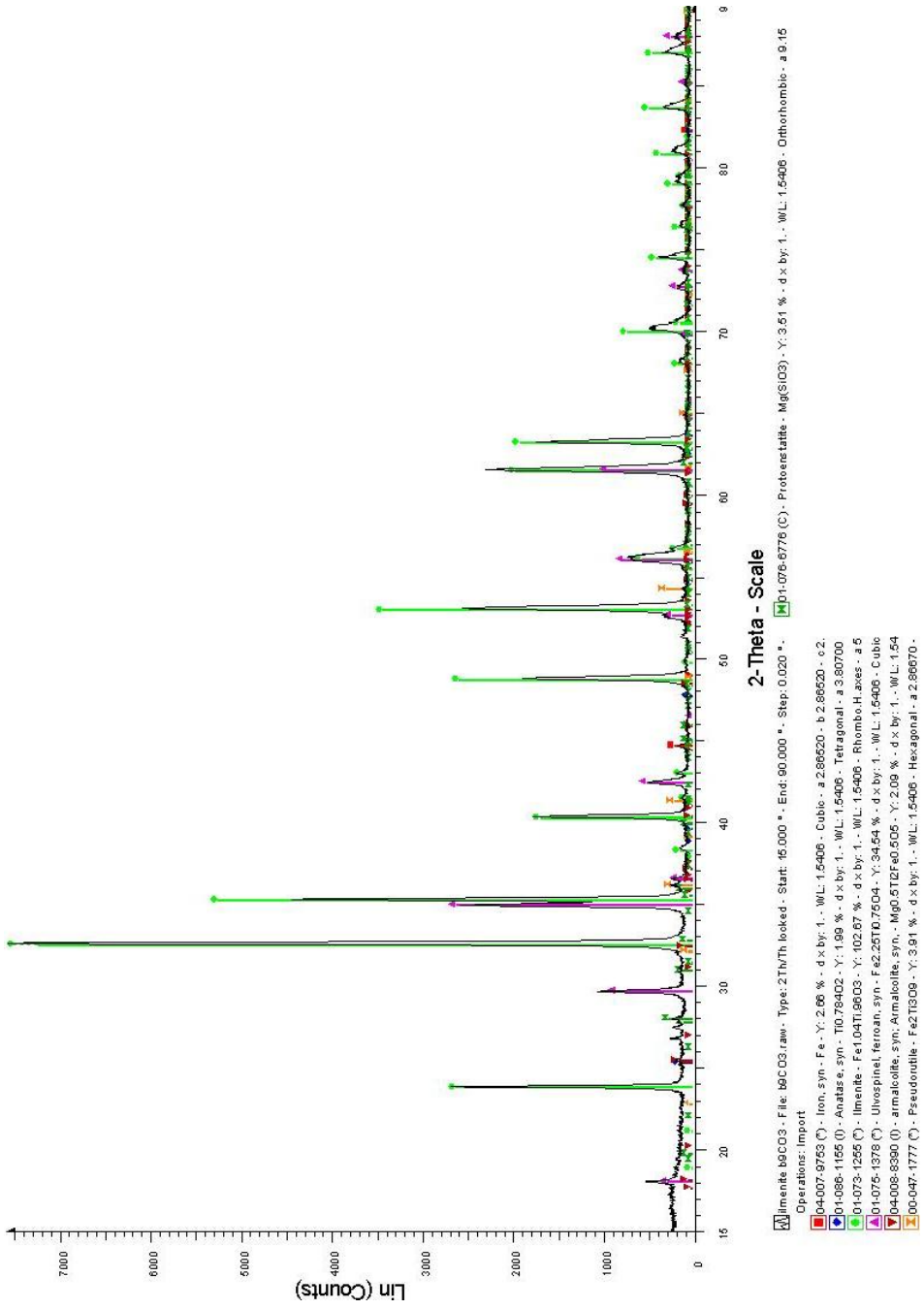

Figure A.14: XRD scan for sample b9CO3 with interpretation and normalized peaks.

Sample b9CO.old

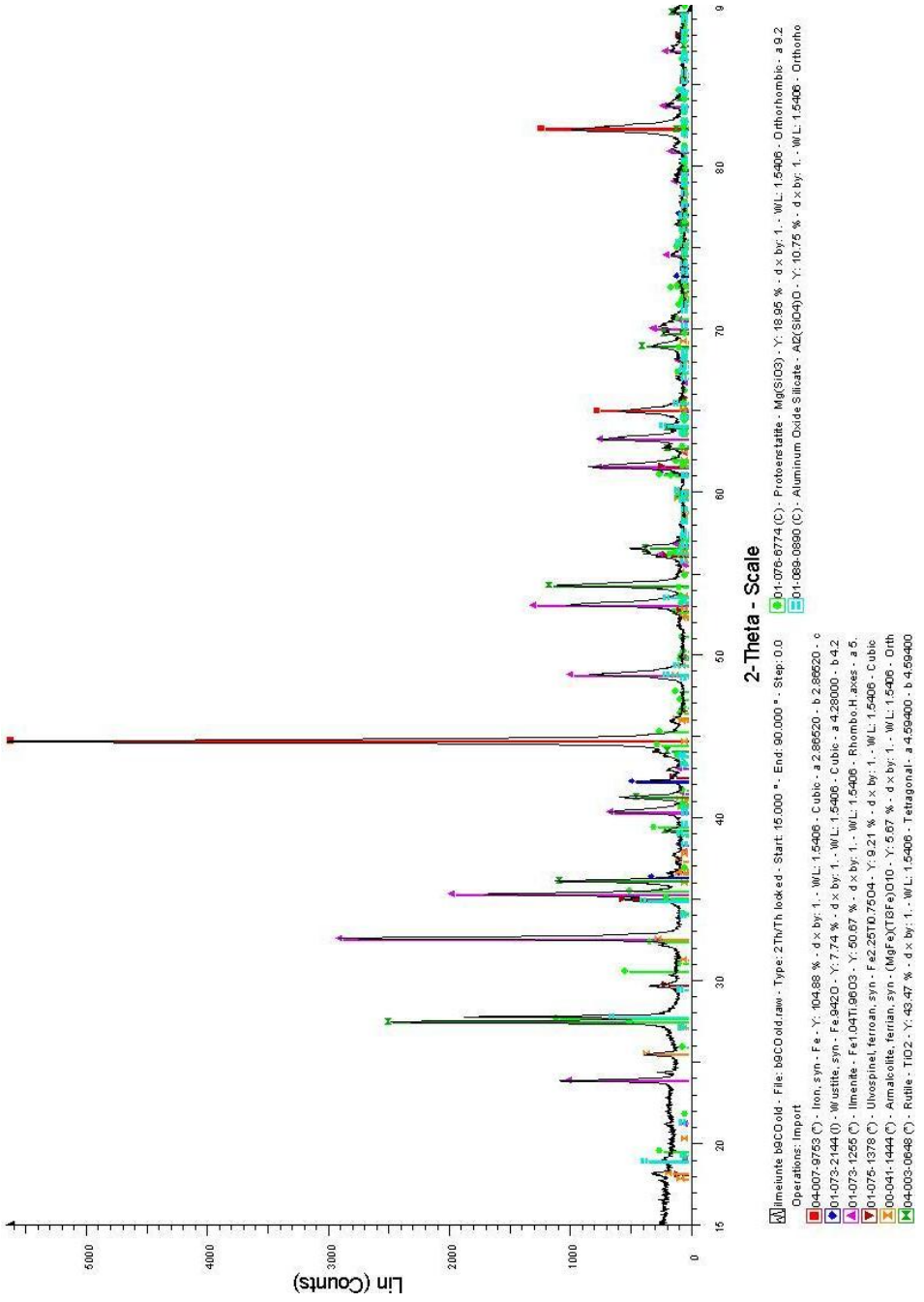

Figure A.15: XRD scan for sample b9CO.old with interpretation and normalized peaks.

Sample b7H$_2$

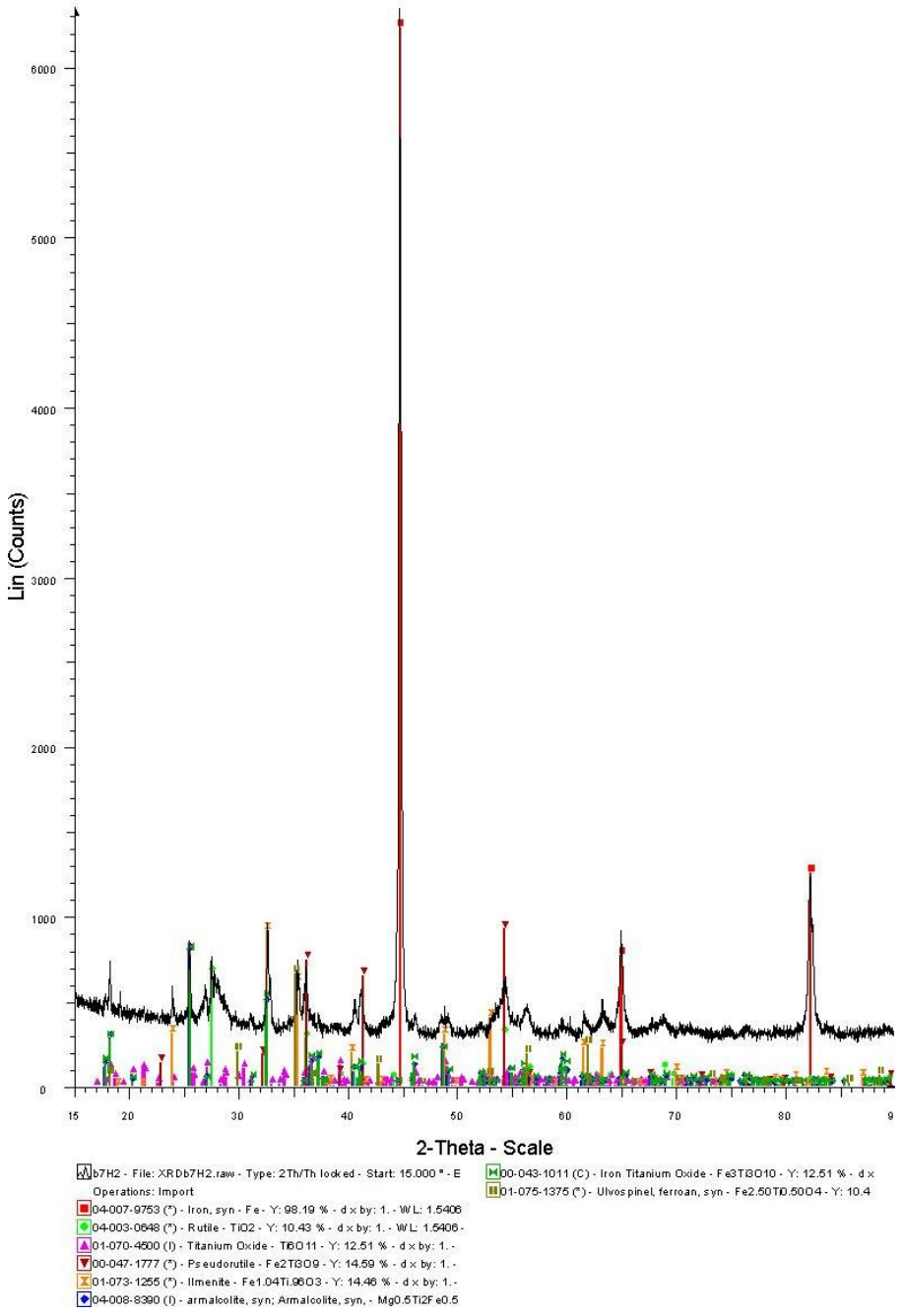

Figure A.16: XRD scan for sample b7H$_2$ with interpretation and normalized peaks.